NTNU

Norwegian University of
Science and Technology

Investigation on Quartz Crucibles for Monocrystalline Silicon Ingots for Solar Cells

Fredrik Winther Thorsen

Master of Science in Mechanical Engineering
Submission date: June 2016
Supervisor: Marisa Di Sabatino, IMTE
Co-supervisor: Adeline Lanterne, IMT

Norwegian University of Science and Technology
Department of Materials Science and Engineering

ABSTRACT

This thesis focuses on the bubble formation and growth in the quartz crucibles used to produce Czochralski (Cz) monocrystalline silicon ingots for solar cells production. Several experiments have been conducted to investigate how much the bubbles grow during the crystal pulling process, and which parameters contribute to their growth.

Two different crucible types have been investigated, before use in the Cz process, after use and after several heat-treatments. From these crucibles, samples have been cut from three different positions along the crucible wall. These samples have been investigated by X-ray tomography, and the size, distribution and volume of the bubbles inside the crucible wall have been measured.

It is observed that the bubbles grow in size and quantity during the Cz process. More bubbles are also detected closer to the inner part of the crucible wall after use in the Cz-process. Small bubbles that are below the detection limit of the X-ray equipment were analysed by scanning electron microscope. The high-temperature heat-treated samples formed a thick cristobalite-layer and many cracks. The lower temperature heat-treated samples formed less cristobalite and less cracks. Comparison was done between the two different crucible types and between the different heat-treatments. The different positions in the samples were also compared.

These results indicate that there are some differences in quality between different crucible producers and that bubble formation and growth are significantly affected by the Cz process parameters, such as temperature and time.

SAMMENDRAG

Denne avhandlingen tar for seg dannelse og vekst av bobler i kvarts-digeler brukt for å produsere silisium ingoter for bruk i solceller ved Czochralski (Cz)-metoden. Det har blitt undersøkt hvor mye boblene vokser i løpet av krystalliseringsprosessen, og hvilke parametere som bidrar til denne veksten. For å undersøke dette, har flere eksperimenter blitt gjennomført for å isolere faktorene som er viktige for at boblene skal vokse.

To forskjellige digeltyper har blitt undersøkt, før bruk i Cz-prosessen, etter bruk og etter flere forskjellige varmebehandlinger. Prøver fra tre forskjellige posisjoner har blitt kuttet fra digelveggen. Prøvene har blitt undersøkt med røntgen-tomografi (CT), og størrelsen, fordelingen og volumet til boblene inne i digelveggen har blitt målt.

Observasjonene viser at boblene vokser både i størrelse og antall i løpet av Cz-prosessen. Flere bobler ble oppdaget nær innerveggen i digelen etter bruk i Cz-prosessen. Små bobler som er mindre enn deteksjons-grensen til røntgen-utstyret ble analysert ved å bruke et elektronmikroskop. Prøvene som hadde gått gjennom en høytemperatur varmebehandling dannet et tykt cristobalite-lag med stor sprekkdannelse. Prøvene som gjennomgikk en lavere temperatur varmebehandling dannet mindre cristobalite og sprekker. Sammenligning mellom to forskjellige digeltyper og de forskjellige posisjonene innbyrdes i digelen ble gjort. Prøvene som gjennomgikk varmebehandling ble også sammenlignet.

Resultatet fra analysene viser at det er forskjell på kvaliteten mellom de forskjellige digel-produsentene og at bobledannelse og -vekst i stor grad påvirkes av parametere som temperatur og tid under Cz-prosessen.

ACKNOWLEDGEMENTS

When working with this master thesis, I have received help from several persons at NTNU and SINTEF. I would first like to thank my supervisor Marisa Di Sabatino Lundberg and co-supervisor Adeline Lanterne for guidance and supervision through the process, and good feedback. Eivind Øvrelid (SINTEF) helped me with setting up the heat-treatment experiments and gave me interesting answers and ideas. Pei Na Kui also helped me with the heat-treatment, and Ove Darell helped me cut the crucibles into suitable working pieces. I would like to thank Ole Tore Buset for training me at using the X-ray tomography equipment, and acquiring high quality data. A big thank you to Stein Rørvik (SINTEF), who kindly helped me with the image analysis and made me able to easily extract valuable and meaningful results from the X-ray images. John-Atle Bones (SINTEF) provided me with the simulation data, and Ove Paulsen (SINTEF) answered many questions regarding crucible examination and heat treatment. Last, but not least, I would like to thank Ingrid for being my biggest supporter.

Trondheim, 13th of June 2016

Fredrik Winther Thorsen

TABLE OF CONTENTS

LIST OF FIGURES

LIST OF TABLES

1 INTRODUCTION

Silicon solar cells are the most used types of solar cells in the world today [1]. The demand for clean and carbon-emission free sources of energy is rising, and solar cells is gaining trust as a candidate to solve this global challenge. Despite the large quantities of silicon present in the earth crust, the road from silicon containing sand to solar cells is long and challenging. The purity of the silicon used in the high quality solar cells has to be extremely high, demanding a thorough quality control in all stages of the production and high quality of the raw materials.

Today, the highest solar cell efficiency is obtained by using monocrystalline silicon wafers in the solar cell module [2]. The wafers are cut from silicon ingots grown by a process called the Czochralski (Cz) method. In this process, silicon feedstock is first stacked in a quartz crucible and melted, and a monocrystalline silicon ingot is then pulled out of the melt. The crucibles used in this process are made from high purity amorphous quartz (SiO_2), and should prevent unwanted impurities from entering the silicon melt during the crystal pulling. The crucible also has to keep its shape during the entire process. Indeed, small disturbances in the melt or minor concentrations of impurities can interfere with the crystal growth, leading to the generation of dislocations. To reduce the price of high quality solar cells it is important to mitigate the occurrence of these events. To do so, a better understanding of the crucible's role and changes during the process is now necessary.

The quartz crucible contains a lot of bubbles. Most of these bubbles were formed when the crucible was manufactured, but some also grow during the crystal pulling process. In general, crucibles consist of two different layers: One bubble free layer (BF) and one bubble-containing layer (BC). The bubble free layer is facing the inside of the crucible. As this side is in direct contact with the silicon melt, it is important to keep this layer free from bubbles through the entire process, to ensure that no bubbles are released into the melt and subsequently into the silicon ingot. It is also important to understand whether the bubbles are formed in the bubble free layer during the pulling process, or if they grow from very small, invisible bubbles to larger visible bubbles. They might also move from the bubble-containing layer to the bubble free layer. In this context, the main goal of this thesis is to improve the understanding of mechanisms

occurring inside the crucible during use, and discuss about the possible impact on the silicon ingot quality and yield.

The work of this thesis is the continuation of the work previously done in a project thesis [3]. In this project thesis, the bubbles inside the quartz crucible wall were characterized by X-ray tomography. By comparing used and unused crucibles, it was concluded that the bubbles grow in size and in number during the crystal pulling process. The unused samples were heat-treated and re-examined as a method of understanding how the bubbles form and grow inside the crucible. The present results will be compared to the findings of this project thesis.

This master thesis will focus on the comparison of the bubble contents in the crucible walls before and after their use in the Cz process, for different crucible suppliers. In addition, the unused crucibles will be heat-treated in different annealing processes to investigate what parameters contribute to bubble growth and formation. Both X-ray tomography and Scanning Electron Microscopy will be used to study the samples. A theoretical background for bubble growth and movement will be given, along with an introduction on the global solar cell value chain to highlight the crucible's role and importance in the final output quality.

2 THEORY

2.1 Solar cell value chain

Silicon solar cells can be divided in three categories: Monocrystalline, multicrystalline and thin film. These different solar cell structures correspond to different quality demands and different potential applications of solar cells. This thesis focuses on the monocrystalline silicon solar cells that allow to reach the highest efficiencies. The process of making these monocrystalline solar cells will be presented in this section.

The solar cell value chain, shown in Figure 1, describes how natural silicon is transformed through several steps into power producing solar cells. The main steps are the silicon feedstock production and refinement, the crystallization and wafering, and the solar cell process which creates working solar cells from the wafers [4]. All the steps in the value chain are important to obtain the highest possible quality and efficiency in the solar cell. This brief presentation will mainly focus on the silicon feedstock production and the crystallization and wafering processes.

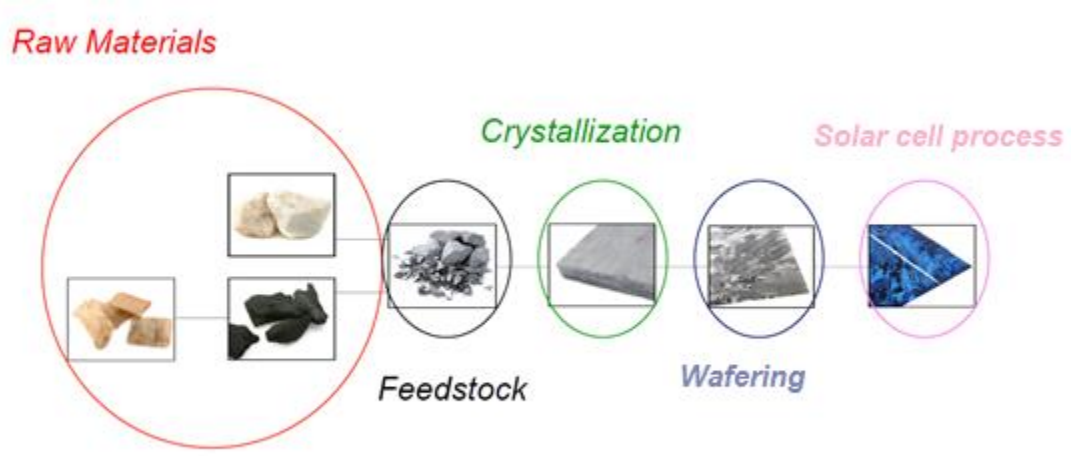

Figure 1. The solar cell value chain [4].

2.1.1 Feedstock

Even though silicon is a highly abundant substance in the earth's crust[5], the road from silicon bound in sand or rocks as SiO_2 to solar cell material is long and challenging. Firstly, the oxygen-bound silicon has to be separated from the oxygen. This is done by the so-called metallurgical route, and involves coal or woodchips to reduce the silicon dioxide and oxidise the carbon to produce silicon and carbon monoxide (CO). The outcome of this process is called metallurgical grade silicon (MG-Si), which has a purity of about 98% [6].

The metallurgical grade silicon has to be refined to the required purity before it can be used in the process of making solar cells. The silicon used in solar cells is called Solar Grade silicon (SoG-Si), and is defined with a purity of 99,9999% (6N) [4]. The allowed contamination concentrations are shown in Table 1.

Impurity	MG-Si [ppm]	SoG-Si [ppm]
B	15-50	<1
P	10-50	<5
O	3000	<10
C	100-250	<10
Fe	2000	<10
Al	100-200	<2
Ca	100-600	<2
Ti	200	1
Cr	50	1

Table 1. Table showing the impurity concentration in MG and SoG-Si [4].

Two main methods are used to produce the high purity silicon used in solar and other photovoltaic (PV) industries: The Siemens method and the Fluidized Bed Reactor (FBR) [4]. The techniques use tri-chlorosilane and silane, respectively, to deposit high purity silicon in a silicon rod (Siemens) or as granulates in the reactor (FBR).

2.1.2. Cz process

When the desired purity is achieved, the silicon is melted and crystallized into a silicon ingot. This process is called the Czochralski process, and will be described in detail here. The Czochralski (Cz) process is a method for growing single crystals from a melt bath. In the photovoltaic industry, it is used to produce monocrystalline silicon ingots for silicon wafer production. Although discovered in 1918 [7], the process is still the most used crystal growing process to produce single crystals today.

The process starts with the stacking of a quartz crucible with polycrystalline silicon feedstock, which is then loaded into a furnace. The silicon is heated to around 1500 °C to ensure the melting. While the temperature is raised, the air is pumped out of the furnace chamber, and argon is purged through the system. This is done to obtain an inert atmosphere, and the desired pressure is in the range of 15-50 mbar during the pulling process [8]. An overview of the main materials involved in the Cz process is shown in Figure 2.

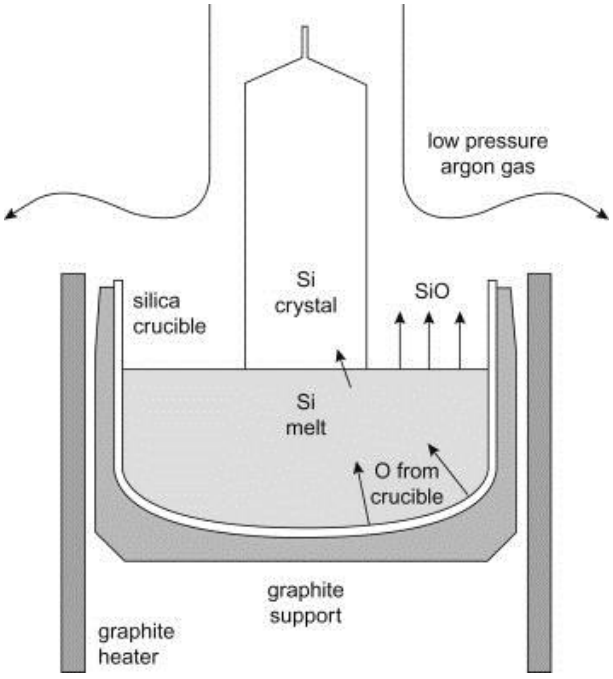

Figure 2. Processes and materials in the Czochralski process [8].

While the silicon melts, the crucible rotates. This is to ensure sufficient mixing of the melt, but also to release most of the bubbles that are trapped inside the melt and close to the crucible wall during the melting. After the melt stabilization, a crystal seed is dipped into the melt and then pulled slowly upwards while being rotated in the opposite way of the crucible. The seed is a thin mono-crystal rod with the desired crystal direction (usually <100> or <111>). When the seed is dipped into the melt, this creates a thermal shock in the seed which generates dislocations inside. To avoid these dislocations to propagate in the growing crystal, a *neck* is grown first. The neck is a thin elongation of the seed, grown so thin and pulled up so rapidly that the dislocations all terminate on the edge of the crystal. This can be seen in section (e) in Figure 3, which illustrates schematically the Cz process.

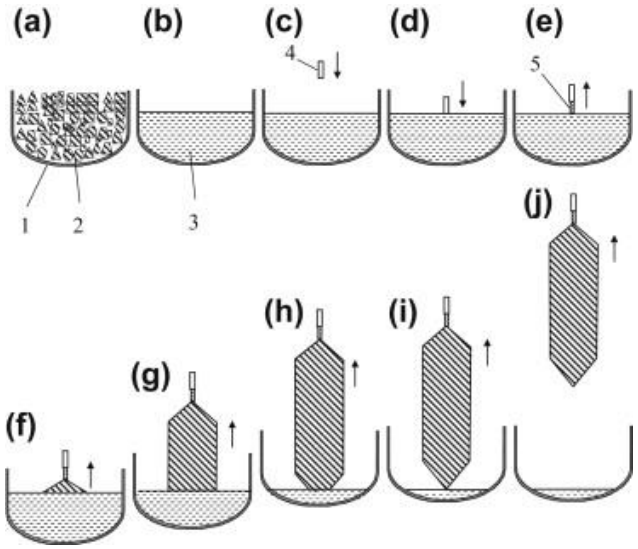

Figure 3. Schematic overview of the Czochralski process [9].

After reaching a successful dislocation free neck growth, the pulling speed is reduced to increase the diameter of the growing ingot. This part of the ingot is called the *crown*, and it is the transition between the neck and the body. Once the desired diameter is obtained, the ingot is grown with a constant diameter (typically between 120 and 250 mm [8]). When the weight of the ingot starts to approach the desired value (around 100 kg), the tailing process is initiated. This is done to minimize the thermal shock created when popping the ingot out of the melt and thus avoiding propagation of the dislocations in the body, as the dislocations will travel a shorter distance upwards than they would if the growth was disrupted at full diameter [8].

After the finished ingot is separated from the melt, it is placed into a receiving chamber to be cooled down. The heaters are turned off, and the crucible cools down while the rest of the melt contained in it freezes. This part of the remaining melt is called the *pot scrap*, and will not be reused due to its high contamination level.

2.1.3 Wafering and solar modules

The ingots are then cut into blocks with the desired shape. The blocks are then glued to a supporting tool and cut into thin wafers, as shown in Figure 4. The wafers form the basis of the solar cells that are used to produce electricity.

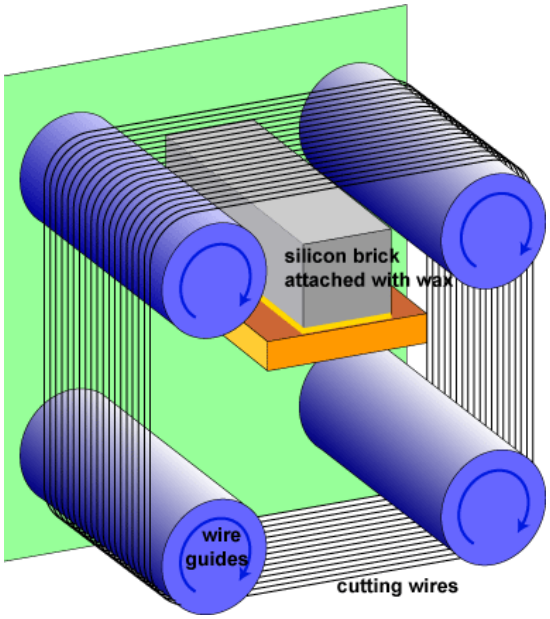

Figure 4. Wafering process: The silicon block is sliced into wafers using cutting wires [10].

After the silicon ingots have been cut into wafers, the wafers are cleaned and the surface is treated to obtain the wanted surface texture. An emitter layer is deposited on the wafer to create the PN-junction. An anti-reflective coating and metallic contacts are then added, before the wafer interconnection in a module, to obtain a functioning solar cell system (see Figure 5).

Figure 5. Interconnection of wafers in a solar module [11].

2.1.4 Detrimental impurities in silicon solar cells

In order to reach high solar cell and module efficiencies, the silicon has to be extremely pure. Contamination of light elements such as carbon and oxygen will be covered separately in Section 2.3.3 and 2.3.4, as they form from the interaction between the silicon melt and the crucible. The metallic impurities will be covered here. Figure 6 shows how much different metal impurities affect the efficiency of a p-type silicon solar cell [13].

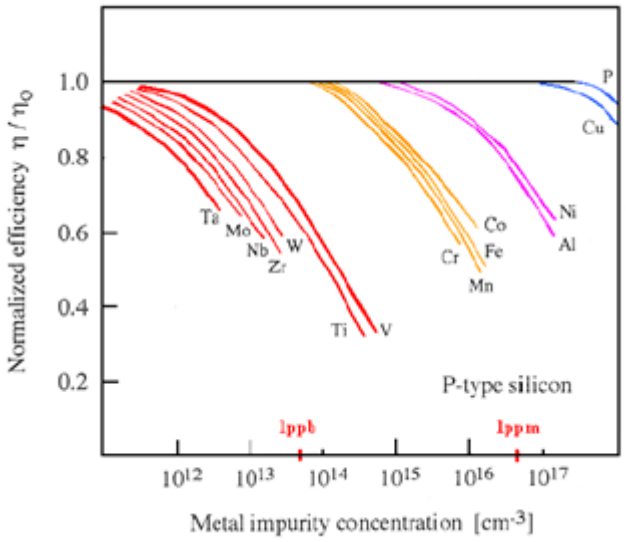

Figure 6. Detrimental impurities and how they affect performance of the solar cell [4].

There is a big difference in how detrimental the impurities are for the solar cell performance. As seen in Figure 6, 1 ppb of for instance W or Nb will decrease by half the efficiency, while 1 ppm of Fe, Cr, Mn or Co is required to do the same damage [4]. The quality of the silicon wafer is checked by measuring the electronic resistivity and the carrier lifetime in the wafer. Both these parameters are governed by the amount of impurities present in the silicon, and they are thus very important to control, to obtain high solar cell efficiencies.

2.2 The crucible composition and manufacturing

Because of the high melting temperature (1412 °C) and the reactivity of molten silicon at high temperatures, there are not many materials that are suitable for the crucible composition [13]. Most metals are rejected because they are only allowed in the crystal with very small concentrations, typically in the parts per trillion atoms (ppta) range [13]. Materials from group III and IV in the periodic table are used as dopants in the crystal, but the allowed concentrations are also too low to have the crucible to be made from them. One of the materials that answers this challenge is the amorphous silicon dioxide, also known as quartz or silica, which is the most used in the PV industry.

The crucible consists of one transparent inner layer facing the melt, and one opaque outer layer. The inner layer consists of dense natural silica, while the outer layer contains a lot of bubbles [14]. The inner layer will be referred to as the bubble free (BF) layer, and the outer layer will be referred to as the bubble containing (BC) layer in this thesis.

2.2.1 The raw material

The raw material in the crucibles used in the Czochralski process is high purity quartz sand. It is defined to contain less than 30 ppm of impurities, that is to say >99.997% silicon dioxide (SiO_2) [15]. Natural quartz resources with this level of purity are only found in the Spruce Pine deposits in North Carolina, US. Natural quartz from other sources can also be used, but has to be purified through several steps to meet the high purity demands.

The most detrimental impurities in the crucibles are found in three chemical groups: Alkalis, transition metals and boron [15]. Traces of alkalis such as lithium, potassium and sodium can have a critical impact on the thermal stability of the quartz crucibles and accelerate the dissolution of the quartz into the silicon melt. Transition metals such as Cr, Cu, Fe, Mn, Ni and Zn can dissolve or diffuse into the silicon and thus strongly decrease the electronic properties of the solar cell as discussed previously. Finally, it is critical that the quartz feedstock has a low boron content, as boron does not respond to conventional chemical refining of quartz [15]. Boron is used as a dopant in the solar cells, and it is therefore important to thoroughly control the level of boron in the silicon melt.

The refining process of natural quartz starts with crushing, size sorting, and comminution of the raw material. Later, the impurities are removed by physical and chemical treatments that are not explained in more detail here [16]. The last step of the quartz refinement is the thermal treatment or calcination. This process reduces the bubble content and hence improves the melting behaviour thanks to the removal of fluid inclusions [16].

2.2.2 Crucible manufacturing

The crucibles used in the Czochralski process are called *fused silica* crucibles. The route for making the crucibles is kept confidential by the different suppliers. However, the main principles can be found in patents [17], [18]. High purity crystalline quartz sand or amorphous quartz powder is first poured into a rotating mould. The centrifugal force holds the sand against the mould walls, and ensures an even distribution and thickness. Heat is applied from an electric arc, and the quartz is melted to an amorphous glass. The fusion will start in the inside, and spread out to the mould wall, which is made from graphite or heat resistant stainless steel. To decrease the amount of bubbles in the finished glass, a method for introducing vacuum is also applied. The different steps of the crucible formation process are detailed below. Figure 7 shows the manufacturing process (left), and a finished crucible (right).

First, a coarse quartz material is introduced in the mould. There are holes in the mould to apply the vacuum, and pull out gasses from the material that can pollute the process and create bubbles

in the quartz. Then, a second layer of finer quartz is introduced on top of the coarse one. This forms a tight "wall" to the air in the inside of the mould, and creates an even higher vacuum outside the quartz. This is because the fine layer of quartz stops air from being drawn into the mix. Once the heat is applied, the finer layer of quartz melts first, forming an even tighter blockage of air. This layer then fuses into a layer of glass with low bubble content. The air and gasses are drawn out, and the fine grains ensure that there are few voids inside the quartz. The coarse quartz layer then fuses in a second time, forming an outside layer with a higher number of bubbles. The importance of the absence of bubbles in the inner layer will be discussed in more details in the section 2.3.1.

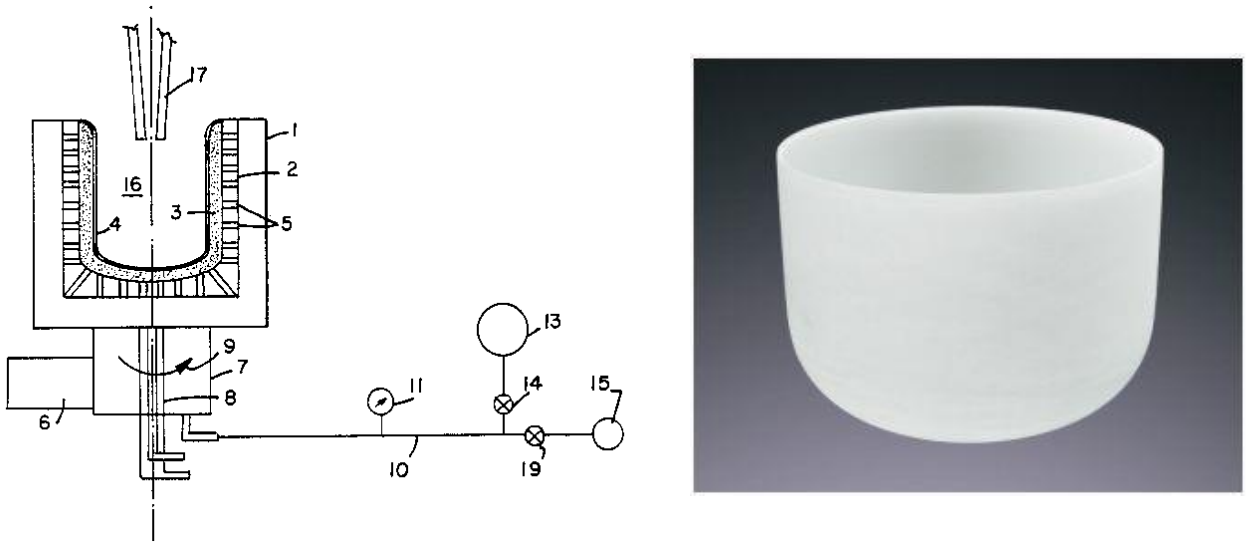

Figure 7. Left: Quartz crucible manufacturing with (3) the BC layer in the quartz crucible, (4) the BF layer, (17) the heater, and (1) & (2) the graphite mould [17]. Right: Picture of finished crucible [19].

A thin layer of unmelted sand is left between the finished crucible and the graphite mould to simplify the removal of the crucible at the end. This sand cannot be reused because of impurities and pollutions in it, and has to be discarded. It is therefore important to use as little "insulation sand" as possible. Pressurized air is pumped into the vacuum holes to help unloading the crucible. Water cooling of the mould and process structure is necessary to improve the lifetime of the structure and the cost of the process. It is also important to keep the mould cold, because the structure expands and contracts much more than the quartz, which can cause stresses and cracks in the crucible. In addition, the mould can be made by two pieces, where the inner sleeve can be removed with the crucible for an easier removal.

The method described above gives crucibles with a much lower bubble content than if they were made with just one type of sand. It is also important to use sufficiently small holes to provide the vacuum in the graphite mould. This will prevent the holes from being blocked, which can cause insufficient vacuum. The pressure during process should be less than 5000 Pa, and preferably less than 1000 Pa [17].

The finely ground quartz material is obtained by milling either amorphous or crystalline quartz using a quartz mill, and the mill container should be made from polypropylene to prevent contamination, as the purity specifications are very strict [8].

2.2.3 Cristobalite formation

During the Cz process, when the quartz crucible is brought up to temperatures over 1470 °C, the quartz transforms from the amorphous α-Quartz to the β-Quartz and then crystallizes to form a β-cristobalite layer on the surface of the crucible [20]. This polymorph is the stable form of silica at these elevated temperatures [20]. It is desired to form a cristobalite layer during the crystal pulling for several reasons. Firstly, it generates a hard armour between the silicon melt and the silica crucible wall. Secondly, the hard cristobalite layer helps the crucible maintaining its shape when its viscosity decreases at high temperatures. The melting point of cristobalite is 1713 °C, which is much higher than the maximum temperature achieved in the Czochralski process, and also higher than the softening point of the amorphous silica, which is at 1544 °C [19]. The cristobalite can clearly be seen (Figure 8) as a non-transparent, brittle, white layer on the used crucible.

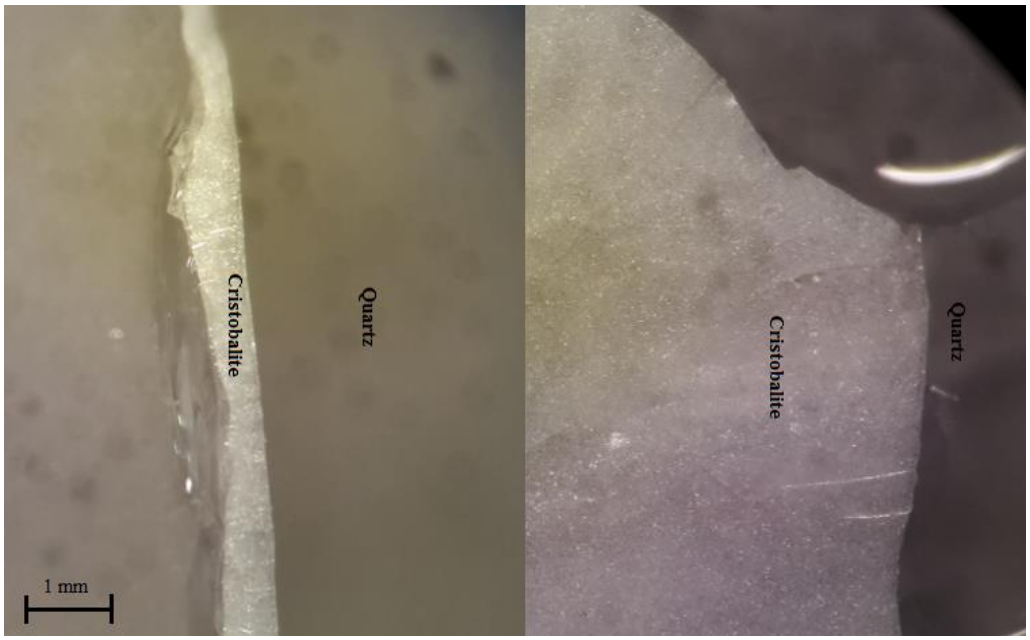

Figure 8. White layer of cristobalite on the glassy silica seen from side (left) and top (right).

When the crucible is cooled down below 280 °C, the cristobalite transforms from a β-cristobalite, which has a cubic crystal structure, into an α-cristobalite which has a tetragonal structure. This phase transition leads to a volume decrease of about 5%, which causes stresses and cracking in the cristobalite layer [(20)]. This, and in addition the crucible deformation, are reasons why the crucible can not be reused after it has been cooled down at the end of the crystal pulling. It can however be reused if it is refilled with silicon while the temperature in the chamber is maintained. This technique is called hot recharging [(8)]. The phase diagram of silica is shown in Figure 9.

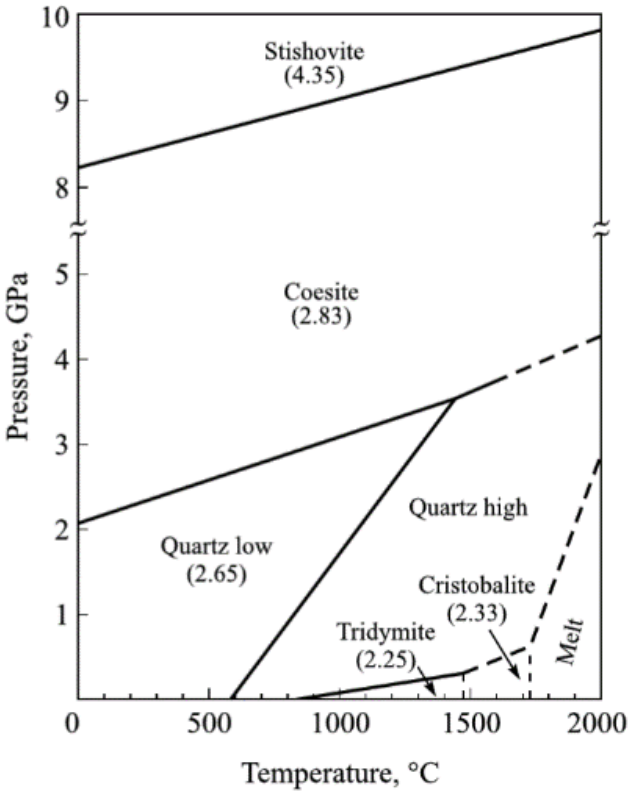

Figure 9. Phase diagram of silica, showing the stability range of the cristobalite [20].

The advantages brought by the cristobalite layer requires the cristobalite layer to be evenly distributed. In case of contaminations present at the crucible surface, the cristobalite can nucleate and promote formation of cristobalite islands around the contaminations. The cristobalite will then grow unevenly during the silicon melt and Cz pulling. The cristobalite islands can then detach from the crucible and enter in the melt [21]. A technique to improve the formation of a continuous cristobalite layer is discussed in the following section.

2.2.4 Crucible coating

Because of the advantages of having an even layer of protective cristobalite on the crucible, and the disadvantages of having uneven growth as described above, the cristobalite formation is controlled to give the wanted properties. To enhance the growth of cristobalite, the crucible surface can be doped with a devitrification agent, such as an alkaline-earth metal [22]. When the coated silica is heated to above 600 °C during the Czochralski process, the devitrification agent reacts with the vitreous (amorphous) silica and forms crystalline nuclei on the surface. As the

melting process continues, the silicon melt and the graphite crucible support acts as a reducing atmosphere which promote radial growth of the cristobalite from the nucleation sites. The cristobalite grows radially until a continuous layer is formed over the entire surface of the crucible.

The most used devitrification agent is barium. A 100 ppm barium doping decreases the activation energy in the crucible surface, from 167 to 120 kJ/mol, which enhances the formation of the cristobalite [23]. Barium is used because it is not detrimental for the crystal growth as it does not enter the growing crystal even with a considerable barium concentration in the melt. Calcium for example, is not suited as a devitrification agent, because it is incorporated into the crystal at a much lower melt concentration than barium [22] and as discussed earlier, even very small concentrations of contaminations can cause defects in the silicon crystal structure.

2.3 Crucible interaction with the silicon melt

2.3.1 Importance of a bubble free layer

As already mentioned, it is important that the layer closest to the silicon melt has a very low bubble content. This has multiple reasons. Firstly, the heat conduction of the crucible changes when there is a lot of air inside the glass. In order to control the growing process, one wants to know the specific properties of the crucibles, which change in the presence of bubbles. Secondly, as the quartz is heated over a long period, its lowered viscosity causes it to start creeping and sagging. If the quartz is filled with bubbles, it will collapse even more. In contrary, the lack of bubbles will improve the support of the quartz weight.

Lastly, as the silicon is melted and the crystal is pulled, the reactive silicon melt consumes the inner layer of the crucible. It is therefore important that this layer is as pure and free from bubbles as possible, to prevent impurities or bubbles from entering the melt.

Indeed, bubbles close to the surface can expand and even explode due to higher pressure inside them than in the vacuum of the crystal puller. The small explosions may lead SiO_2 particles entering the melt, which can lead to a structure loss issue (introduction of dislocations inside the crystal) if the particles enter in contact with the solidification front. In addition, bubbles that get uncovered through the melting or crystallization process creates a cavity where gas bubbles can grow [24].

2.3.2 Gas bubbles and pinholes in the silicon

Gas bubbles of SiO can be produced in the melt-crucible interface. The crucible can also react with the carbon in the graphite hot zone parts to form silicon monoxide. The two reactions producing SiO are: [8]

$$SiO_2(s) + C(s) \rightarrow SiO(g) + CO(g)$$

$$SiO_2(s) + Si(s) \rightarrow 2\,SiO(g)$$

The SiO gas bubbles produced at the melt-crucible interface can stick to the crucible wall for a long time. If these bubbles reach the crystal solid-liquid interface, they can form small gas bubbles in the crystal, often referred to as pinholes [8]. The SiO particles can also agglomerate and form small dust particles that can float on top of the silicon melt. If these particles get into the growing crystal, they can lead to generation of dislocation inside the crystal, an issue called structure loss [25], and hence destroy the final properties of the ingot.

When the silicon is stacked in the crucible, argon from the atmosphere will be present in between the silicon "chunks". When the silicon is melted, some of this argon gets trapped in the interface between the crucible and the silicon melt. This can create argon gas bubbles. If the inside crucible wall is uncoated, the low surface tension will cause most of the bubbles to be released from the crucible surface and travel to the melt surface before start of the crystal growth. When the crucible inside is coated, it has a higher surface tension, and therefore the bubbles will hang on for much longer [22]. This means that they can be released into the melt

during the crystal pulling. If the bubble enters in contact with the solidification front, the crystallization of the silicon around the gas bubble from the melt leads to the formation of a pinhole (gas bubble inclusion in the crystal). This can also cause a structure loss issue [24]. Both these events cause a disturbance in the monocrystalline structure, which is detrimental for the quality and the lifetime of the solar cell. Silicon wafers with pinholes or dislocations cannot be used for solar cells fabrication. It is therefore highly wanted from the industry to prevent bubbles from entering the melt during the crystal growth.

Most of the bubbles leave the crucible wall during the "stabilization" step after melting, but this is not always the case. The melt convection created by the heat from the thermal elements and the crucible and crystal rotation removes bubbles from the crucible wall over time [26]. This may causes the pinhole occurrence to decrease as the runtime increases. The problem with long runtime is that the crucible is consumed by the melt, which generates even more SiO gas and risk of contamination from the crucible itself. Proper stacking of the silicon feedstock and correct surface tension on the crucible inner wall is important to reduce the problem of argon gas bubbles [27].

2.3.3 Oxygen

As the crystal is pulled, the inner part of the crucible wall is consumed by the silicon melt. Since the crucible material contains two compounds, oxygen and silicon, it is important to control what happens when it is in contact with the reactive silicon melt. The allowed oxygen level in the crystal is quite high, typically in the 10-15 parts per million atomic (ppma) range [8]. Still it is important to eliminate most of the oxygen that dissolves from the crucible to prevent levels exceeding the limit.

In order to remove most of the oxygen and silicon monoxide, a low pressure argon gas is purged through the furnace chamber. The inert gas removes up to 98-99% of the oxygen that is dissolved from the crucible [8]. As a result of this, only 1-2% of the dissolved oxygen from the crucible ends up in the silicon ingot.

2.3.4 Carbon

The lifetime in the silicon wafers produced from the ingots grown by the Czochralski process, is greatly influenced by the amount of carbon in the silicon [28]. As discussed in Section 2.3.2, silicon monoxide gas is produced by dissolution of the crucible in the silicon melt, which can lead to the production of carbon monoxide. In addition, the silicon monoxide reacts with the carbon in the graphite support to produce silicon carbide and carbon monoxide through the following reactions [29]:

$$3C\ (s) + SiO\ (g) \rightarrow SiC\ (g) + 2CO\ (g)$$

$$SiO\ (g) + 2C\ (s) \rightarrow SiC\ (s) + CO\ (g)$$

Solid silicon carbide particles produced by the reaction between the SiO and graphite can be driven by the melt flow towards the melt-crystal interface and cause structure loss in the growing crystal. Moreover, because the vapour pressure of carbon is extremely low, the CO molecules trapped in the melt will cause carbon to be incorporated in the solid silicon according to the freezing segregation law [29]. It is known that carbon can become a nucleation site for oxygen precipitates in the silicon crystal, which lowers the lifetime [30]. To achieve long lifetime in the silicon wafers, the carbon content has to be reduced by controlling the gas formation in the crucible-melt interface.

One method is to apply a strong magnetic field to control the convection in the silicon melt. This is called the MCz method [28]. This gives better lifetime in the silicon because it reduces the dissolution of the crucible in the melt by controlling the melt convection. However, the MCz system has several challenges. Firstly, it is costly to buy and to operate the superconductive magnets and the necessary cooling system. Secondly, the magnetic fields reaches thousands of Gauss (G) in magnitude, which is far off the recommended maximum 600 G for 8 hours exposure recommended by the ACGIH [28].

Another method to achieve longer lifetime in the silicon wafers, is by using a melt-phobic, "liquinert" crucible [28]. The lifetime increase (seen in Figure 11) is achieved by reducing the carbon content in the silicon ingot, thanks to the liquinert crucible that reduces the formation of

SiO gas by limiting the reactivity in the crucible-melt interface. As a result of the carbon reduction, the oxygen precipitation sites are reduced. This causes a lower oxygen concentration (see Figure 10).

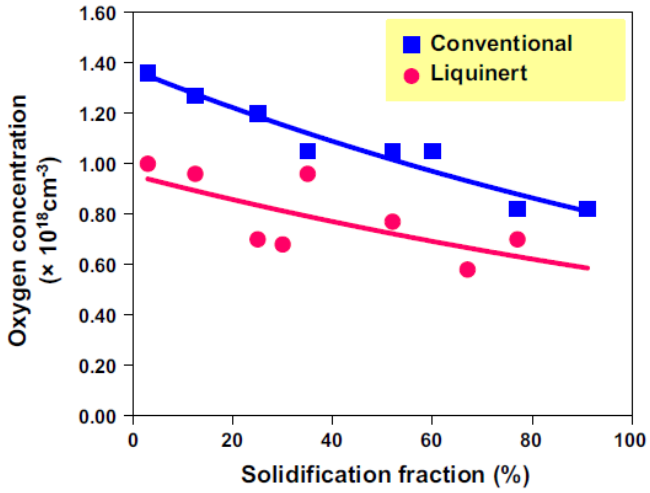

Figure 10. Comparison of the oxygen concentration in the silicon ingot between liquinert and conventional crucibles [28].

The measured oxygen concentration in silicon ingots produced by a conventional and a liquinert crucible is shown in Figure 10.

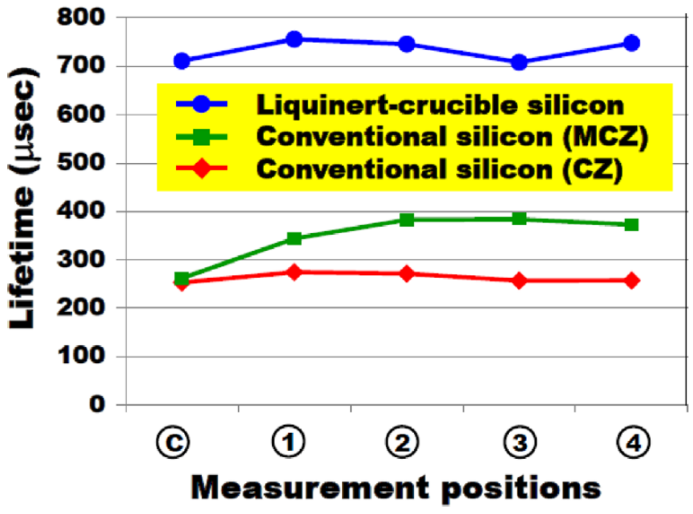

Figure 11. Lifetime measurement on different positions on wafers produced by conventional Cz, MCz and with liquinert crucible [28].

The liquinert crucible produces silicon with higher lifetime than what is produced with conventional crucibles, even with MCz technology (Shown in Figure 11) [28].

2.3.5 Heat transfer through the crucible

Silica has low thermal conductivity, but it can transfer heat through radiation because of its transparency. In the inner layer (later referred to as the BF layer), the material is nearly completely transparent, while the outer layer (BC layer) contains a lot of bubbles that decreases the transparency. It is therefore obvious that the distribution of these bubbles will play a critical role in managing the heat transfer and temperature control of the melt, which has shown to be critical to achieve when growing a Czochralski crystal [8].

The composition of the gas inside the bubbles is still a matter of debate. Most likely it is air, maybe with traces of carbon, or water vapour [31]. To illustrate how the heat-transfer is affected by bubbles in the crucible, a crude example is made with air filled bubbles. Thermal conductivity data for silica and air at ambient temperature and pressure are obtained. This is not representative for what happens inside the crucible during the crystal pulling process, but it gives an idea of how the heat transfer properties change due to the presence of bubbles.

For air at ambient pressure and temperature, the thermal conductivity, k, is 0.0262 W/m*K [32]. For silica it is 3.8 W/m*K [33], which is 150 times higher (but still not very high, as Si has 65 W/m*K) [33]. Some of the samples tested in this thesis showed a bubble content of up to 12%. Taking an approximated case of a crucible with a bubble content of 10%, this gives a total thermal conductivity of the crucible material to be 3.4 W/m*K, which is 90% of what it would be without any bubbles. This means that a crucible filled with 10% bubbles, needs 10% more heat to transfer the same amount of heat through the wall and into the silicon melt. This is interesting, as the thermal conductivity of the crucible might change when the bubbles grow during the pulling process, and make it difficult to control the temperature in the melt.

2.4 Bubbles inside the crucible wall

2.4.1 Bubble movement inside the crucible wall

When the temperature is raised in the furnace, the quartz softens, and the viscosity decreases. This may cause the bubbles to move vertically inside the crucible wall, but this movement is so small that it can be neglected [34]. Indeed, as seen in Figure 12, even at 1550 °C for 50h, a bubble of 1 mm diameter will only move 0.34 µm.

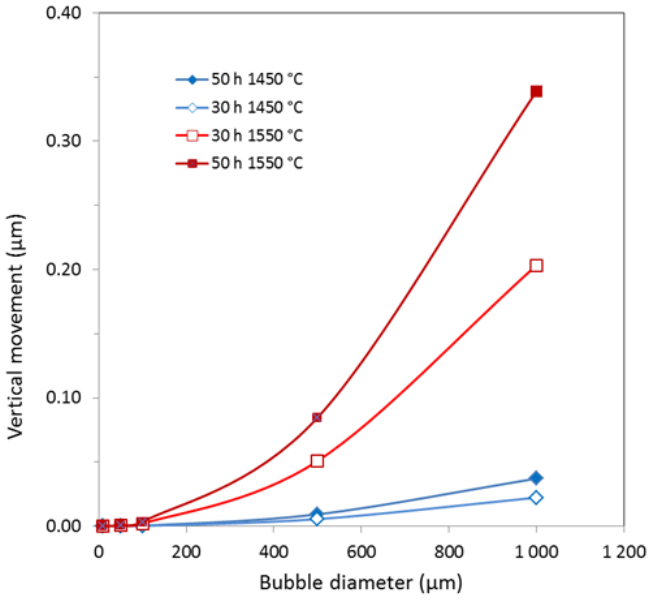

Figure 12. Vertical bubble movement inside the crucible wall [34].

This implies that the variation of bubbles observed in this study can only be due to a change of the bubbles' size (by expansion of the gas inside the bubbles with increasing temperature) or to the formation of new bubbles, but not to movement of existing bubbles.

2.4.2 Bubble growth

As concluded in the project thesis [3] the bubbles in both the BC and the BF layer grow both in number and volume during the Czochralski pulling process. Other research, including heat-

treatment of the silica, concludes that the bubbles grow in size after an annealing at 1500 °C in a 20 Torr argon atmosphere for 10h [35], as seen in Figure 13.

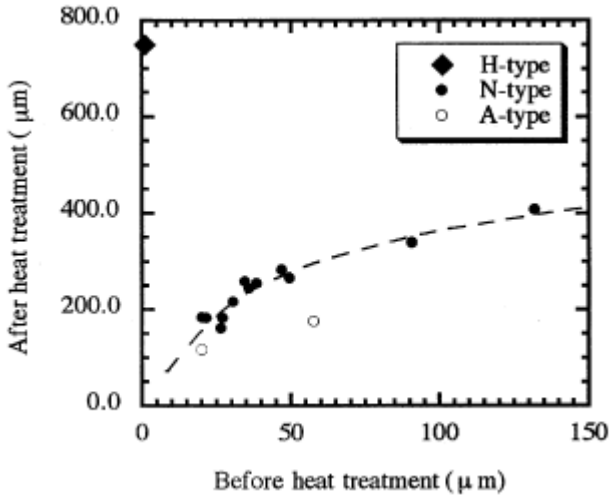

Figure 13. Bubble growth in heat-treated silica [35].

It was concluded in this work that the growth of the bubble is due to the carbon present in the bubbles before the heat-treatment. As the temperature was raised, the carbon reacted with the silica to form CO and SiO gases, as discussed in Section 2.3.2. This can lead to a huge expansion of the bubbles. After heat-treatment, the gas inside the biggest bubbles was measured to be more than 96% CO. The SiO was deposited and dissolved on the inside of the bubble surface, which is why only the CO was detected. The carbon inside the bubbles is likely to have come from the carbon crucible used to manufacture the silica crucible [35].

3 EXPERIMENTAL

3.1 Materials

The materials mostly discussed in this thesis are silicon (Si) and silicon dioxide (SiO_2). Silicon belongs to the IV group of the Periodic Table (atomic number is 14), and is the second most abundant element in the earth crust (27.7%) after oxygen. The crystal structure of silicon is cubic, which is the same type as diamond. Like water, silicon expands when it freezes [5]. Some physical parameters of silicon and silicon dioxide are found in Table 2.

Physical parameters	**Symbol**	**Si**	**SiO_2**
Heat capacity at constant pressure ($J\ kg^{-1}\ K^{-1}$)	*Cp*	703	1175
Thermal conductivity ($W\ m^{-1}\ K^{-1}$)	*k*	65	3.8
Density ($kg\ m^{-3}$)	ρ	2330	2218
Coefficient of thermal expansion (K^{-1})	α	4.1510^{-6}	$0.55\ 10^{-6}$
Melting temperature (K)	*Tm*	1685	–

Table 2. Physical parameters of silicon and silicon dioxide [33].

Silicon is not found in nature in its pure form, but often bound to oxygen forming SiO_2. Silicon dioxide, also called silica, as a compound is highly abundant. Bound as silicates in the form of sand, quartz and natural crystals, silica makes up 75% of the earth crust [20]. The material used in the crucibles for the Czochralski process is made from fused silica. As mentioned in Section 2.2.2, this is a high purity, amorphous structure with a low thermal conductivity and high heat tolerance. The temperature dependent viscosity of fused silica is shown in Figure 14 [33].

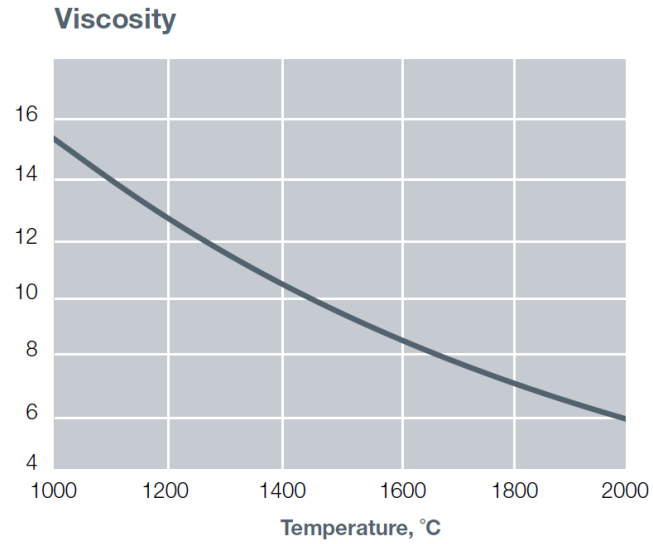

Figure 14. Viscosity in fused quartz [36].

The melting of silica point is not known. However, the softening point is known to be 1544 °C [22]. As seen in Figure 14, the viscosity will decrease as the temperature rises.

3.2 Investigation route

In order to investigate what parameters contribute to bubble growth and formation, a testing method was developed. Samples were obtained from three different positions in both a used and unused crucible. All samples were investigated by X-ray tomography to measure the bubble content, and the unused samples were heat-treated in three different ways. The results from the X-ray tomography before use, after use and after heat-treatment were compared to the results from the project thesis [3], where a different type of crucible, called crucible A, was tested in the same way. The crucible tested in this master thesis is called crucible B. To be able to compare the different crucible types, both crucible A and B were tested in HT4. The different heat-treatment methods are shown in Table 3.

Heat-treatment	HT1 (done earlier)	HT2	HT3	HT4
Temperature	1500(melt)->1420	1400	1400	1400
Holding time	30 h (1420)	24 h	4 h	4 h
Pressure	Ambient	Ambient	Vacuum	15 mbar
Atmosphere	Argon	Argon	Vacuum	Argon
Sample holder	Quartz	Quartz	Graphite	Graphite
Crucible	A	B	B	A+B

Table 3. Heat-treatment methods.

High magnification microscopy was done in parallel with the X-ray investigations. By using a scanning electron microscope (SEM), the sample surface was checked for small bubbles that can not be seen by using X-ray. As crucible B was being examined with X-ray and heat-treated, the SEM was only performed on samples from crucible A. This was part of the further work described in the project thesis [(3)].

The heat-treatment done in the work with this thesis was performed at a lower temperature than the heat-treatment from the project thesis. This is due to the high crack formation in the samples in the project thesis [(3)]. The temperature was chosen to be 1400 °C because, as seen in Section 3.1, the viscosity of the fused silica is not critically higher at 1400 °C than at 1500 °C. Even though the crucible undergoes higher temperatures during the crystal pulling process, it was decided more valuable to test the crucible at 1400 °C with different pressures and holding times. This would give more valuable and comparable results, rather than using a higher temperature and getting untrustworthy results.

3.3 Crystal pulling simulation

To obtain temperature data for the crucible during the crystal pulling process, a simulation model made by SINTEF was used. The model simulates the crystal pulling in 10 steps, showing the growth of the ingot body. This makes it possible to measure temperatures in different positions inside the crucible and see how the temperature at a specific point develops during the pulling process. Figure 15 shows what kind of data can that be extracted from the simulation.

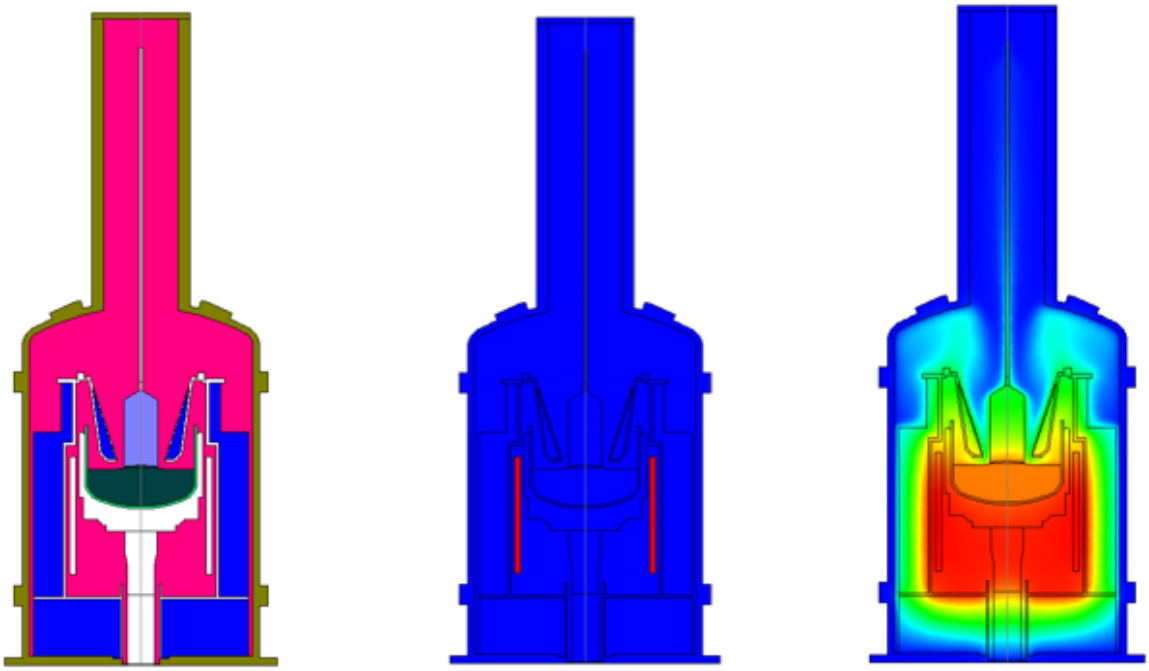

Figure 15. Left: Different materials. Middle: Heaters placement. Right: Heat distribution.

The model is built up by drawing the furnace geometry in 2D, and then adding to this the material properties of the different components in the furnace. The situation modelled in Figure 15 is pictured in the middle of crystal pulling, where the ingot can be seen being pulled out of the melt. The different colours in Figure 15 (left) represent different materials. The brown outer line is the furnace cover, and the pink inside is the gas filled areas. The blue represents the insulation, and the white represents the graphite crucible support and heaters. Lastly, the green represents crucible containing the grey molten silicon from which the light blue silicon crystal is been pulled out of. The thermal conductivity data are set to 4 W/m*K for the crucible, 64 W/m*K for the silicon melt and 0.03 W/m*K, which corresponds well to the data used in Section 2.3.5.

Figure 15 (middle) shows the placement of the heater elements in the furnace. It is worth noting that the crucible support moves upwards during the process, as the melt level decreases (i.e. as the ingot grows). It is desired that the melt level stays at the same height during the entire process, which means that the crucible support will have to move in the same speed upwards as the melt level drops inside the crucible. This means that the crucible moves up between the heaters, and that at the end of the run it is raised above the heater elements. The heat from the

heater elements will heat up the crucible support and the crucible itself in order to melt the silicon feedstock. Since the crucible is moving upwards, this means that the bottom corner of the crucible will be close to the heater through the entire process. This implies that the corner of the crucible will experience a higher temperature over a longer period than the top of the crucible, which is never in contact with the melt. A zoomed version of the heat-distribution shown in Figure 15 (right) is shown in Figure 16.

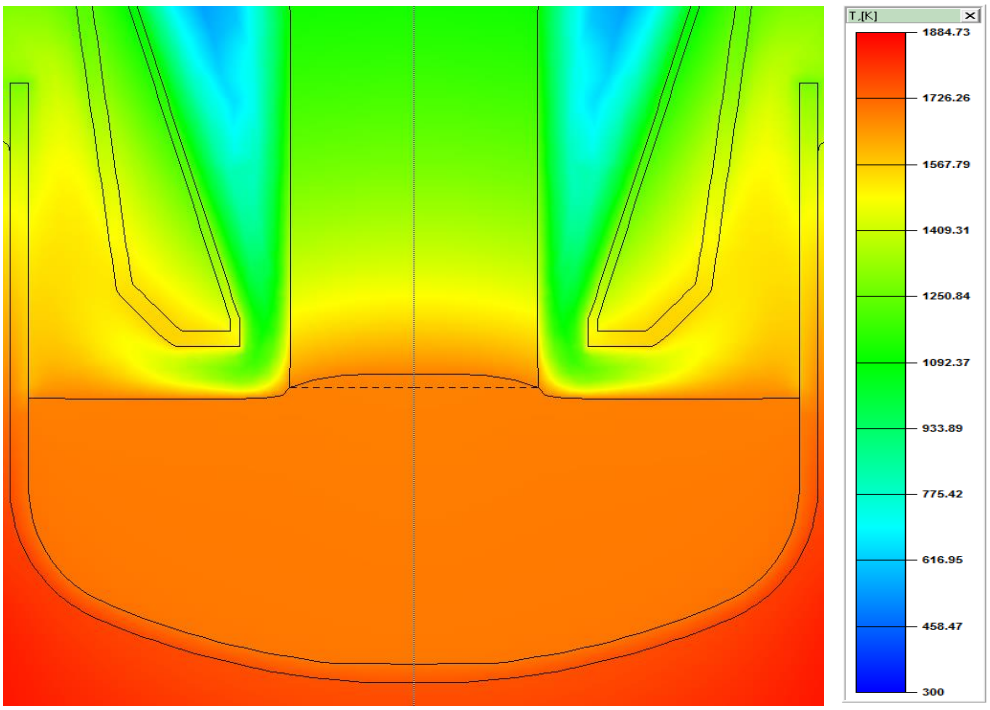

Figure 16. Temperature chart of the crucible with the silicon melt and the crystal pulled out of it.

When the silicon is melting, the heaters are at "full power", producing around 100 kW [8] of heat going through the crucible wall. Figure 15 (right) and Figure 16 shows the heat distribution during the crystal pulling, where it is clearly seen that there is a difference in temperature in the different crucible positions. In addition to being closer to the heaters, the bottom of the crucible is in contact with the silicon melt through the entire process, causing it to maintain a higher temperature. This means that the different parts of the crucible are exposed to different "heat-treatment" during the run. This should indicate that the bubble growth and movement will be much greater in the bottom of the crucible, since the glass will be softer here, and it is also the most critical place to have bubbles near the melt because the crucible is consumed over time when it is in contact with the reactive silicon melt.

3.4 Sample collecting

In order to investigate the bubble formation in the quartz crucibles, two quartz crucibles of type B were provided by NorSun's factory in Årdal. NorSun produces high quality n-type monocrystalline silicon wafers by the Czochralski method. The first crucible was used to produce a silicon ingot in Årdal and it was cut into different sections (as seen in Figure 17) in Trondheim. Three positions in the crucible were selected for this investigation. The samples from these positions were cut as 10x10x10 mm cubes. This was done with an Accutom high precision diamond blade saw by Struers.

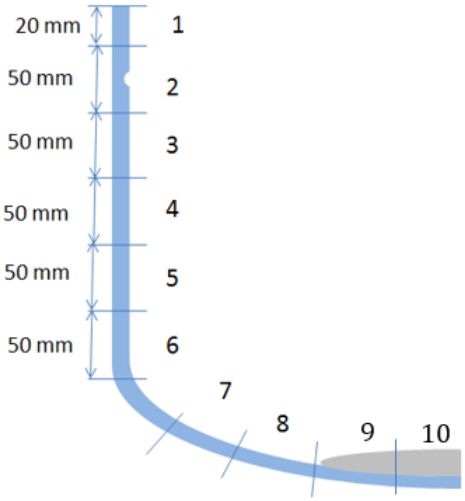

Figure 17. Cutting scheme of the quartz crucibles showing the different positions.

Later, the same process was repeated for the new and unused crucible. It was decided to focus on three positions, namely position 1, 7 and 10 (see Figure 17). This is to check if there is any variation through the crucibles profile, and whether the silicon melt will have any impact on the processes happening inside the crucible wall. The different samples from position 1 in crucible B investigated in this thesis are shown in Figure 18. All the samples have a dimension of 10x10x10 mm. The samples from crucible A can be seen in the project thesis [(3)].

Figure 18. Unused. Used. HT2. HT3. HT4.

The samples were cut by a diamond blade with a high precision control unit. The challenge was to fasten the samples properly when they were cut. The fastening mechanism was made from steel and was probably designed for straight samples. The small curvature on the quartz samples made them unstable when the cutting started. As a result, the samples were not completely square and equal in size, but equal enough to be compared. This will be further discussed in Section 3.9. A light microscope was used to show the bubble containing and bubble free layer in the crucible wall, as shown in Figure 19.

Figure 19. 50x magnification light microscopy image from wall of a used crucible, clearly showing the bubble free (BF) layer to the left and bubble containing (BC) layer to the right.

3.5 X-ray tomography (CT)

The X-ray apparatus used, is a Nikon XT H 225 ST. The fine cut samples are placed inside the chamber on a special holder. After the source is warmed up, a process called "Shading correction" is performed to compensate for the background in the radiation chamber. Then the sample holder is moved into position. Voltage, current and other parameters are loaded from an existing CT-profile. A procedure developed at SINTEF was followed. The sample is scanned with X-rays with a voltage of 130 kV and 100mA, while the sample is being rotated 360°. This process takes about two hours.

The machine acquires pictures for the entire volume and compiles them together to create a 3D-model of the sample. These can then be made into a picture "stack" consisting of around 1000 images on top of each other. Each of these pictures show the cross section of the sample with a depth of one voxel (i.e. a three dimensional pixel). This is limited by the resolution set when acquiring the pictures. One voxel in this case corresponds to approximately 9.1 µm. A program called CT Pro 3D helped reconstruct the pictures to give me the optimal contrast, beam-hardening correction, centre of rotation and crop to provide the best results. The picture stack was then reconstructed and ready for further analysis.

3.6 Image analysis

An image analysis program called ImageJ was recommended by SINTEF to analyse the pictures obtained from the X-ray tomography. First, the pictures showing just air or just the sample holder were removed from the stack. Then a colour threshold was chosen automatically by ImageJ which allows it to separate between bubbles and glass in the pictures of the sample. With the help of a SINTEF research scientist, ImageJ was used to measure the bubble and glass

area in each slice (screenshot from the analysis is shown in Figure 20), and then put it together in a spreadsheet.

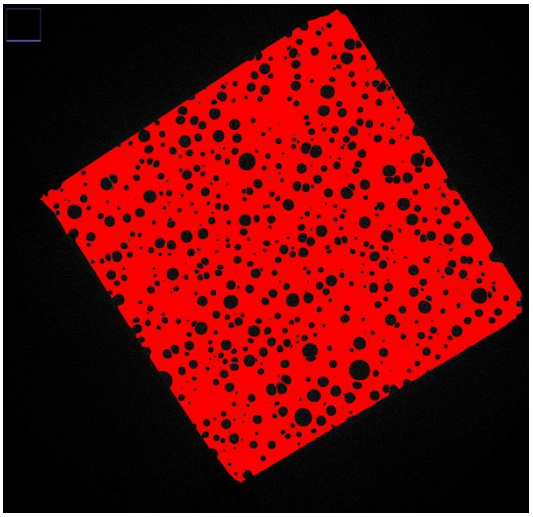

Figure 20. Screenshot from the image analysis process done in ImageJ.

The macro uses the colour difference to calculate the different areas, and then adds them together to compute, e.g., the total bubble area or the total glass volume. From this, the bubble/glass ratio, and also data for the position and distribution of the different bubbles, can be obtained. The image analysis has a measuring limit of 9 µm, as this corresponds to one voxel (three dimensional pixel). Any bubbles smaller than this can not be measured.

3.7 Heat treatment

3.7.1 Heat-treatment 1

In the project thesis, heat treatment was performed to simulate the melting and crystal pulling conditions of the Czochralski process. The samples were heated to 1500 °C and then kept at 1420 °C for 30 hours, as this reflects the long runtime in the crystal pulling process [(8)]. This caused massive crack formation in the samples, as the high temperatures induced cristobalite formation and growth on the sample surface. When the samples cooled down, the difference in thermal expansion between the cristobalite and silica glass and the phase transition in the

cristobalite creates high tension in the glass/crystal interface, which induced crack formation (Section 2.2.3). Also, the bubbles in the samples got deformed and the shape was distorted after heat-treatment. This made the results from the image analysis untrustworthy, as the program has difficulties separating bubbles from cracks.

3.7.2 Heat treatment 2

To cope with this problem, a new heat-treatment was done at a lower temperature, to reduce the amount of cristobalite formed. The cristobalite forms at 1470 °C (Section 2.2.3). The samples were put in a quartz sample container inside a tube furnace (see Figure 21) and argon was purged through the chamber to remove as much air as possible. The samples were then heated to 1400 °C at 200 °C/hour, and kept there for 24 hours. An argon flow with 10 psi of pressure was pumped continuously through the system, creating an inert atmosphere with ambient pressure. Even though this is less similar to the temperatures experienced during the crystal pulling, it was considered that the bubbles would grow significantly also at this temperature, as the viscosity of the silica is not critically higher. Since the formation of cristobalite is much lower at this temperature than at 1500 °C, the crack formation should be less detrimental for the end results. The furnace was operated by an engineer at NTNU.

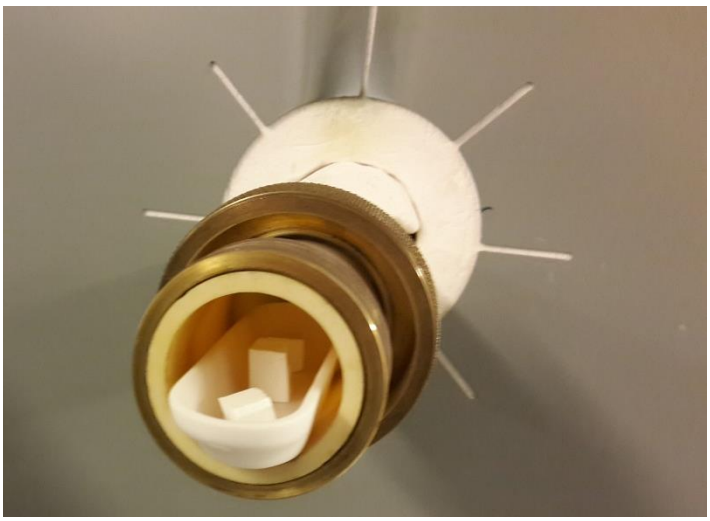

Figure 21. Samples in a container inside the furnace, after heat treatment.

3.7.3 Heat-treatment 3&4 in VGF furnace

To test what impact the pressure has on the bubble formation process, it was decided to use a VGF (Vertical Gradient Freeze) furnace to perform another heat-treatment of the crucible samples. This furnace is primarily used to crystallize multicrystalline silicon ingots used in solar cells, but its ability to rapidly heat samples in a low pressure argon atmosphere made it ideal for the purpose. The alternative was to use a full scale Czochralski puller to perform the heat-treatment, but this was decided to costly and complicated due to the large power and gas consumption.

Preparations

Before the experiment could start, a risk analysis and training in using the equipment had to be performed. Since there is high current, voltage and temperature present, it is important to be careful when using the equipment and knowing how to use it properly. After the required training was completed, the samples could be prepared. Samples from position 1, 7 and 10 were placed in a graphite crucible with a diameter of 10 cm, which was placed inside the furnace. Graphite felt was put around the crucible to insulate and make the heat in the furnace more uniform. The samples were placed with the BC layer facing the graphite, as would be the case during the crystal pulling process. The samples placed in the crucible, the open furnace and the vacuum pump are seen in Figure 22.

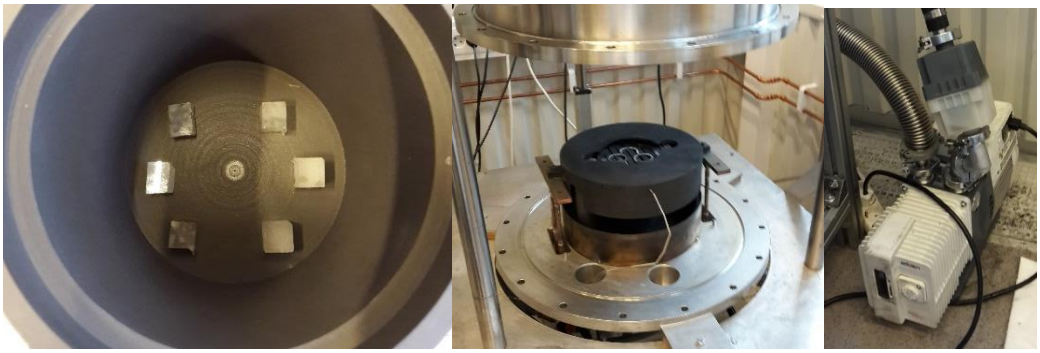

Figure 22. Left: Samples placed in the graphite crucible, middle: Open furnace, heater seen inside the graphite, right: The oil fume filter on top of the vacuum pump.

The vacuum pump was turned on the check the furnace chamber for leaks. After about 1 hour, the chamber pressure had reached 1.49E-1 mbar. This was higher than expected, but it could be explained by degassing from the samples and the insulation. The pump was then switched off to check how much air would leak into the chamber. In ten minutes, the pressure had reached 2.47E-1 mbar. This means that the pressure increased by 9.8E-2 mbar in 10 minutes. It was concluded that the furnace was adequately leak-proof. The pump exhaust emitted a white oil fume which was considered both a health risk and a contamination risk in the lab, and was solved by fitting a special oil vapour filter to the pump exhaust.

The heat-treatment was done in two parts: One in vacuum (HT3), and one in a low pressure argon atmosphere (HT4). A light microscope was used to compare the inner and outer surface of the samples before and after heat-treatment.

Heat-treatment 3: Vacuum

This heat-treatment was done in vacuum to check whether the pressure is deciding if the bubbles are allowed to grow when the glass is soft. If the pressure inside the bubble exceeds the pressure outside it, and the glass is soft, this could make the bubble grow as the gas inside expands. To test this, the chamber was closed and the pump started. When the pressure reached 5E-2 mbar, it was considered a vacuum, and the heater power was turned on. This was done manually at 15% power on the bottom heater and 7% power on the top heater. The pump was kept on during the entire experiment.

The crucible and insulation were placed around the bottom heater, making the power demand here larger to maintain the same temperature rise. When 1000 °C was achieved, the heaters were turned into automatic mode, and computer control was initiated. The furnace temperature was increased to 1400 °C at a rate of 1000 °C/h, and kept at this temperature for 4 hours. The temperature was then lowered to ambient temperature with a rate of 600 °C /hour. The cooling was done slightly slower to prevent the sample from cracking. As the temperature ramped up to 1400 °C, the pressure rose to 2.9E-1 mbar, but as the temperature stabilized at 1400 °C, the pressure normalized around 4.5E-2 mbar.

Heat-treatment 4: Argon

The last heat-treatment was performed in an atmosphere designed to resemble the actual conditions inside the crystal pulling chamber during the Czochralski process. The inlet flow of argon therefore had to be controlled together with the vacuum pump so that the pressure stabilized at the wanted level. As the pressure increased along with the temperature in the vacuum experiment, the pressure in this heat-treatment was chosen to be in the lower part of the pressure range used in Czochralski crystal pulling. This ranges from 15-50 mbar [8], so 15 mbar was chosen as a starting pressure. The pressure was first pumped down to 3.0E-1 mbar, and then the argon inlet was opened to stabilize the pressure at 15 mbar. This was done by having a steady argon flow of 100 l/min as seen in Figure 23.

Figure 23. Argon flow through the furnace.

The same temperature route was chosen in the furnace software as in the vacuum experiment. This demanded more power from the furnace, because the inlet argon cooled down the inside of the chamber. When the temperature reached 1400 °C, the pressure had only risen to 15.8 mbar, and stabilized there.

3.8 SEM

The X-ray tomography is a good tool to examine the sample in 3D, and to obtain data from all the bubbles in the sample. However, it has a measuring limitation of 9 µm, which can exclude some very important results. If there are smaller bubbles present in the glass that grows into visible bubbles, this might explain the difference in results from the unused and used crucible samples. To investigate this, a SEM (Scanning electron microscope) was used. A schematic figure of the SEM is seen in Figure 24.

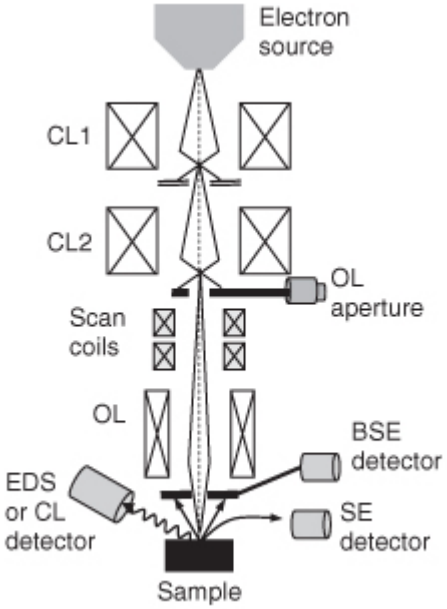

Figure 24. Schematic figure of the Scanning Electron Microscope [37].

The SEM operates by accelerating an electron beam towards the sample (see Figure 25). When the electron beam hits the sample, they have both elastic collisions with the sample atoms and inelastic collisions with the sample electrons. Some of the elastic collisions causes the electrons to backscatter out of the sample. This is a signal called Backscatter Electron (BSE) [37].

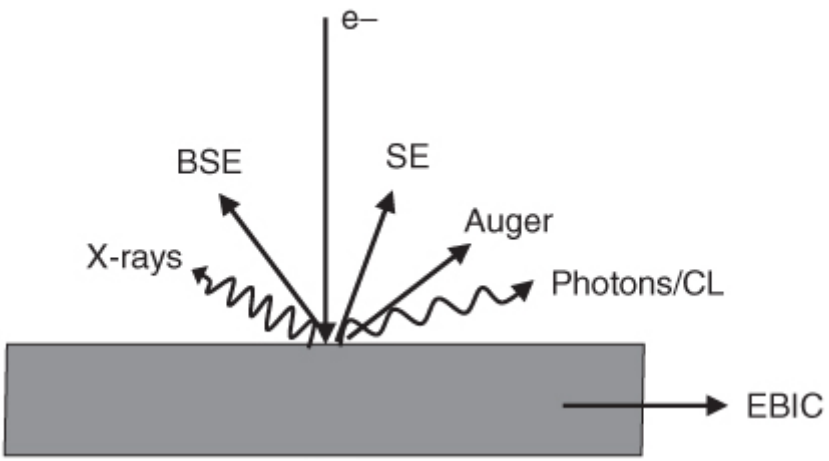

Figure 25. Ingoing electron beam and outgoing signals in the SEM [37].

The inelastic collisions with the sample electrons cause an energy loss of the incoming electrons, and many of them are absorbed in the sample. Because the total energy is preserved, this energy is transferred to the sample electrons, mostly as kinetic energy. The raised kinetic energy allows the sample electrons to move and further collide inelastically with other electrons. Most of the electrons are brought to rest eventually, but electrons that are excited close to the sample surface can escape into the vacuum in the microscope chamber. These electrons are called Secondary Electrons (SE). The SE signal is used to image the surface structure (topography) of the sample.

3.8.1 Sample preparation

The samples were embedded in epoxy and polished with 3 µm diamond paper. They were placed on the side, so that both the BC and BF layer was visible on the polished surface. The samples were then covered with aluminium foil, except for the area to be investigated, and a special carbon tape was used to connect the sample with the aluminium. This was to ensure there was electronic contact between the sample and the sample holder. The samples were then put in a heated cabinet for degassing before they were ready for the investigation. The uncoated sample was collected from crucible sample A1, and the coated sample was from crucible sample A7. The gold coated sample placed in the holder in the SEM can be seen in Figure 26.

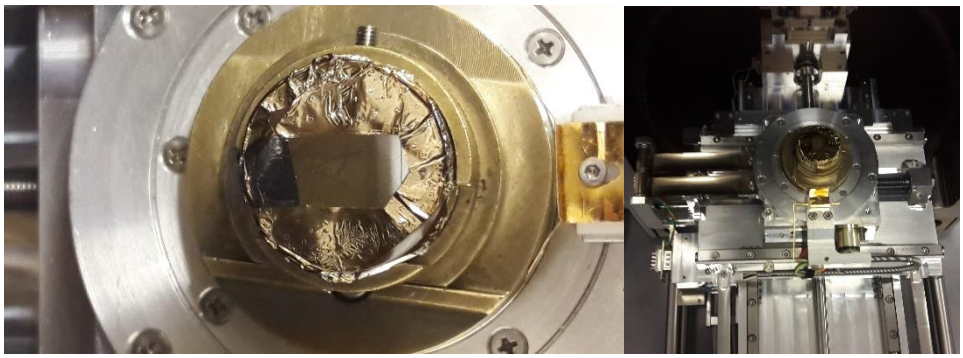

Figure 26. Gold coated sample placed in holder in SEM.

3.8.2 Charging problems

The SE signal was used to obtain images that show the bubbles on the surface of the quartz samples. The challenge with using this method on quartz, is that the quartz material is electronically non-conductive. This means that the electrons are tightly bound to the atoms, unlike metals where the electrons can move more freely and conduct electricity. This causes a problem called "Charging effect" [38]. The charging effect arises when the electrons are accumulated in the sample, and then "charged" out and into the receptor which creates a distorted and moving image on the SEM monitor. Metals and other electronically conducting materials do not have this problem, but it is a known problems for insulating materials. There are several methods that are designed to compensate for the problem; two will be mentioned in detail here. They are:

- Low voltage mode
- Conductive coating of the sample

Low voltage

To decrease the amount of electrons going into the sample, the voltage can be lowered. By doing this, the charging problem is reduced, because the sample is able to transport the electrons sufficiently fast. This means that the sample will not need to be coated with an electronically conductive material. The problem is that the intensity of the electron beam is much weaker when using e.g. 5kV instead of the normal 20 kV. This makes it harder to obtain good contrast in the images, but gives much better resolution than e.g. having higher voltage and using a low vacuum [39].

Coating

To increase the sample's ability to conduct electricity, it can be coated with an electrically conducting material. This is usually done with gold or carbon, and in such a thin layer that it does not change the original topography of the sample. Usually this is between 2 and 20 nm in thickness [(40)]. Previous investigations have been done with a gold coating, and this was also tried in this thesis [(41)]. To see how this worked, one sample was investigated without any coating, and another with gold coating. The results are discussed later.

3.8.3 Energy-Dispersive X-ray Spectroscopy (EDS)

When X-ray photons enter the sample, the sample electrons are excited and can move through the different energy levels of the atom. When they settle back to the normal energy level, the excess energy is released out of the sample as a photon. This photon's energy corresponds to the energy difference between the different states in the respective atom. This means that the photon reveals what kind of atom is present. In this way, the different compounds and compositions in the sample can be analysed [(42)]. The results are presented in X-ray spectres, which are given later in this thesis. Only the coated samples were investigated by this method, as the higher conductivity gives better results.

3.9 Measuring accuracy

The measuring done on the bubbles using the X-ray tomography has a detection limit of 9 µm. The method gives a high precision measurement of the bubbles in the samples that are above this limit. However, there are several other factors that play a role in determining how accurate the results from the experiments are. These will be discussed in this section, in addition to the normalization done to compensate for the minor volume difference in the samples.

3.9.1 Crack formation

During the heat-treatments, some of the vitreous silica is transformed into cristobalite, as presented in Section 2.2.3. The phase transformation in the cristobalite and the difference in thermal expansion causes the cristobalite to crack during cooldown. In the samples with a thick cristobalite layer, this means that the sample will be filled by cracks, shown in Figure 27. The crack formation was dominant in the samples after HT1 [3], but there were also several cracks in samples after HT2.

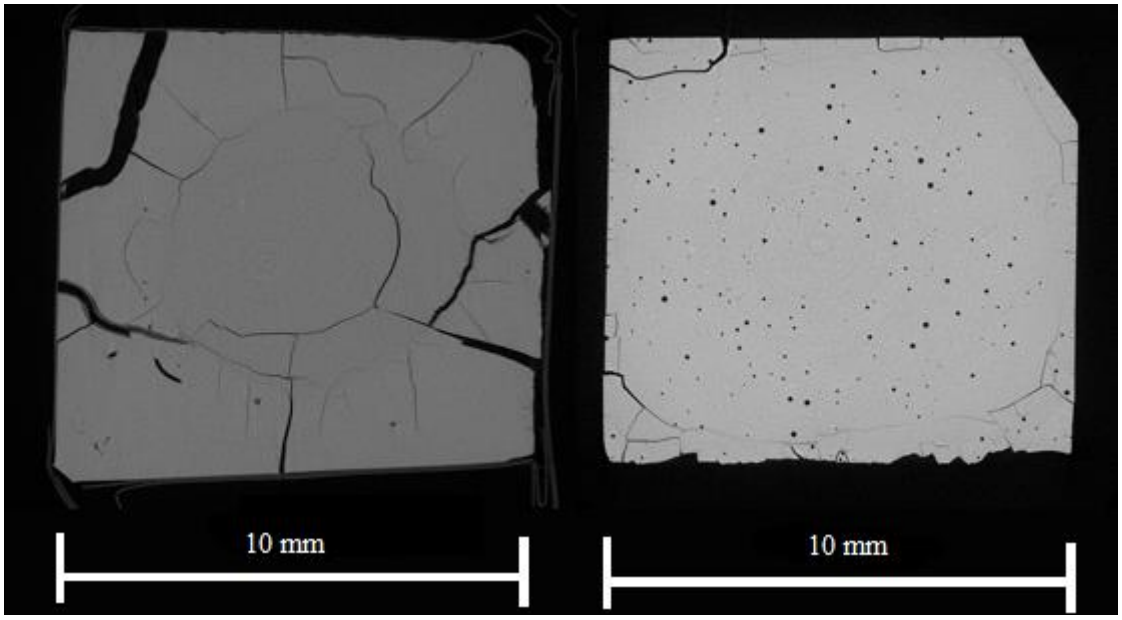

Figure 27. Crack formation in samples from position 1 after HT1 (left) and HT2 (right).

The cracks in the samples are detrimental for results of the image analysis. As mentioned earlier, it uses a colour threshold algorithm to detect the bubbles in each image and summarizes them for the entire volume. The cracks are in many cases counted as bubbles because they have the same colour in the image, as seen in Figure 27. It is therefore not possible to completely trust the numeric data from the analysis of crack-filled samples. As mentioned earlier, the heat-treatment method was optimized to prevent cracks from forming, and the samples from HT3 and HT4 had no cracks. This means that the results from HT3 and HT4 were more trustworthy than the results from HT1 and HT2. This was taken into account when the data from the testing was analysed.

3.9.2 Sample preparation

The samples were cut from a used and an unused crucible, with help from a SINTEF-engineer. The crucibles were initially cut into pieces of 5x5 cm, according to the cutting plan showed earlier, in 3.4. For the samples from position 1, 7 and 10, samples of 1x1 cm were cut out to be examined. The possible measuring error can occur if the samples are not completely cubic, as either the BF or BC layer then is more represented in the sample. This would explain if there are small differences between samples from the same position in the same crucible.

To calculate the sample shape deviation that can result from the cutting, an example is made here. The diamond blade used to cut the samples is ~1 mm thick. It is therefore assumed that the samples can have a 1 mm deviation in both the cut surfaces. In worst case, this would cause the sample to have a trapeze-like profile. This is shown in Figure 28. It is assumed in this example that the BC and BF layers originally are distributed in 50% of the sample each. This means that the uneven cutting could cause the BF/BC relation in the sample to be changed from 50/50 to 47/53, which gives an 11% difference in the bubble free content in the sample.

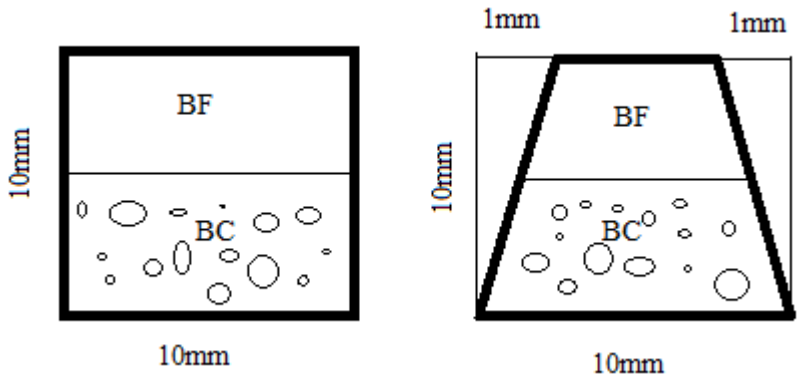

Figure 28. Exaggerated example of cutting deviation.

It is assumed that the bubble distribution in the crucible is homogenous in the tangential direction, which means that samples obtained from the same position right next to each other will give the same result in the bubble analysis. Based on this, the samples used in the different heat-treatments could be compared directly, as they were cut out right next to each other.

3.9.3 Bubble volume calculation

The calculation of the bubble volume in the samples is done by interpreting the image analysis data in Excel. The image analysis uses the colour threshold to calculate the total area of "voids" in each slice from the 3D-model obtained from the X-ray tomography. To calculate the bubble volume, Excel uses the slice thickness, which corresponds to one voxel (Section 3.6), and multiplies it with the void area in each of the slices. This gives a correct total volume of bubbles in the sample, but the size distribution will not be completely accurate. Because the spheres are counted as discs with different diameters multiplied by the slice thickness, the diameter of the bubbles will be counted as a sinus-wave containing the different diameters in the entire sphere. This means that the middle sized bubbles are represented more in the statistics than the big bubbles, since the big bubbles also contain smaller diameter discs. The total bubble volume is still correct.

The excel template compensates for the errors by using a logarithmic x-axis. Since the x-axis is logarithmic and crosses several decades, the sinus curve is "pushed flat" sideways. This means that the error in the bubble size distribution is small. Still, the tool works best to compare samples directly, rather than using the bubble distribution data from each sample separately.

3.9.4 Volume normalization

Because the wall thickness was different in the three different positions, the volume of the samples varied accordingly. To compare the results easily, the data from the image analysis was therefore normalized. This was done by dividing the volume of bubbles in the sample by the sample volume. In this manner, the results could easily be compared between different samples within the same plot. It also meant that small variations in the sample volume does not affect the ability to compare samples. All the comparisons of bubble volumes and distributions in the results were normalized for this purpose.

3.9.5 EDS chemical analysis

The chemical analysis done by EDS has a 2% uncertainty in the measurements. This means that low abundancy substances in the substrate may not be detected. It is therefore possible that there are substances present in the sample that is not detected. To improve the accuracy of the chemical analysis, WDS (Wavelength Dispersive Spectrometry) could be used. The WDS technique has a detection limit of 0.1 wt%, i.e. ca. 1000 ppm. This will be suggested in the future work.

3.9.6 Reproducibility

The results from the X-ray tomography and image analysis could easily be reproduced by using the same X-ray profile and image analysis macro (3.5-3.6). The image analysis macro can be found in Chapter 9: Appendix. The factor that could change the results if the experiments were done again is the sample cutting. It is estimated that, in the worst case, the cutting can cause an 11% error in the distribution between BF and BC layer in the sample. This should, however, be avoidable by using proper fastening of the sample and a cutting device with accurate measuring.

4 RESULTS

4.1 Temperature simulation in the crucible

During silicon meltdown and stabilization, the temperature in the melt is higher than during the crystal pulling [8]. As the melt is consumed, the crucible is moved upwards to keep the melt level consistent during the entire process. The heat going from the thermal elements have to go through the quartz crucible to reach the silicon, which means that the crucible experiences higher temperatures than the melt itself. Knowing this, an estimation of the crucible temperature variation during the whole Cz process is a necessary first step to better understand the evolution of the material properties as well as the formation of bubbles in the crucible wall.

4.1.1 Temperature differences in the crucible

Using the CGSim simulation, temperature distribution graphs and quantitative data are obtained for the crucible during the crystal pulling. The simulation only covers the body growth of the ingot, not the meltdown or the cooling stages. However it gives a good indication on the differences in temperature that the crucible experiences during the crystal pulling. The results give a good insight into what part of the crucibles experience higher temperatures, and how long they are exposed. This is shown in Figure 29.

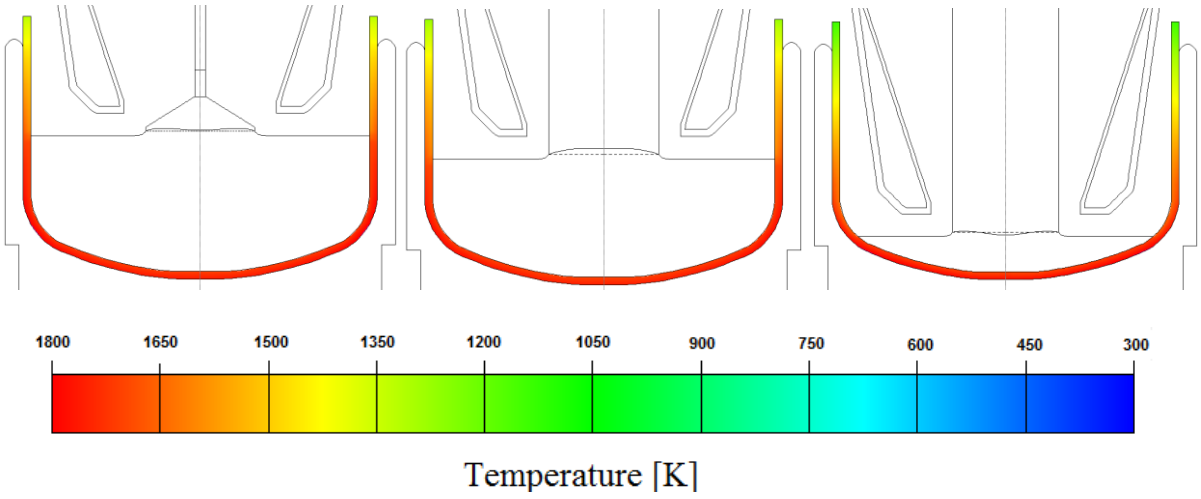

Figure 29. The heat distribution in the crucible at start (left), middle (middle) and end (right) of crystal pulling.

As seen in Figure 29, the temperature of the different positions in the crucible changes during the pulling process. The temperature in the bottom part of the crucible maintains a temperature between 1700K and 1800K, which is equivalent to 1427-1527 °C. The top part of the crucible experiences a lower temperature as the melt level decreases. To show the variation between the different positions of the crucible, a temperature gradient between position 1 and 7 was obtained (See Figure 17 in Section 3.4 for the location of position 1 and 7). The results can be seen in Figure 30 in case of the middle situation in Figure 29.

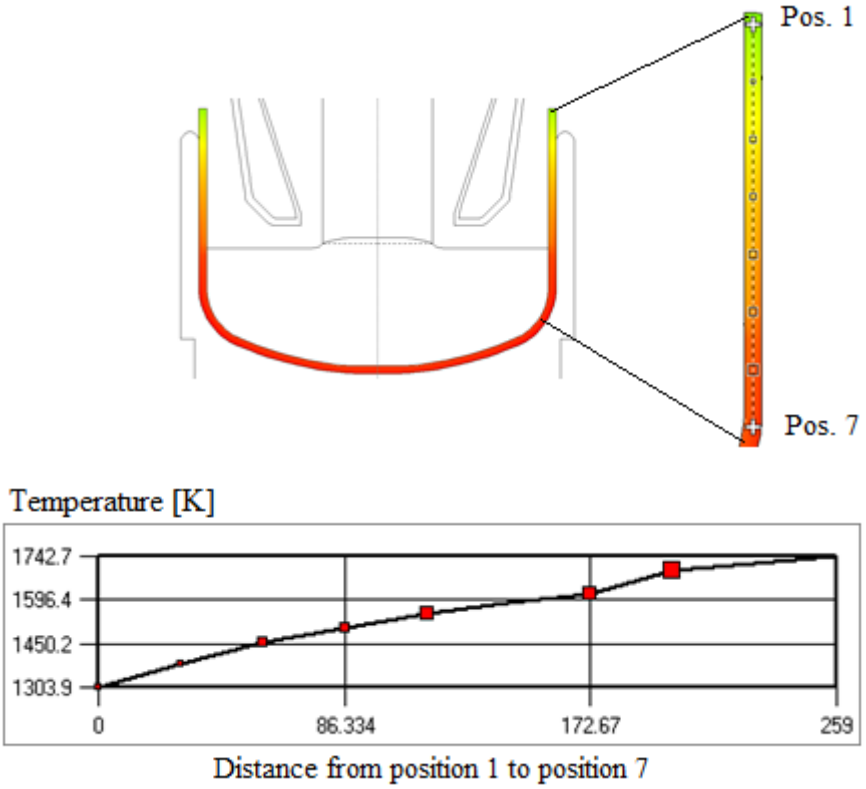

Figure 30. Top: Illustration of the position of the temperature gradient simulation line inside the crucible wall. Bottom: Temperature gradient in the crucible wall, from position 1 to position 7.

As seen from the graph in Figure 30, the temperature varies by almost 340 °C from position 1 to position 7. In position 1 the temperature is 1031 °C, while in position 7 it is 1470 °C. This important difference can have an impact on the speed and quantity of the bubble formation and growth. In the rest of the crucible, the results reveal that the temperature is almost constant from position 7 to the bottom (as seen in Figure 29), and only decreases down to 1450 °C in position 10.

4.1.2 Temperature gradient through the crucible wall

The variation of the temperature through the crucible wall was also simulated by using a "line probe" technique, which retrieves data from points along a defined line. The results are shown in Figure 31, 32 and 33. The temperatures and graphs are retrieved from the middle situation in Figure 29, which corresponds to the process during the ingot body growth. The distance between the measured points at position 1 (Figure 31) is 10.8 mm, and the thickness of the wall

is 11 mm. The points are taken on the inside of the crucible, and not in the boundary layer between it and the graphite support.

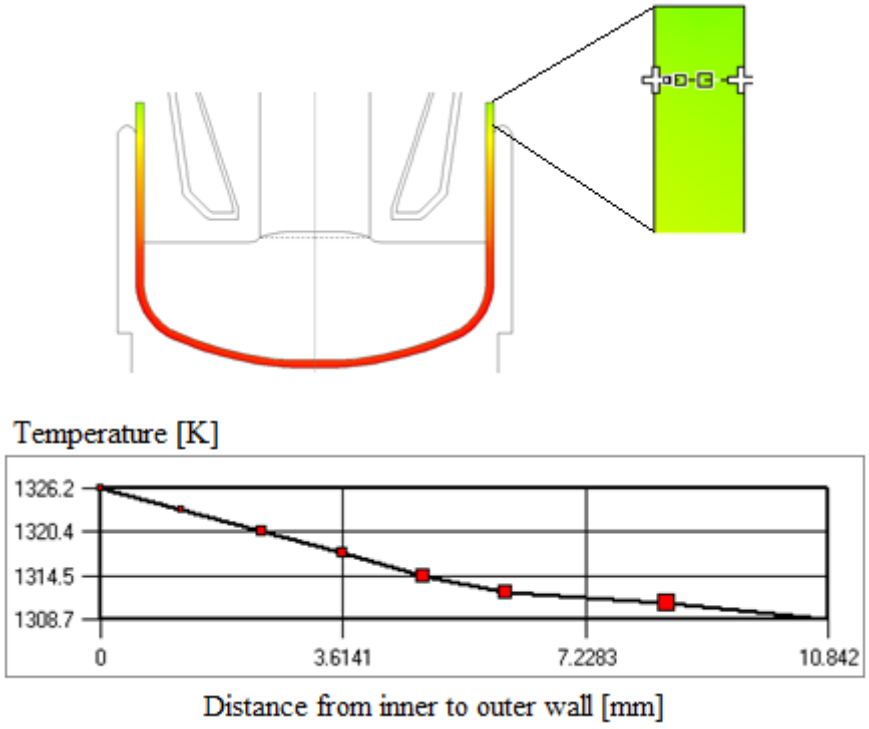

Figure 31. Top: Illustration of the position of the temperature gradient simulation line inside the crucible wall. Bottom: Temperature gradient through the top of the crucible wall (position 1).

The results in Figure 31 show that the temperature is almost 20 °C higher in the inside part of the crucible wall compared to the outside at this position. The temperature obtained close to the outside wall is 1036 °C, and 1053 °C close to the inside wall.

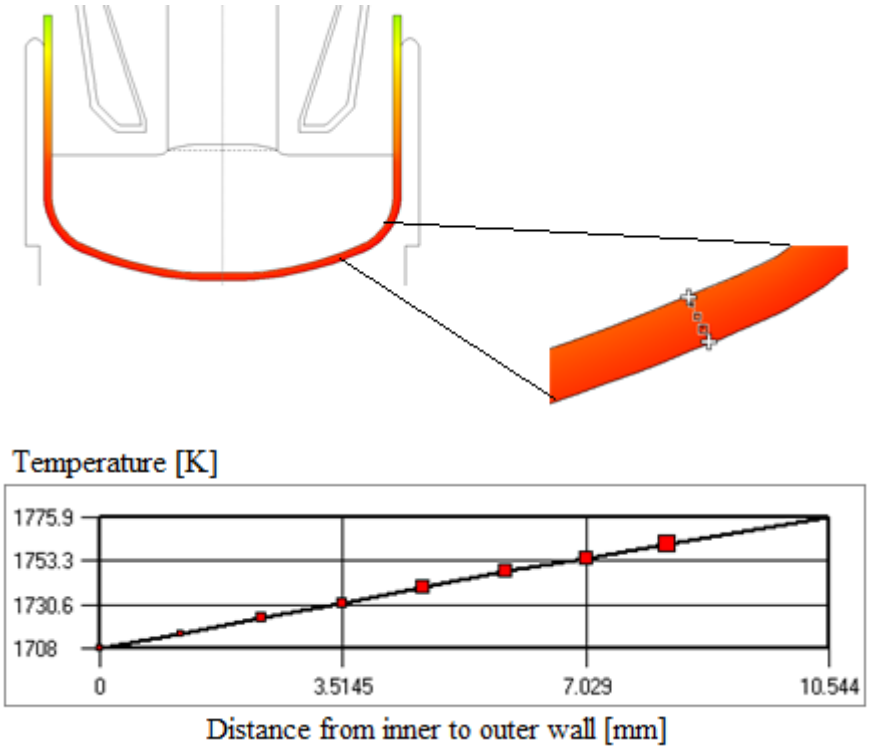

Figure 32. Top: Illustration of the position of the temperature gradient simulation line inside the crucible wall. Bottom: Temperature gradient through the middle of the crucible wall (position 7).

A similar simulation was performed at position 7 and 10 (see results in Figure 32 and 33 respectively). For position 7, the outer part of the wall has the highest temperature. The temperature difference between the inner and outer part of the crucible wall is almost 70 °C, the outside measuring 1503 °C and the inside measuring 1435 °C. The temperature in the outer wall is almost 500 °C higher than in position 1.

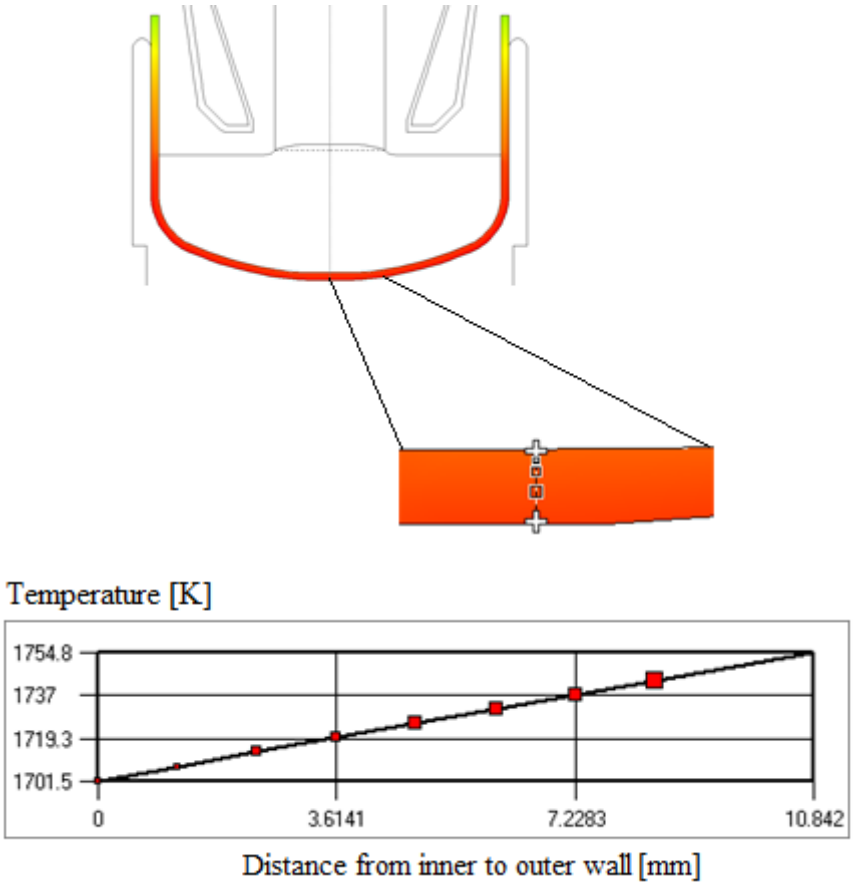

Figure 33. Top: Illustration of the position of the temperature gradient simulation line inside the crucible wall. Bottom: Temperature gradient through the bottom of the crucible wall (position 10).

The temperatures in position 10 are a little lower than in position 7, but in the same range. The inner part has the lowest temperature of 1428 °C, and the outer part has a temperature of 1482 °C, as seen from Figure 33. This means there is a difference of 54 °C between the outer and inner edge of the crucible wall.

4.2 Improvement of heat-treatment results

4.2.1 Heat treatment 1

The 1 cm^3 samples cut from crucible A in position 1, 7 and 10 were heat-treated with the HT1 process described in Table 3 with a holding time of 30 h at 1420 °C. The X-ray tomography observations of the sample before and after the heat-treatment are shown in Figure 34 along with an X-ray tomography image of a crucible from the same supplier after being used in the pulling process. This work has been performed in the previous project [3], however to compare it with the new results, the main findings are presented below.

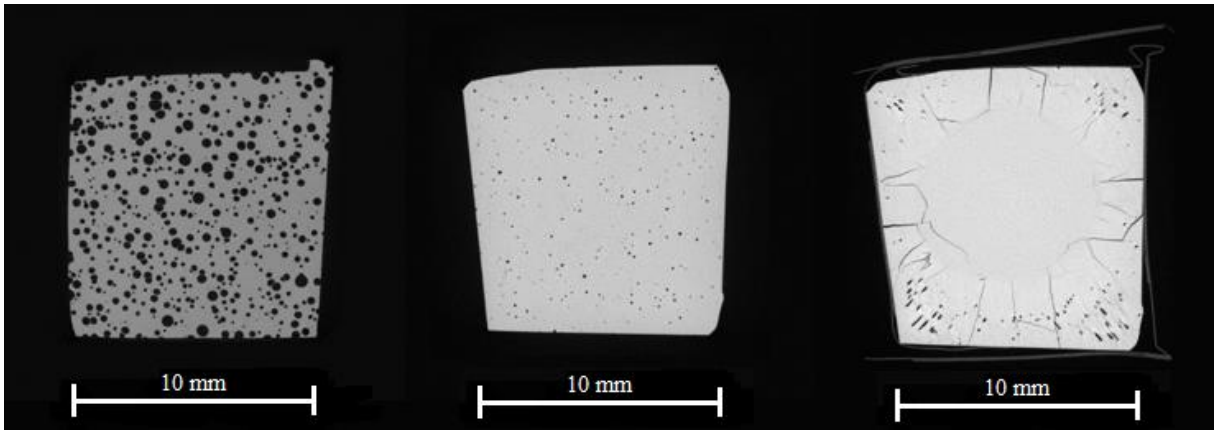

Figure 34. X-ray tomography images of crucible A at position 1. Left: Used in the Cz process, middle: Unused and right: Heat-treated.

The heat-treatment performed on crucible A (right in Figure 34) induced cracks in the samples with the formation of a thick cristobalite layer on the outside. The cracks are formed when the cristobalite undergoes a phase transition and shrinks with a different rate of contraction than the glass (2.2.3). It was also experienced that the bubbles seemed to be pushed away from the centre of the sample, and out towards the edges. The bubbles also seemed distorted in shape and looked very different to the bubbles in the unused or the used sample.

4.2.2 Heat treatment 2

The 1 cm^3 samples cut from crucible B were heat-treated with the HT2 process described in Table 3 with a holding time of 24 h at 1400 °C. The X-ray tomography observations of the sample before and after the heat-treatment are shown in Figure 35 along with an X-ray tomography image of a crucible from the same supplier after being used in the pulling process. The HT2 process used a lower temperature and slightly lower holding time than the HT1 process to reduce the crack formation in the samples.

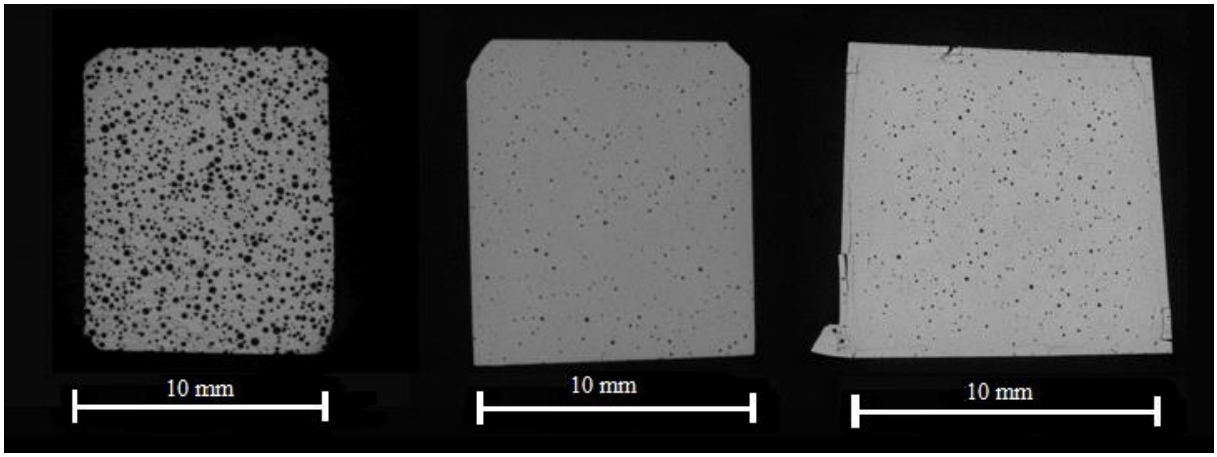

Figure 35. X-ray tomography images of crucible B at position 1. Right: Used in the Cz process, middle: Unused and right: Heat-treated.

Heat-treatment 2 produced less cristobalite and fewer cracks. Indeed, as seen in Figure 35, there are only a few small cracks on the edges, but the inside seems intact. It is here seen that the bubbles are very similar to the ones in the unused sample. This is supported by the calculations, shown in Section 4.3.

4.2.3 Comparing crack formation in heat-treated samples

Because the silicon is extremely reactive in the molten form, the crystal pulling process is done under inert conditions at a low pressure. Impact of this lower pressure was studied by comparing three heat-treatment methods performed under various atmosphere, HT2, HT3 and HT4 (see Figure 36). All of these methods were done at 1400 °C, but the holding time was reduced to 4

h in HT3 and HT4 and the pressure was lowered to vacuum in HT3 and 15 mbar in HT4. In addition to the previous heat-treatment (HT2), HT3 and HT4 were performed on crucible B on samples cut from position 1, 7, and 10.

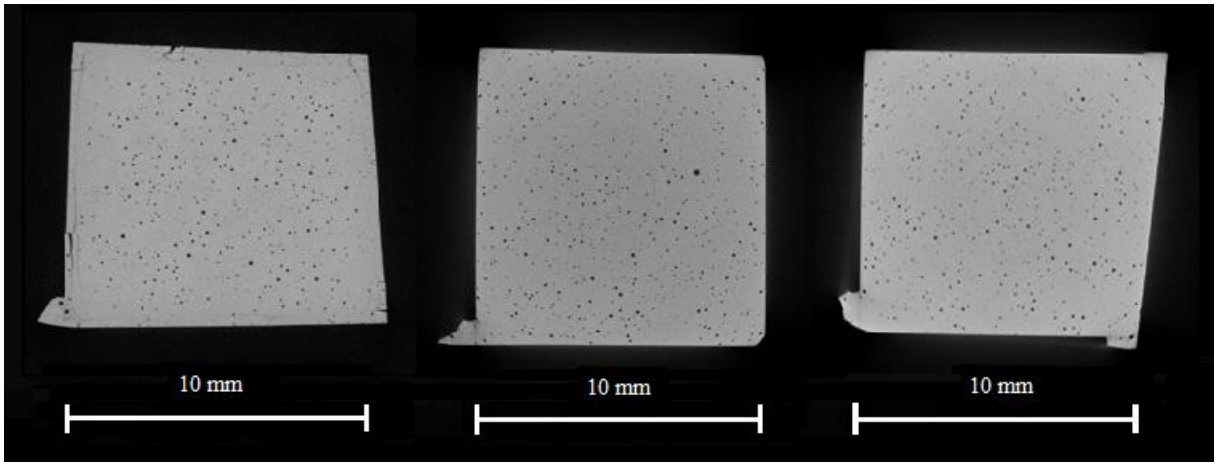

Figure 36. Comparing the X-ray tomography image of various heat-treated samples. Left: HT2, middle: HT3 and right: HT4.

Figure 36 shows the images of the three different heat-treated samples. It is clearly visible that the HT2-sample has some cracks on the surface, while the two other samples does not have it. Except from this, no further differences could be seen from the X-ray images.

4.2.4 Cristobalite formation after heat-treatment

A light microscope with 4x magnification was used to capture the cristobalite formation before and after the heat-treatments performed on the samples cut from crucible B. The micrographs are shown in Figure 37, 38, 39 and 40 for the unused, after HT2, after HT3 and after HT4 samples respectively.

Figure 37 presents the inner and outer surface of the unused sample from position 1 in crucible B. The outside wall is much rougher than the inner wall, and the inner wall seems very uniform with just minor scratches, which most likely comes from the sample handling after cutting.

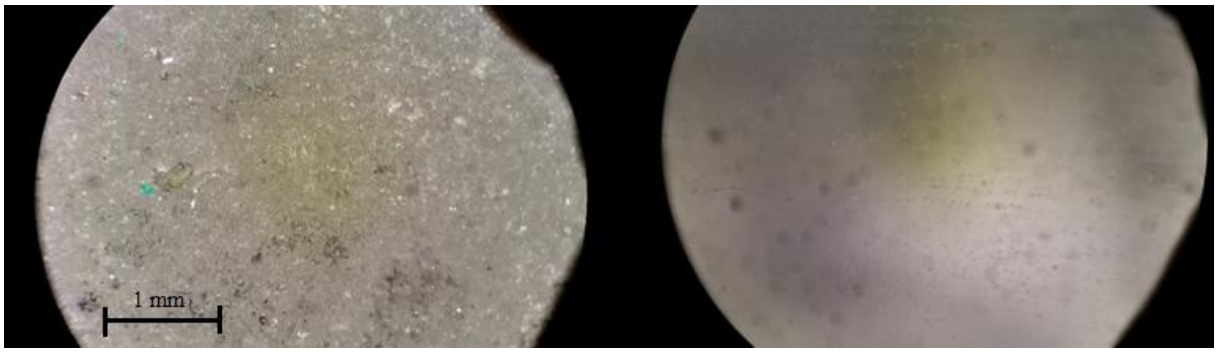

Figure 37. Light micrographs of the sample of position 1 from the unused crucible. Left: The outer wall, and right: The inner wall.

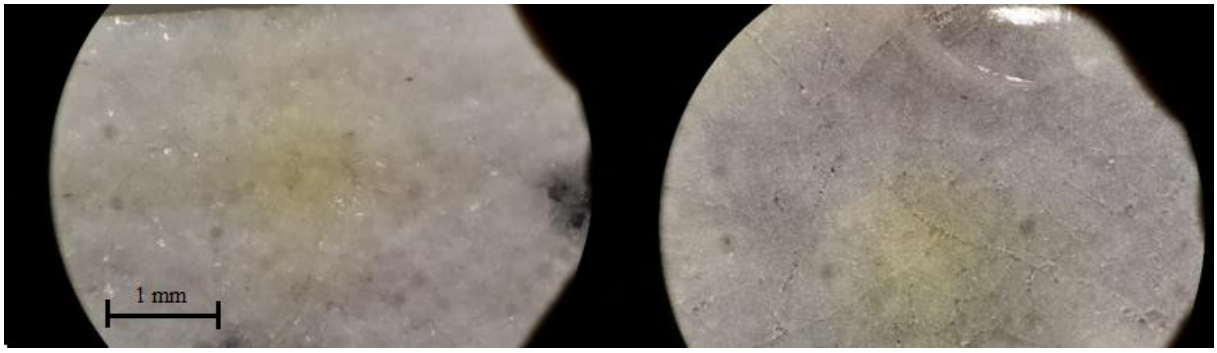

Figure 38. Light micrographs of the sample surface of position 1 after HT2. Left: The outer wall, and right: The inner wall.

After HT2, there was a lot of cristobalite formed on the sample surface. It can be seen as a white opaque layer in Figure 38. In the top corner of the inner wall, a piece of cristobalite has chipped off. The cracks on the surface are easily visible in the Figure 38 (right).

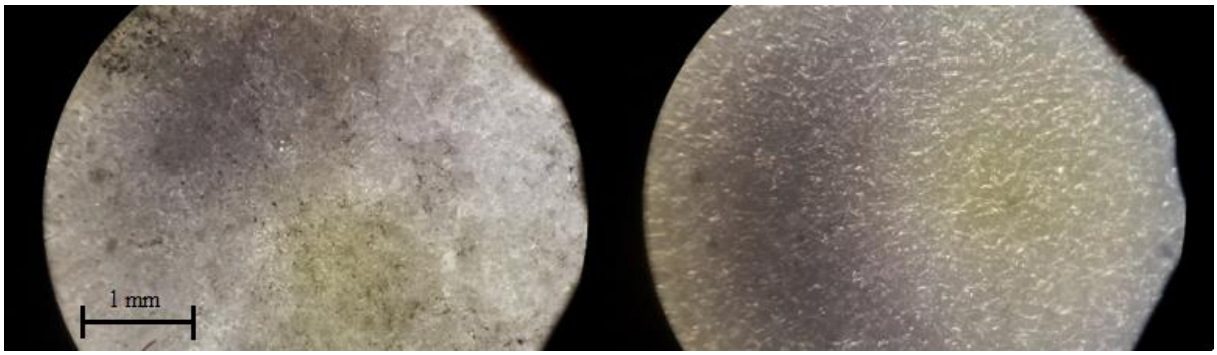

Figure 39. Light micrographs of the sample surface of position 1 after HT3. Left: The outer wall, and right: The inner wall.

In Figure 39, it is seen that in the case of HT3 the outer part is rough, while the inner wall seems very uniform with a thin crystalline layer outside the amorphous silica.

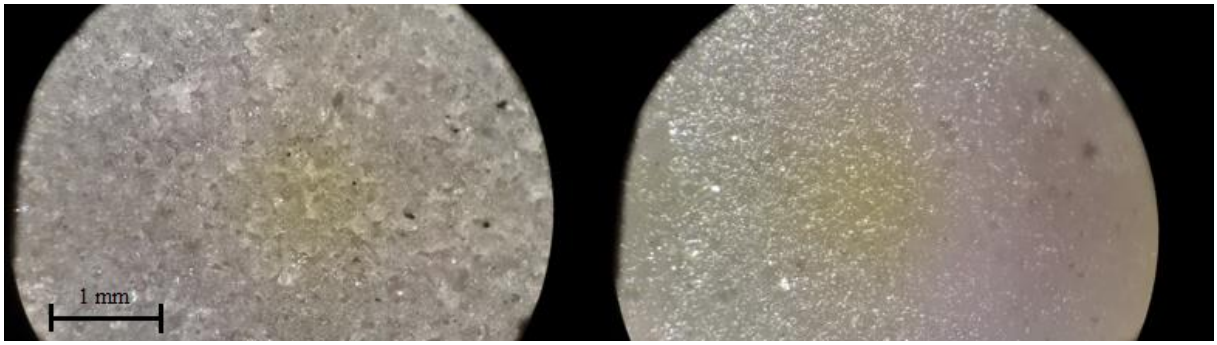

Figure 40. Light microscopy image of the sample surface of position 1 after HT4. Left: The outer wall, right: The inner wall.

Finally, Figure 40 shows that surface of the sample after HT4. The surface looks similar to the HT3-samples, but the inner wall is less homogenous in the surface pattern. As with the HT3-samples, the very thin cristobalite layer is visible on the inner wall.

4.3 Bubble content in unused, used and heat-treated samples

As in the project thesis [3], images from the CT were gathered in image stacks and analysed using a macro in ImageJ. This produced raw data, which could be interpreted by an Excel program to make graphs showing the bubble size distribution, and where the bubbles are situated in the samples. The data from the different heat-treatments done on the samples from position 1, 7 and 10 in crucible B are compared to see how it affected the bubbles in the crucible wall. Later, the results will be compared to similar tests done on the second crucible type (crucible A) during the project thesis [3], to see if there are any significant/obvious differences between the different manufacturers.

As discussed in Section 3.9, the results were normalized by dividing the bubble volume by the sample volume. In this manner, the figures will show the bubble volume relative to the sample volume, which will give a clear indication on the amount of bubbles present in the samples. It will also allow us to compare them, as the graphs will show the bubble content of all the samples in the same reference system. For simplification, the sample cut from e.g. crucible A at position 1 will be noted A1 in the graphs legend.

4.3.1 Comparison of bubble size distribution

The characterization performed on crucible B is presented below. Three positions in the crucible will be compared; position 1, position 7 and position 10.

Position 1

Figure 41 shows the bubble size distribution at position 1, and Figure 42 shows a version of Figure 41 with zoom on the unused and heat-treated samples.

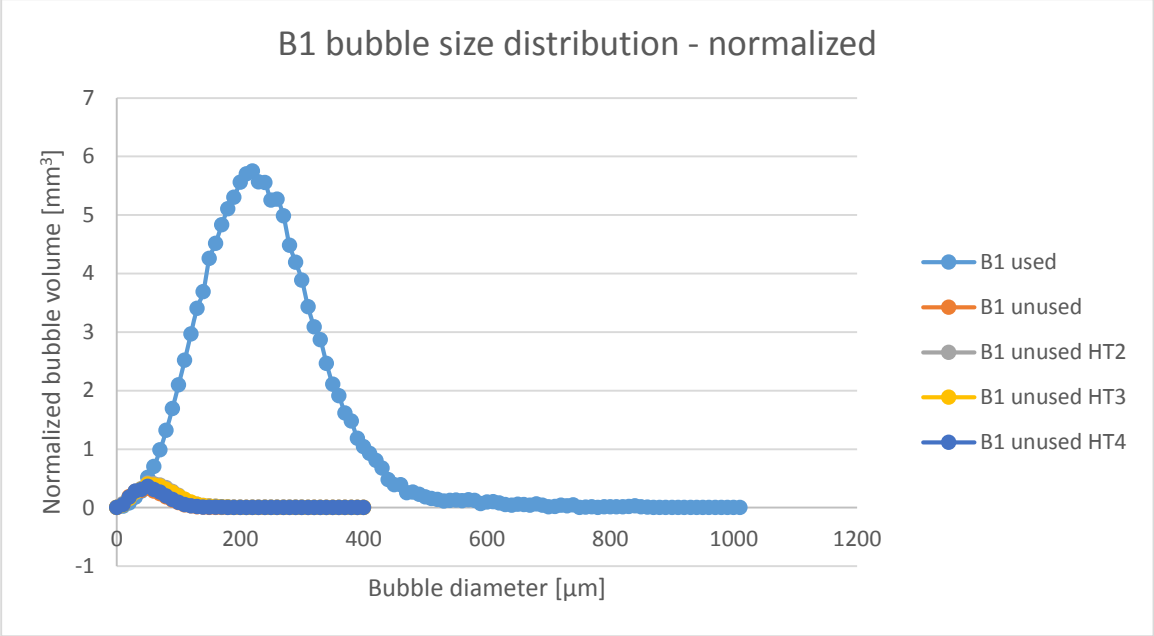

Figure 41. Comparison of the bubble size distribution in crucible B at position 1.

The analysis of the X-ray data concludes that the used crucible sample has a total bubble content of 12.84%, with much larger bubbles than any of the other samples, as seen in Figure 41. The unused crucible has the lowest bubble content, with 0.22%. The heat-treated samples have slightly higher bubble contents (see Figure 42), where the HT2, HT3 and HT4 have 0.33%, 0.31% and 0.23% respectively. The used crucible have bubbles with diameter mostly around 200 µm, while the unused and heat-treated samples have most bubbles with diameter of approximately 50 µm. There are bubbles present in the used sample up to 600 µm, while in the unused they are not larger than 200 µm.

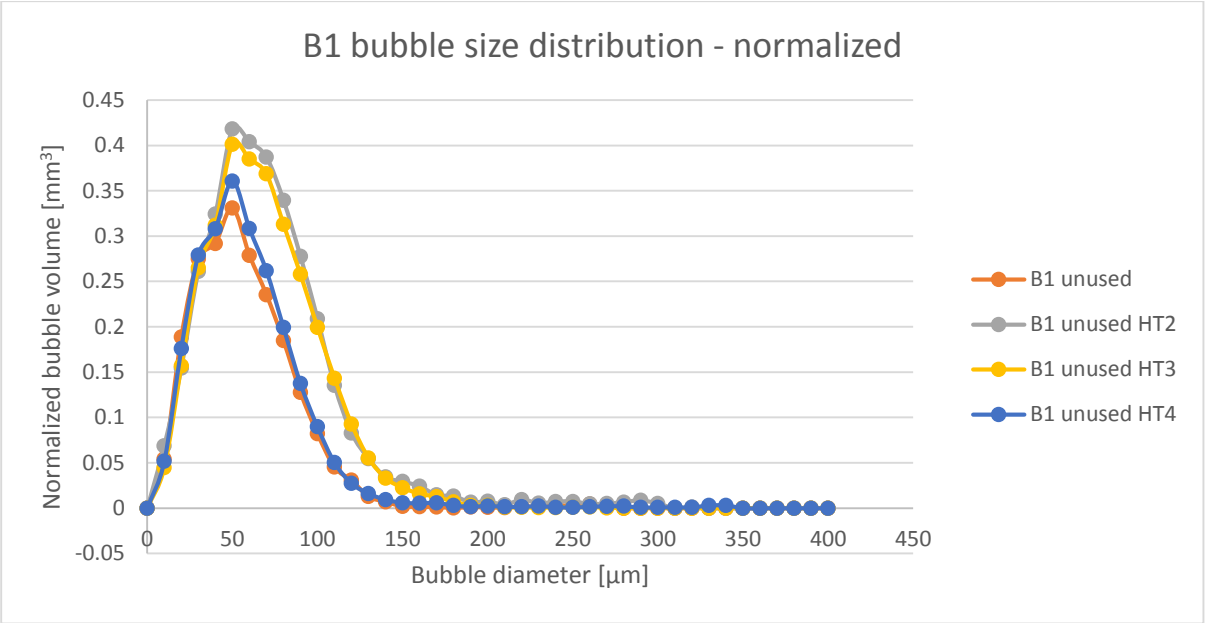

Figure 42. Comparison of the bubble size distribution at position 1, zoom on the unused and heat-treated samples.

In Figure 42, the bubbles in all the samples have the same peak diameter, but the HT2 and HT3 samples have a higher volume of bubbles with diameter over 50 µm than the two other samples. Moreover, HT2 has the highest total bubble content. Comparing before and after heat-treatment, the bubble content has increased from 0.22% to 0.23% with the HT4.

Position 7

Figure 43 shows that the bubble content is lower in position 7 than in position 1. Figure 44 also presents the bubble size distribution, but focuses on the unused and heat-treated samples from position 7.

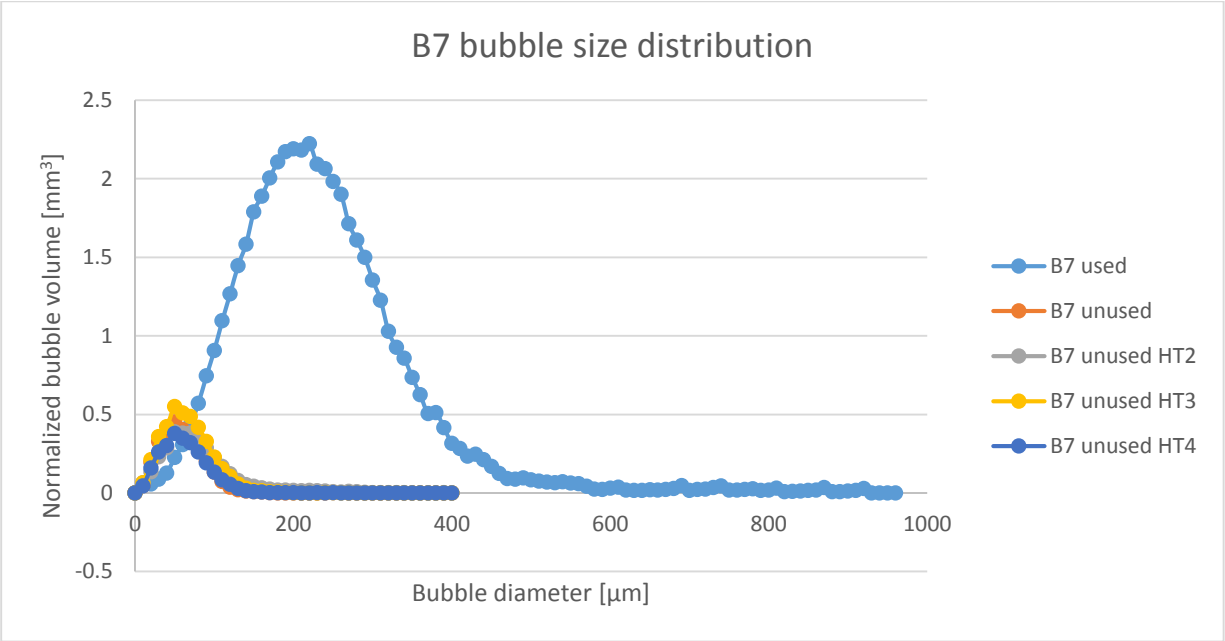

Figure 43. Comparison of the bubble size distribution in crucible B at position 7.

In the case of position 7, the bubble content measured in the used crucible sample is 4.97% in this position. The unused sample has a bubble content of 0.29%. HT2, HT3 and HT4 have 0.34%, 0.40% and 0.26% respectively. Most of the bubbles in the used sample have a diameter around 200 µm, while the other samples have bubbles around 50 µm in diameter. The bubbles in the unused and heat-treated samples are not larger than 200 µm in diameter, while in the used sample there are bubbles present up to 600 µm in diameter.

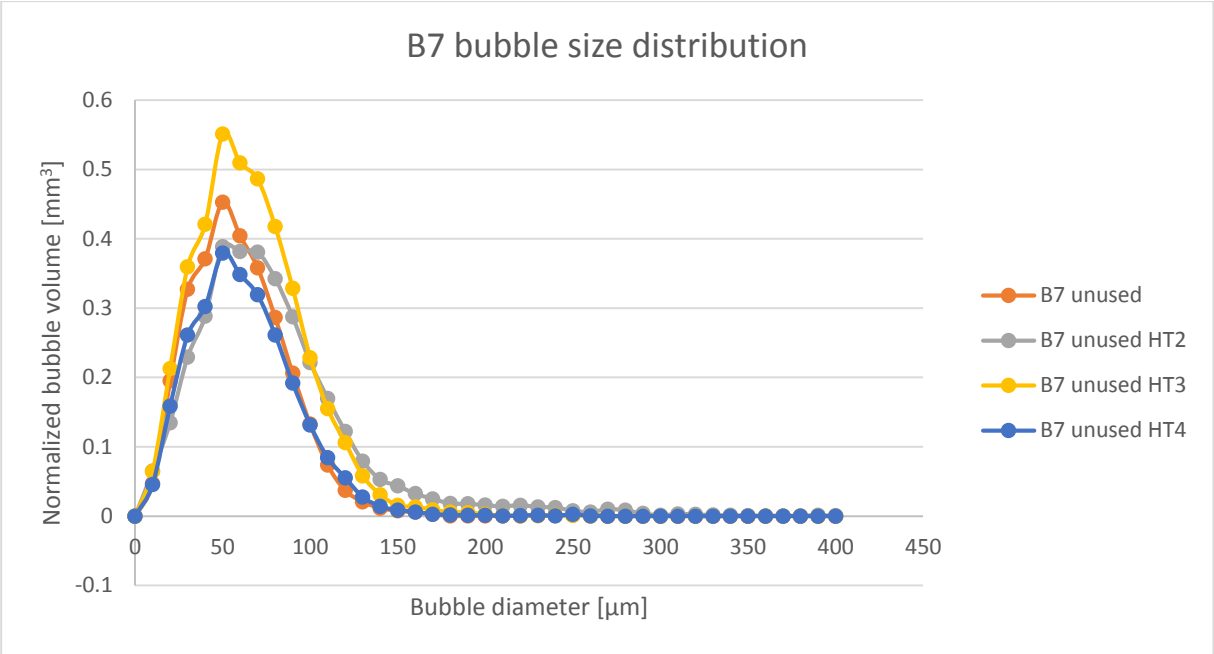

Figure 44. Comparison of the bubble size distribution at position 7, zoom on the unused and heat-treated samples.

As seen in Figure 44, the lowest bubble content is found in HT4, while the highest is in HT3. All the samples have a peak diameter of 50 µm. The bubble content has decreased from 0.29% to 0.26% from the unused to HT4.

Position 10

Figure 45 shows that the bubble content in position 10 is between what is measured in position 1 and 7. Figure 46 shows a zoomed version to compare the unused and heat-treated samples from position 10.

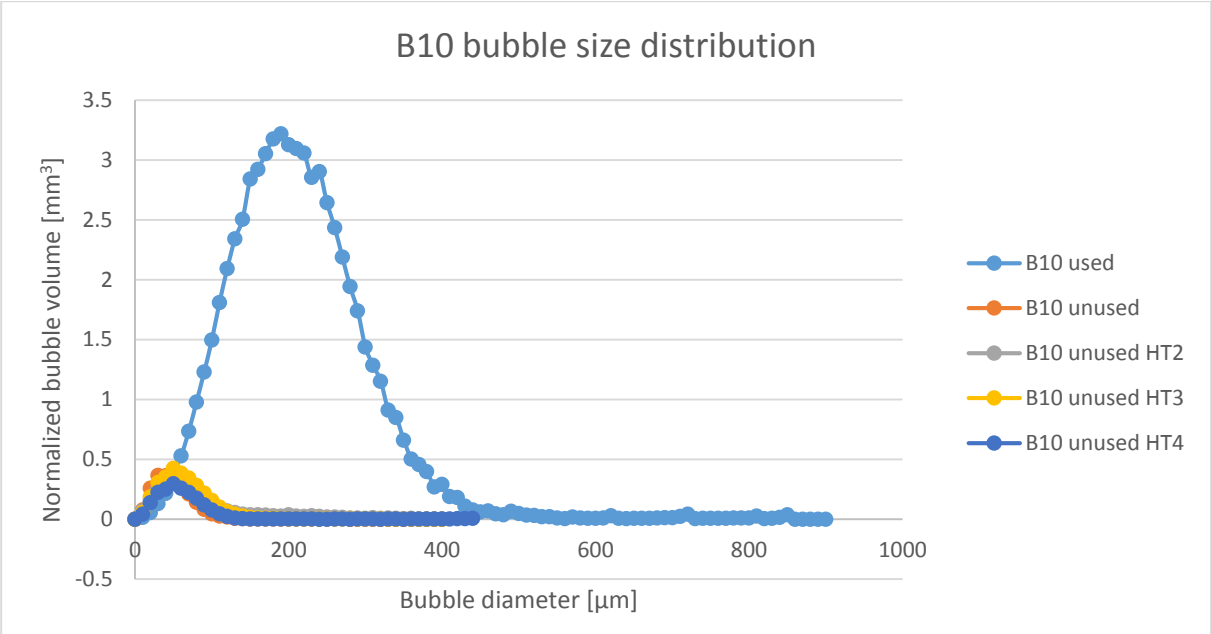

Figure 45. Comparison of the bubble size distribution in crucible B at position 10.

Finally, in position 10, the bubble content in the used crucible sample is measured to be 6.53%. The unused sample has 0.23% bubbles, while the heat-treated samples have 0.30%, 0.30% and 0.19% in HT2, HT3 and HT4 respectively. While the used sample has bubbles with diameter mostly around 200 µm, the unused and heat-treated samples have most bubbles around 50 µm in diameter. The bubbles in the used sample reach up to 500 µm in diameter, while the unused and heat-treated samples only have bubbles up to around 200 µm.

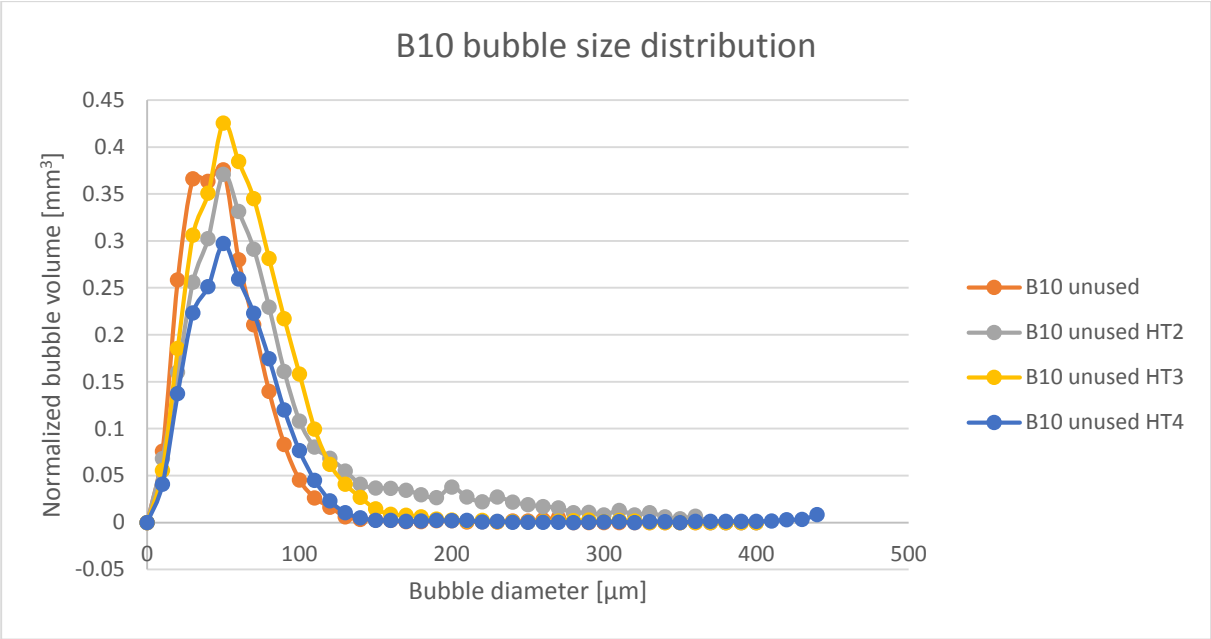

Figure 46. Comparison of the bubble size distribution at position 10, zoom on the unused and heat-treated samples.

In Figure 46, the HT4 sample has the lowest bubble content, while the HT2 and HT3 are equally high. HT2 has bubbles with larger diameter than the other samples, with up to 400 µm diameter bubbles present. The bubble content has decreased from 0.23% to 0.19% from the unused to HT4.

As seen in this section, the used crucible samples have a much higher bubble content, which consists of larger bubbles, than the unused and heat-treated samples. There is also a big difference in bubble content between the used samples, whereas the sample from position 1 had over twice as high bubble content as the sample from position 7 and almost twice as high bubble content as the sample from position 10. The samples from HT2 and HT3 have a minor growth in bubble content compared to the unused samples, while the HT4 samples (except in position 1) have lower bubble content than the unused samples. The unused and heat-treated samples have a low variation in bubble content between the different positions, unlike the samples from the used crucible.

4.3.2 Comparing bubble distribution through the crucible wall

The data extracted from the X-ray measurements can also show the distribution of bubbles inside he crucible wall. The data obtained on from crucible B in unused, used and heat-treated samples, were used to produce the following graphs in order to compare the bubbles' location in the wall. In these graphs, the normalized bubble volume has been calculated at different positions through the crucible wall. As in the previous section, position 1, 7 and 10 have been studied here.

Position 1

Figure 47 presents the bubble distribution in from position 1 in crucible B while Figure 48 focuses on the unused and heat-treated samples.

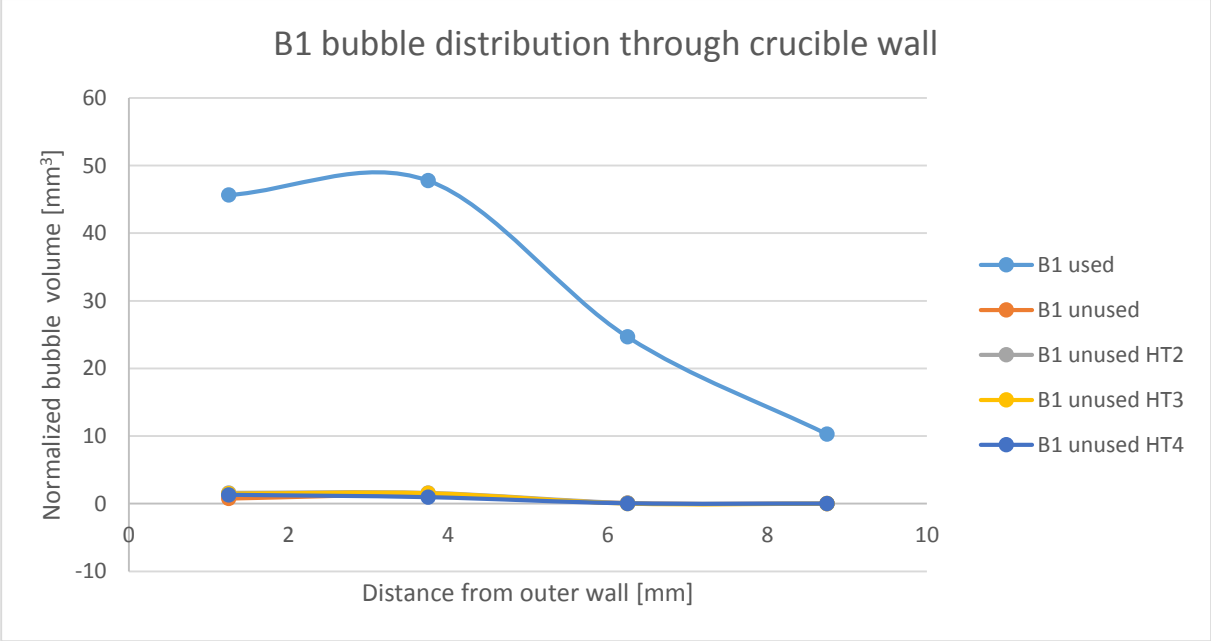

Figure 47. Bubble volume distribution through the crucible wall in position 1.

Figure 47 reveals that the used crucible sample has bubbles present over the entire profile. There are less bubbles (lower bubble volume) near the inner wall, but it is not free from bubbles.

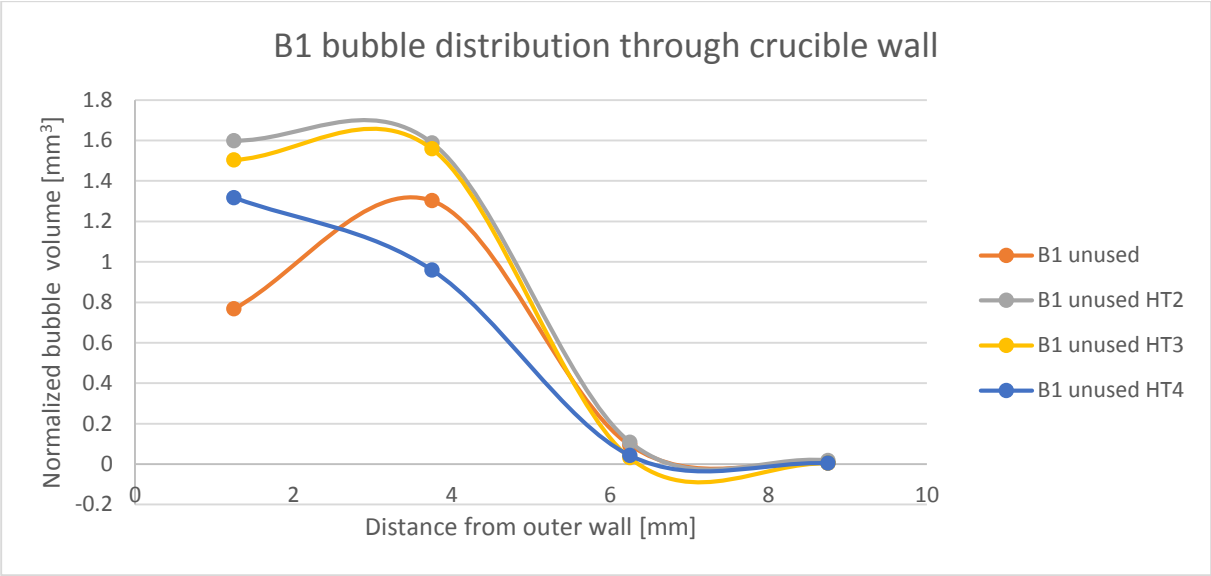

Figure 48. Bubble volume distribution through the crucible wall in position 1 without the used sample.

In Figure 48, while the amount of bubbles and the distribution of them is slightly different in the outer parts of the unused and heat-treated samples, all of the samples have close to no bubbles in the inner half part of the crucible wall. Between those samples, the HT2 case has the highest bubble volume.

Position 7

Figure 49 and 50 shows the bubble distribution in position 7. Figure 49 compares the used samples to the unused and heat-treated samples, while Figure 50 focuses on the unused and heat-treated samples. Compared to position 1, the used sample from position 7 has a lower bubble content close to the inner wall. Also, the unused sample shows a high bubble content in the inner part of the wall.

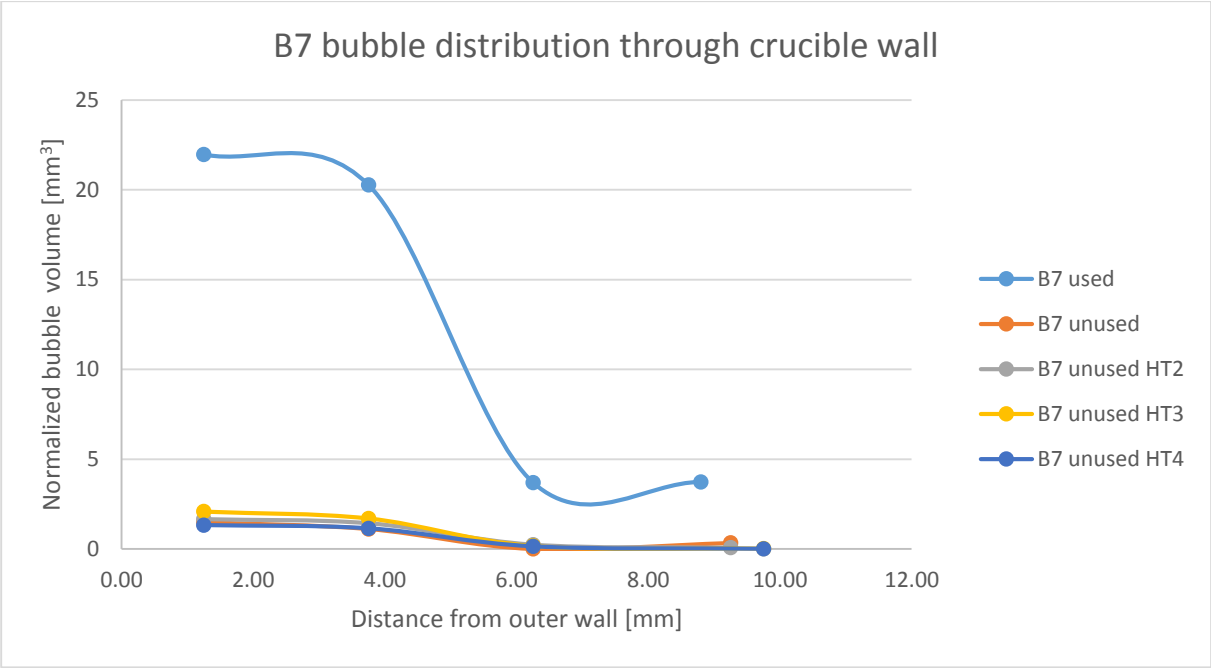

Figure 49. Bubble volume distribution through the crucible wall in position 7.

As seen from Figure 49, the amount of bubbles is around five times greater in the outer part than the inner part of the used sample.

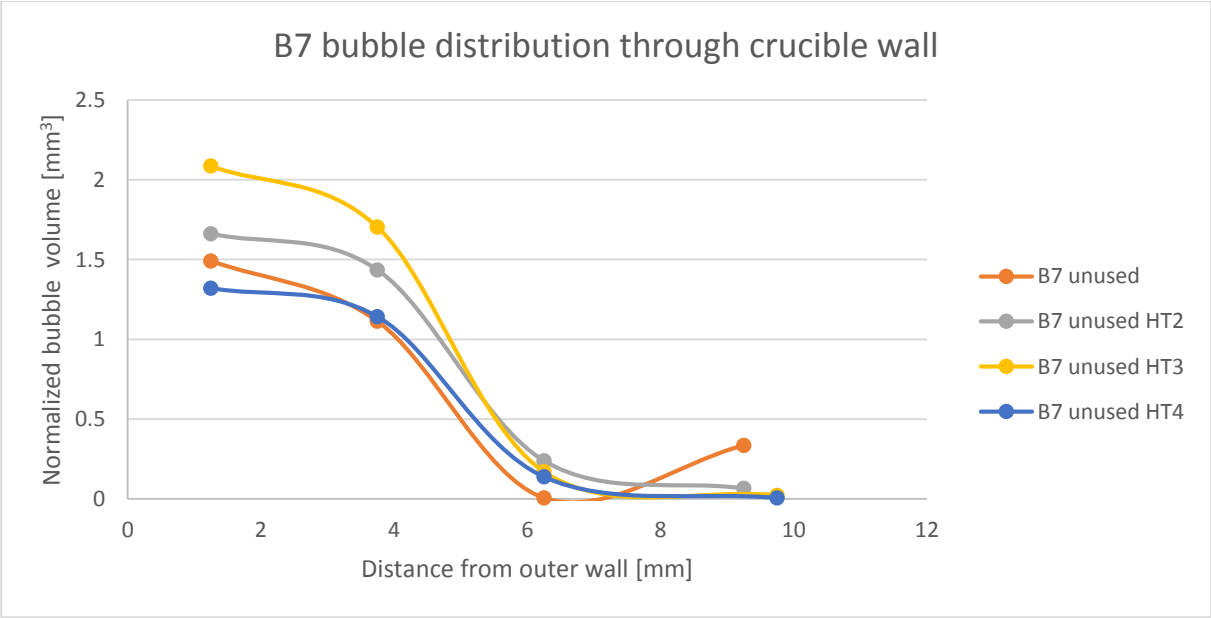

Figure 50. Bubble volume distribution through the crucible wall in position 7 without the used sample.

Figure 50 shows that the HT2 and HT3 samples have the highest bubble content in the outer part, while only the HT3 and HT4 samples are completely bubble free in the inner layer. The unused samples have bubbles present in the inner layer close to the inner wall.

Position 10

Figure 51 presents the bubble distribution in position 10 and Figure 52 focuses on the unused and heat-treated samples. Compared to position 1 and 7, the used sample from position 10 has a lower bubble content close to the inner wall. The used sample has almost no bubbles present close to the inner wall. However, the used sample from position 10 has a higher bubble content close to the outer wall compared to the sample from position 7.

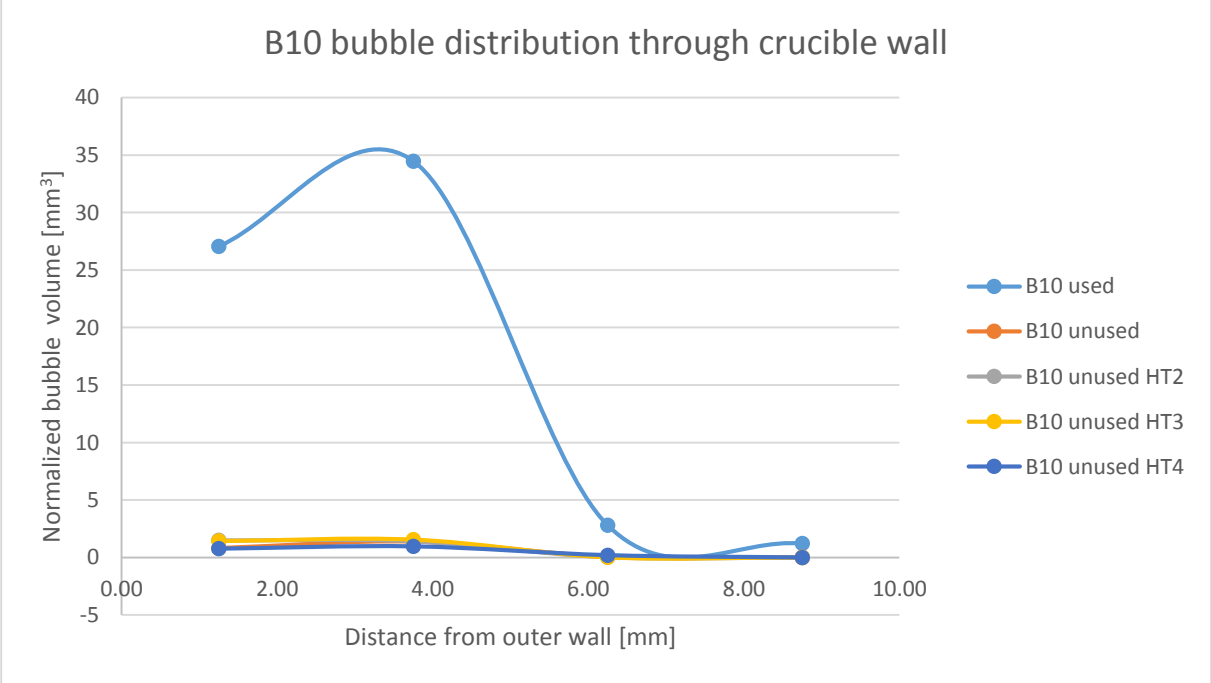

Figure 51. Bubble volume distribution through the crucible wall in position 10.

Figure 51 reveals that the used sample has a low bubble content in the inner part, almost as low as the unused samples.

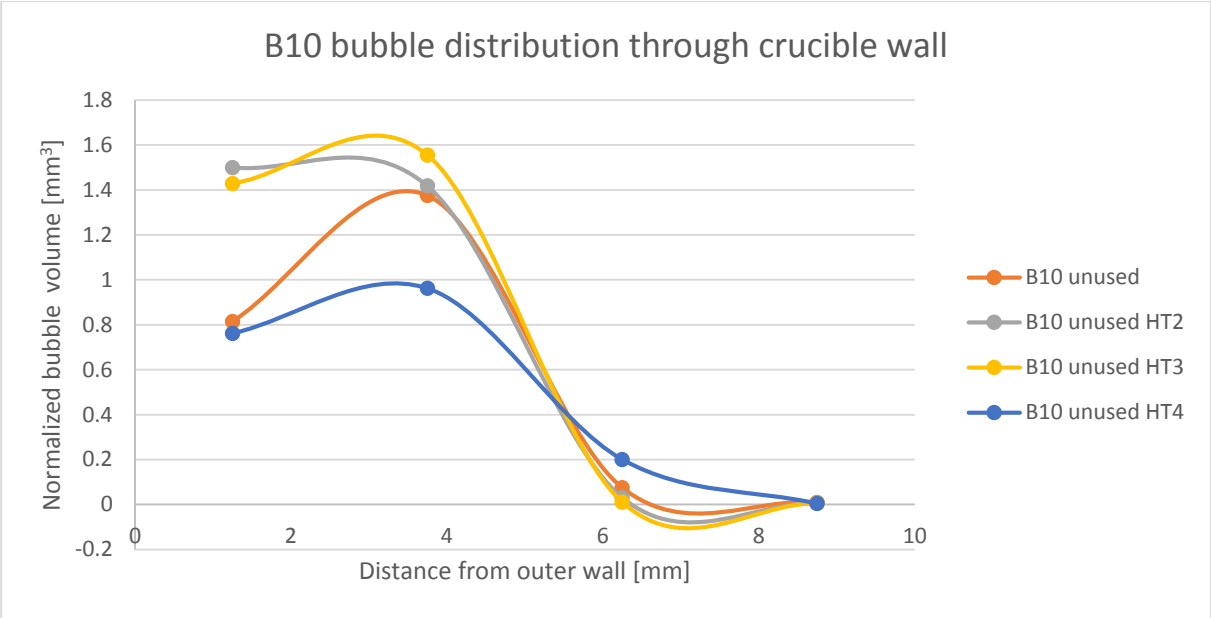

Figure 52. Bubble volume distribution through the crucible wall in position 10 without the used sample.

In Figure 52, the HT4 sample has the lowest bubble content in the outer part, but highest in the inner. The HT2 and HT3 samples have the highest bubble content in the outer part, but a very low bubble content in the inner half, and no bubbles in the inner quarter.

The distribution of bubbles in the crucible wall is similar in the unused and heat-treated samples within the respective positions. All the unused and heat-treated samples have a completely bubble free inner 1/4, except from the unused sample from position 7. The bubble content in the inner part of the used crucible sample from position 1 is high, while it decreases in position 7 and 10. The used sample from position 10 has an almost bubble free inner half part. The HT2 and HT3 samples have a higher increase in bubble volume in the outer part of the crucible wall than the inner side, compared to the unused samples from the same position.

4.4 Comparison between different crucible types

The tests and analysis performed in this thesis and shown previously, have been done on a used and an unused crucible of the same type called crucible B. To see if there are big differences between crucibles from different suppliers, the results were compared to the crucible A case. This is interesting for industrial purposes, as it will be information that the industry can use to know what types of crucibles perform best with regard to the bubble growth and the material quality. This section will then compare the samples from crucible A and B, before and after use in the Cz pulling, as well as after performing HT4 process.

4.4.1 Bubble size distribution comparison

In this first part, the normalized bubble volume is compared. Figure 53 presents the results of the crucible used in the pulling process, while Figure 54 focuses on the unused samples and Figure 55 on the samples after HT4.

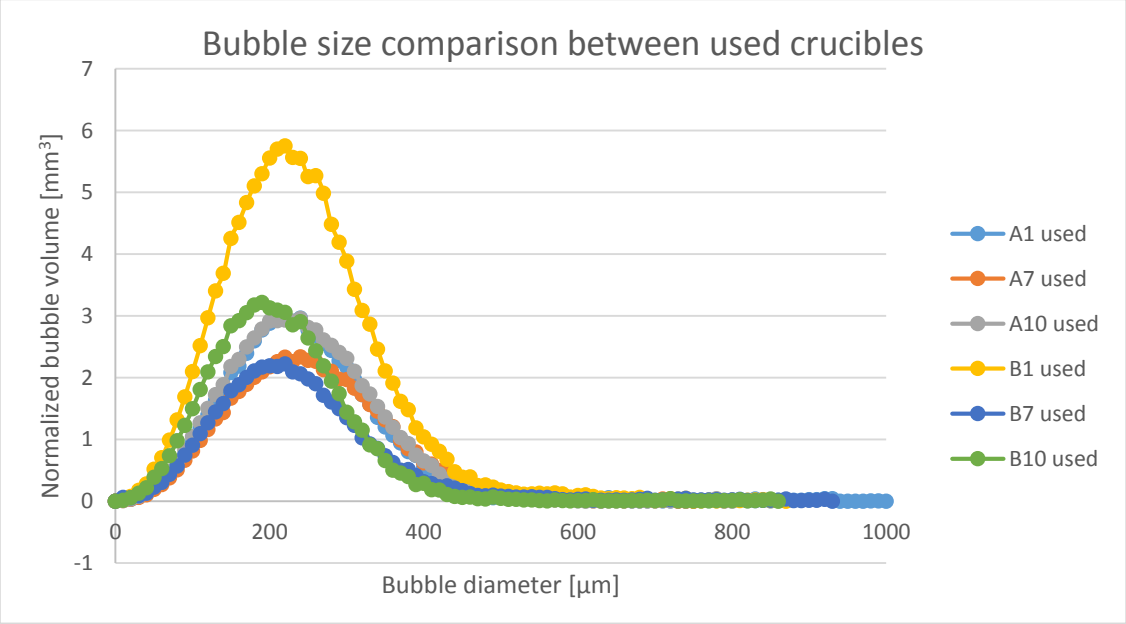

Figure 53. Comparison of the bubble volume content between crucible A and B after use in the Cz pulling process at positions 1, 7 and 10.

In Figure 53, it is clearly seen that position 1 from the B-crucible has the highest bubble content, with almost twice the amount of bubbles (normalized) as the others. Position 7 from both the A and B-crucible have the lowest amount of bubbles, while position 10 from both crucibles are placed in the middle.

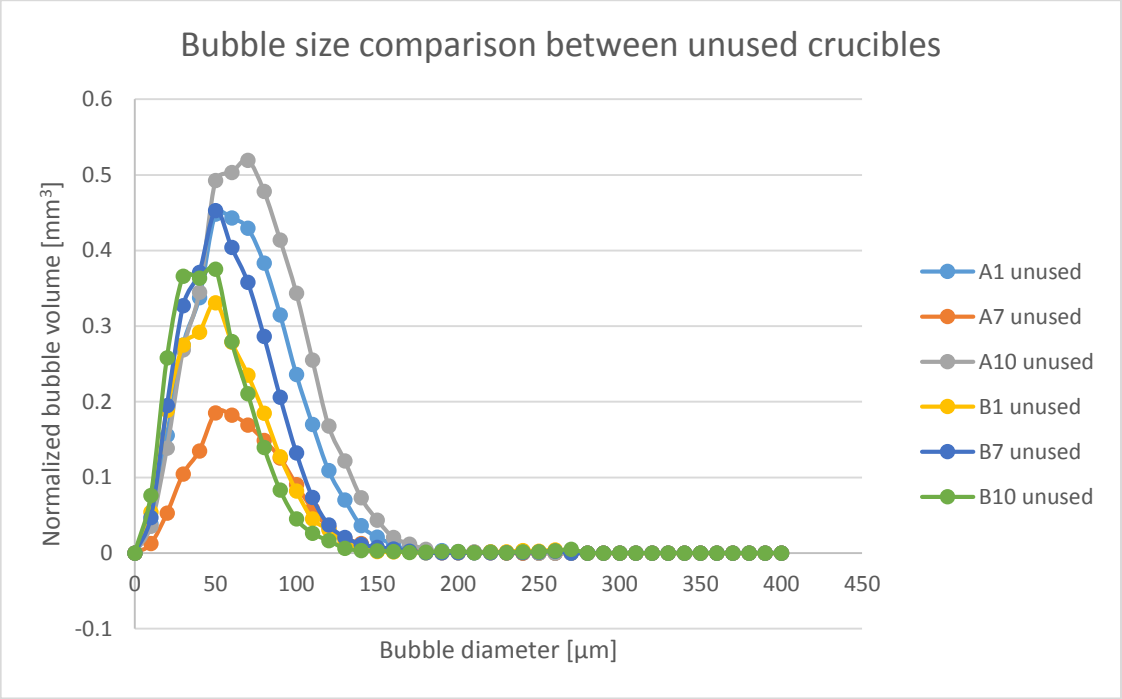

Figure 54. Comparison of the bubble volume content between crucible A and B before use in the Cz process at positions 1, 7 and 10.

For the unused samples (see Figure 54), position 7 from the A-crucible still has the lowest bubble content, while position 7 from the B-crucible has one of the highest. The highest bubble content is found in position 10 from the A-crucible.

As revealed in Figure 53 and 54, the highest growth in bubble volume is found in position 1 from crucible B. The bubble content increased from 0.22% before use to 12.84% after use in the Cz pulling process. Position 7 from crucible B has the lowest bubble volume growth, with an increase in bubble content from 0.29% to 4.97%. The samples from the different positions in crucible A have a more similar bubble growth, and crucible A has a lower total bubble volume growth than crucible B. Crucible A has a total bubble content of 0.30% before use, and

6.43% after use in the Cz pulling process. Crucible B has a total bubble content of 0.25% before use and 8.11% after use in the Cz process.

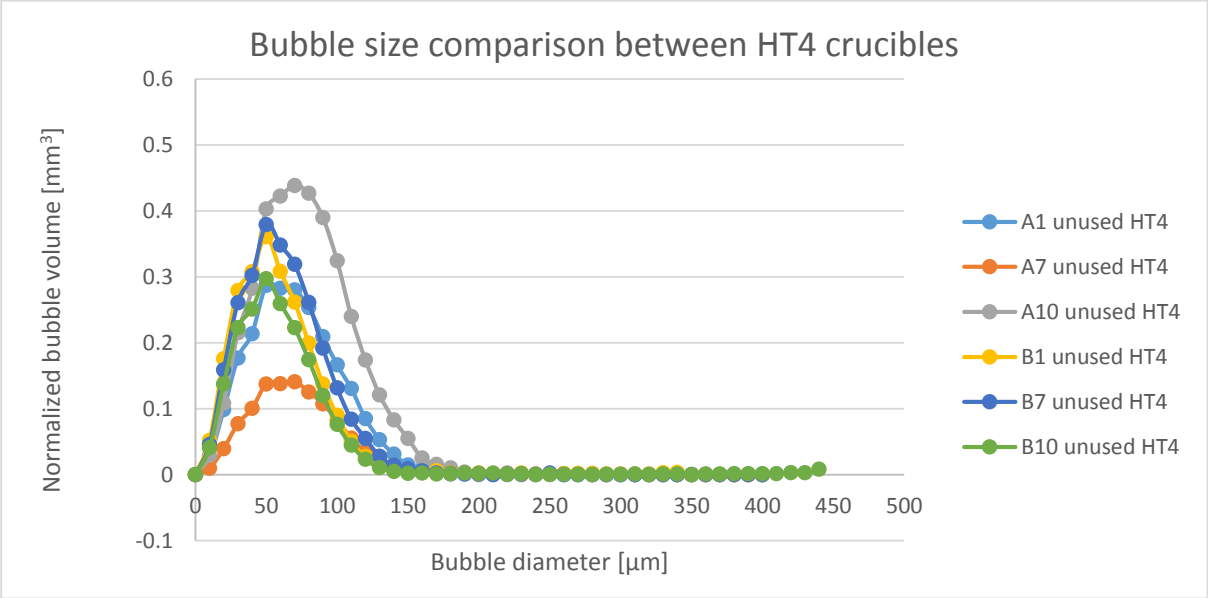

Figure 55. Comparison of the bubble volume content between crucible A and B after the HT4 process at positions 1, 7 and 10.

After HT4 (see Figure 55), the bubble contents look very similar to the results from the unused samples. The highest and lowest bubble content is still found in A10 (position 10 of crucible A) and A7 respectively. In all the samples except from B1, the bubble content has decreased after the heat-treatment. In B1 it has increased from 0.22% to 0.23%, which is very marginal compared to the increase between the unused samples and the samples used in the Cz process.

4.4.2 Comparing bubble distribution through the crucible wall

This second part continues on the comparison between crucible A and B but now focuses on the variation of the bubble volume through the crucible wall from the outer part (BC layer) to the inner part (BF layer). Figure 56, 57 and 58 show the bubble distribution through the crucible wall in the samples from both crucible A and B. The bubble distribution in the samples used in the Cz pulling process, the unused samples and the samples from the HT4 process are shown in Figure 56, 57, and 58 respectively.

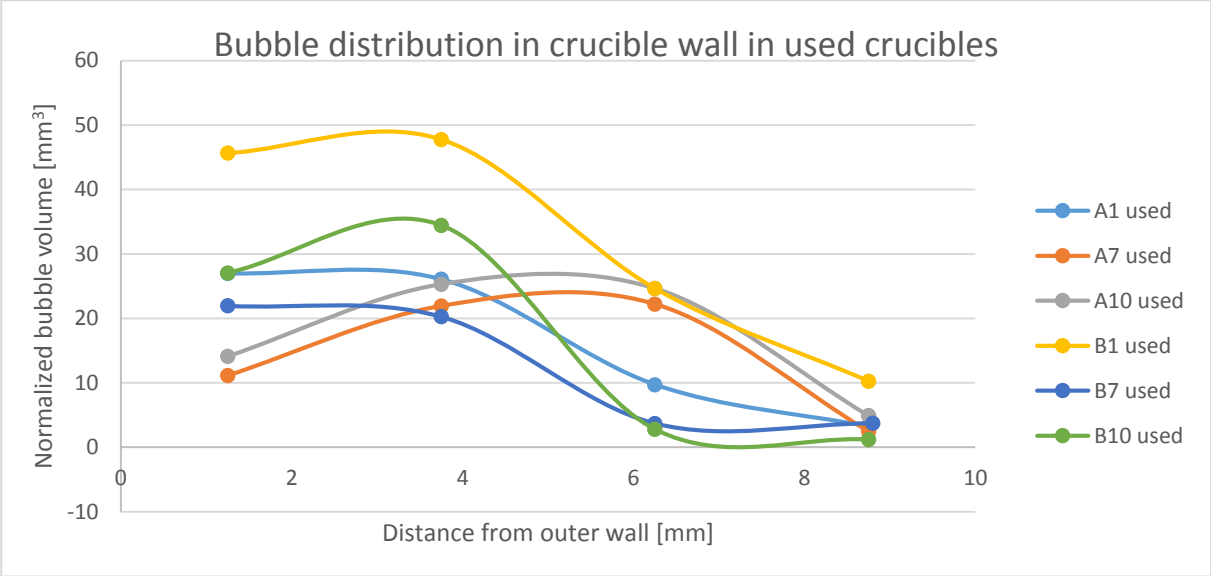

Figure 56. Bubble volume distribution through crucible wall of samples cut from used A and B crucibles at position 1, 7 and 10 after use in the Cz pulling process.

In Figure 56, the different crucibles have a various distribution of bubbles both between the positions and between the crucible types. However, a lower bubble content is always measured close to the inner wall. A7 and A10 has higher bubble content in the middle of the crucible than in the outside, the others have a decreasing bubble content close to the inner wall.

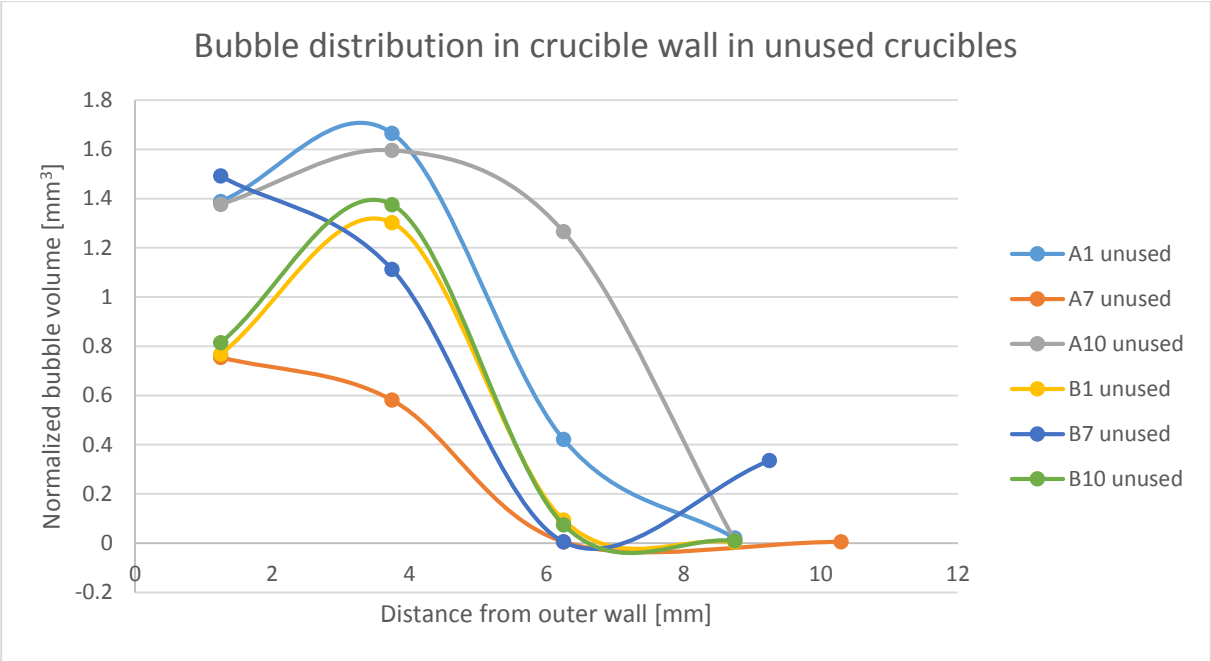

Figure 57. Bubble volume distribution through crucible wall of samples cut from used A and B crucibles at position 1, 7 and 10 before use in the Cz pulling process.

In Figure 57, B7 has a high bubble content in the inner part, close to the melt. The other samples have close to no bubbles in this region. For most of the samples, the highest concentration of bubbles is round around 4 mm into the sample (from the outer side). Sample A7 has the lowest bubble content, while A10 has the highest.

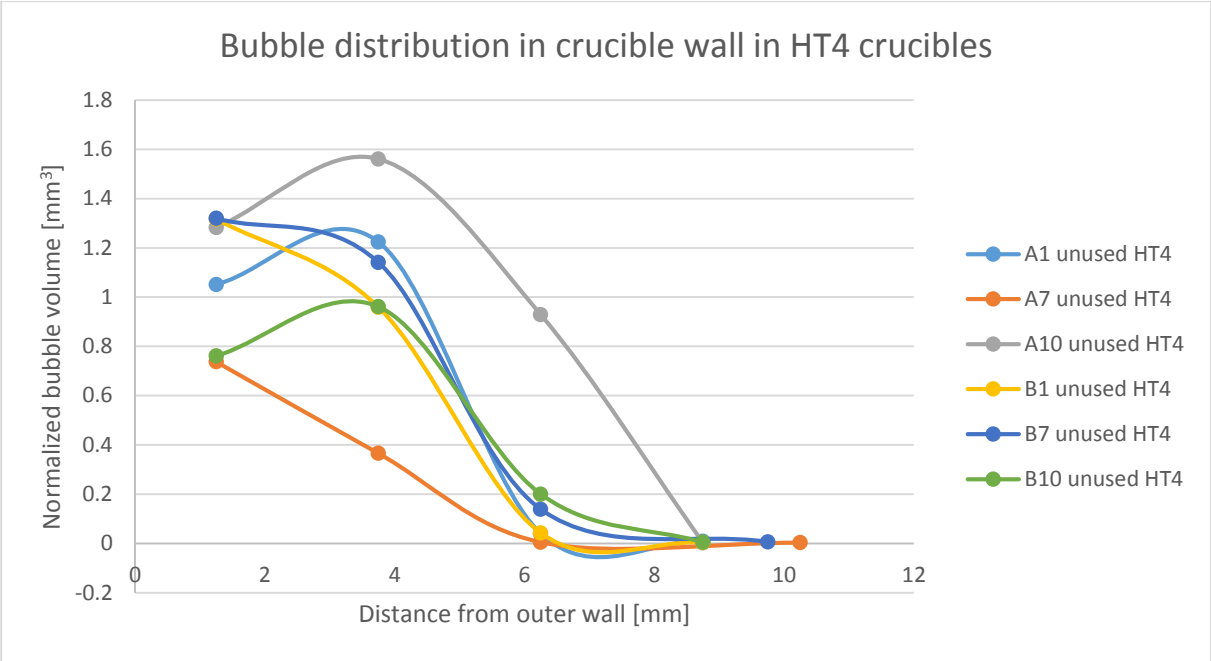

Figure 58. Bubble volume distribution through crucible wall of samples cut from used A and B crucibles at position 1, 7 and 10 after the HT4 process.

The distribution of bubbles in the HT4 samples, shown in Figure 58, look very similar to the unused. In this case, all the samples have no bubbles in the inner part of the crucible wall.

4.5 Electron microscopy

The detection limit of the X-ray tomography is 9 µm. If there are smaller bubbles than this present in the quartz that grows into visible bubbles during the Cz process, this might explain the difference in results from the unused and used crucible samples. A Scanning Electron Microscope (SEM) was used to investigate the samples. The goal was to examine if there are bubbles present in the quartz that can not be measured by the X-ray tomography.

4.5.1 SEM

Uncoated sample

SEM measurements have first been done on uncoated samples. As discussed in Section 3.8.2, charging effect issues were faced during this measurement. Figure 59 illustrates this charging effect during the analysis of the sample cut from position 1 from crucible A.

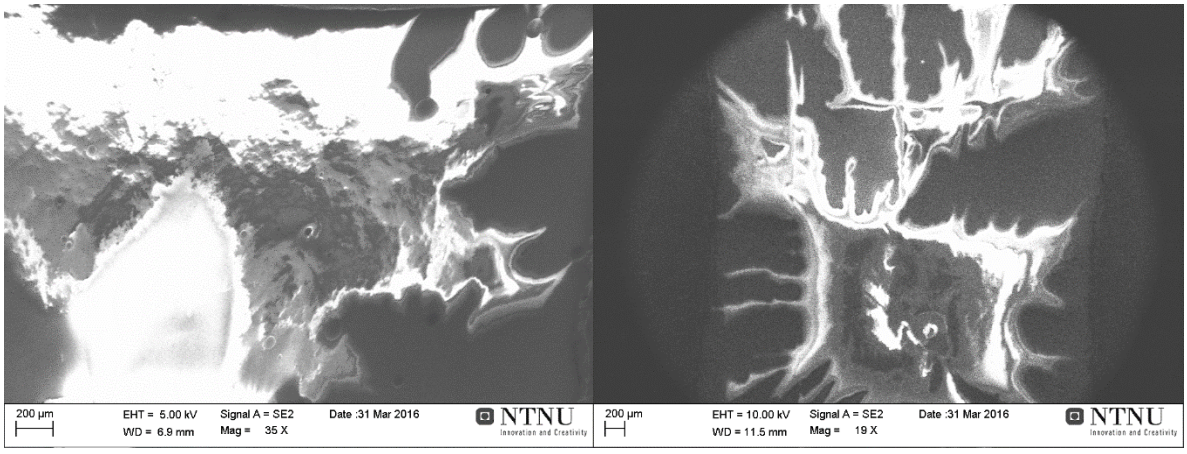

Figure 59. SEM images showing the charging effect. Left: 5kV, right: 10kV.

The charging effect led to some challenges when investigating the topography of the samples. The pictures in Figure 59 were taken with a relatively high voltage, 5kV in (left) and 10kV in (right). The voltage and aperture had to be very small to have as little charging effect as possible. The best results came when a low voltage of 1-2 kV was used, together with a 20 µm aperture.

Still there was some charging and the low voltage and small aperture caused the contrast to be lower than optimal. Figure 60 shows the results obtained from the BC layer on the same sample as in Figure 59, with a lower voltage of 2 kV. The result with a voltage of 1kV is seen in Figure 61.

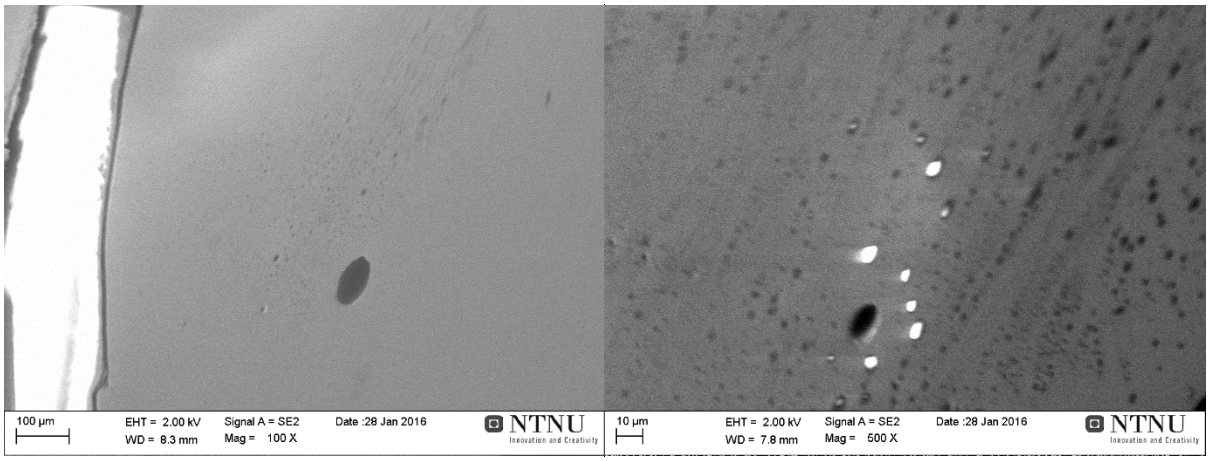

Figure 60. Left: 100x magnification from the BC layer on the uncoated sample. Right: 500X magnification.

Big bubbles with 100 µm diameter are seen together with small bubbles in the left part of Figure 60. The white part on the left in Figure 60 (left) shows the charging effect. Figure 60 (right) shows that there are very small bubbles present in a high number, which could not have been recorded in the X-ray tomography, as they are significantly smaller than 9 µm. Some of the bubbles shown in Figure 60 are less than 1 µm in diameter.

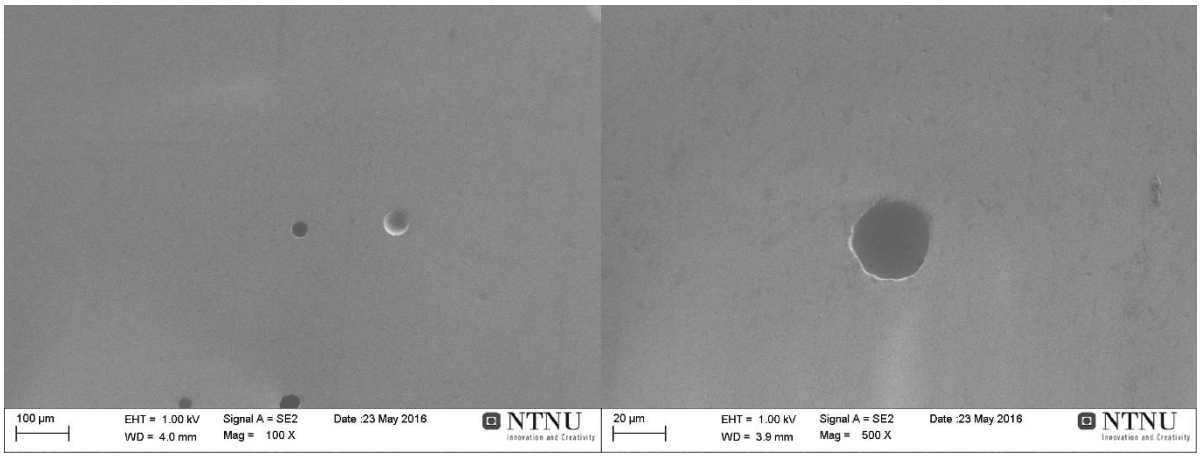

Figure 61. Lower voltage SEM images from the uncoated sample with 100X (left) and 500X (right) magnification.

Figure 61 shows the results obtained with a lower voltage of 1 kV in the BC layer. The right image in Figure 61 shows a zoom of the left image. With a voltage of 1 kV, the charging effect is reduced, but the smaller bubbles are not so easily found. Figure 61 shows the same magnification as Figure 60, but fewer small bubbles. The smallest bubbles present are around 20 µm in diameter.

Coated sample

To improve the previous results, the samples were coated with gold as presented in Section 3.8.2. Indeed, the gold coated sample has a better conductivity and the voltage can therefore be much higher. This gives clearer images, but also a risk that the coating has changed the original topography of the sample. The results can be seen in Figure 62 in the case of an unused sample cut at position 7 in crucible A. The image is taken from the BC layer.

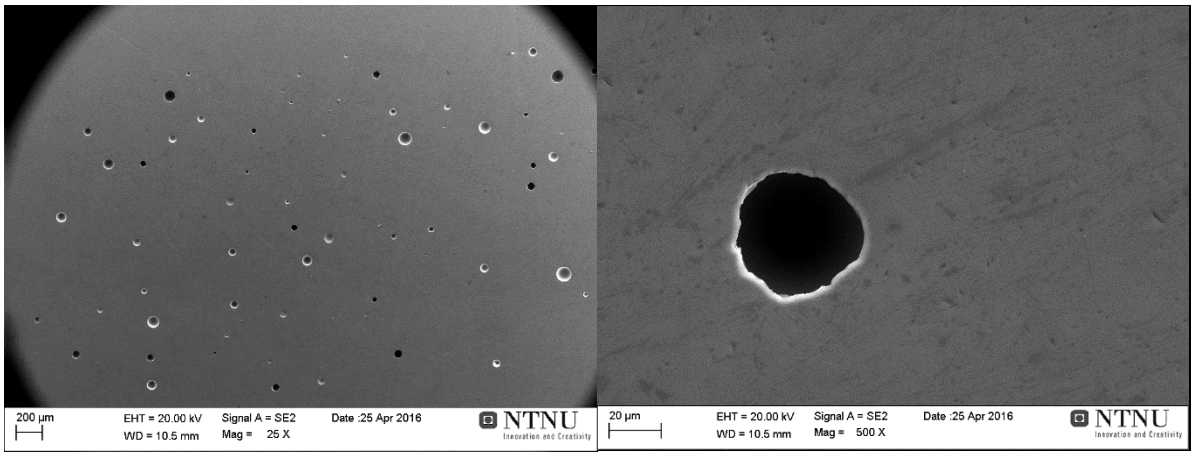

Figure 62. SEM images of the gold coated sample, from BC layer with magnification of 25X (left) and 500X (right).

The bubbles in the BC layer can be clearly seen in Figure 62 (left) while Figure 62 (right) focuses on one bubble with a higher magnification. The bubble is not perfectly circular, but well defined. In addition, the structure of the surrounding quartz is seen. The bubbles seem to be between 10-100 µm in diameter, but smaller bubbles are not easily seen. This is most likely due to the gold coating, which covers over the small bubbles in the sample.

Figure 63 shows low (left) and high (right) magnification images from the BF layer on a sample cut from position 7 in crucible A.

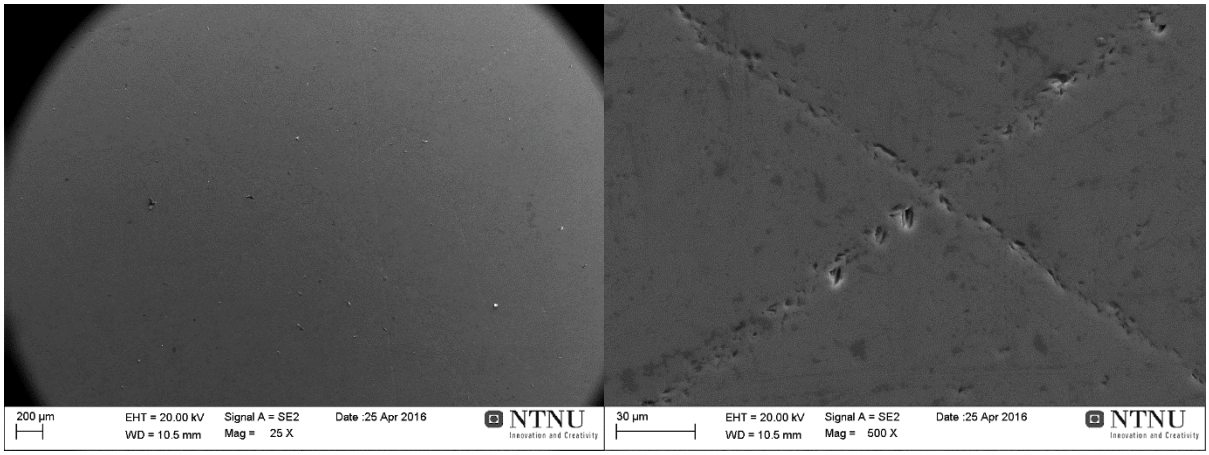

Figure 63. SEM images of the gold coated sample, from BF layer with magnification 25X (left) and 500X (right).

In the BF layer, no small bubbles are seen. The only structures seen on the surface, except from some few medium sized bubbles, are grinding lines from the polishing. These lines are just a few µm across, but can still be easily seen. It should therefore not be a problem to see the small bubbles if they were present. This is most likely due to the gold coating, which covered over the small bubbles in the BC layer of the sample.

Finally, in Figure 64 (left), the transition between the BC and the BF layer was captured with the SEM, and one can clearly see the bubbles in the BC region and near no bubbles in the BF region. In Figure 64, the SEM picture is compared to a light micrograph of position 1 from crucible A. Bubbles from further into the sample body are visible in the light microscope, because the sample is transparent and the bubbles can be seen through the glass, unlike in the SEM.

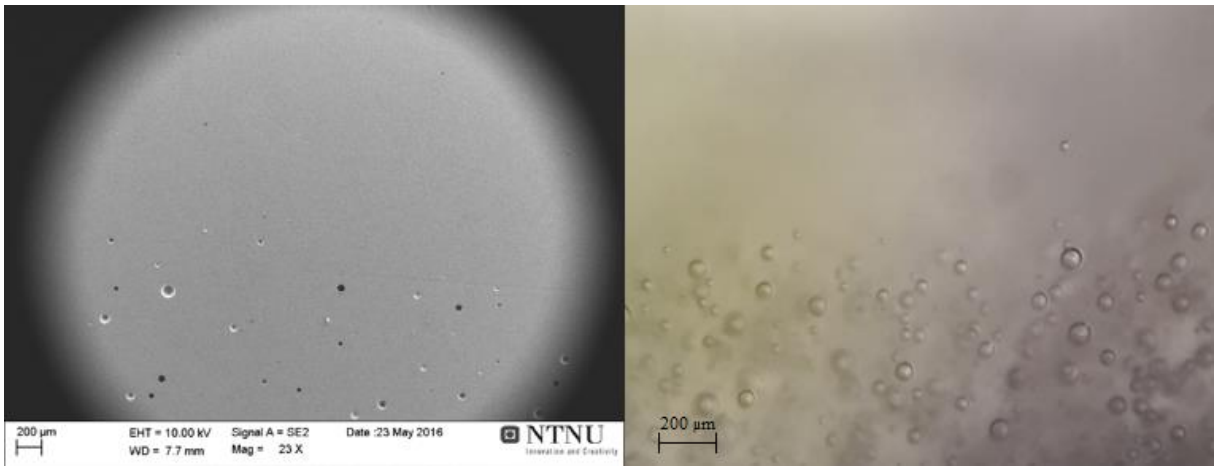

Figure 64. Left: Gold coated sample, SEM image from transition between BC (bottom) and BF (top) with 23X magnification. Right: Light micrograph of the transition to compare the bubbles.

4.5.2 EDS analysis

EDS was used to analyse the chemical composition of the crucible sample. Figure 65 shows the three measuring points in the sample. Figure 66, 67 and 68 show the chemical analysis results from these three measuring points done on the gold coated crucible sample from position 7 in crucible A.

The EDS analysis was done by point scanning three points in the sample. Two points are positioned on the surface, and one point is positioned on the edge of a bubble (see Figure 65). The results show that the element present is mostly silicon and oxygen, and gold and a little carbon. The results from the different test spots are very similar. The results from point 1 show high occurrence of silicon and oxygen, and traces of gold and carbon. The analysis from the bubble edge shows a lower oxygen content than the other points. It also shows very small traces of sulphur in this point. The reference point shows very similar results as point 1.

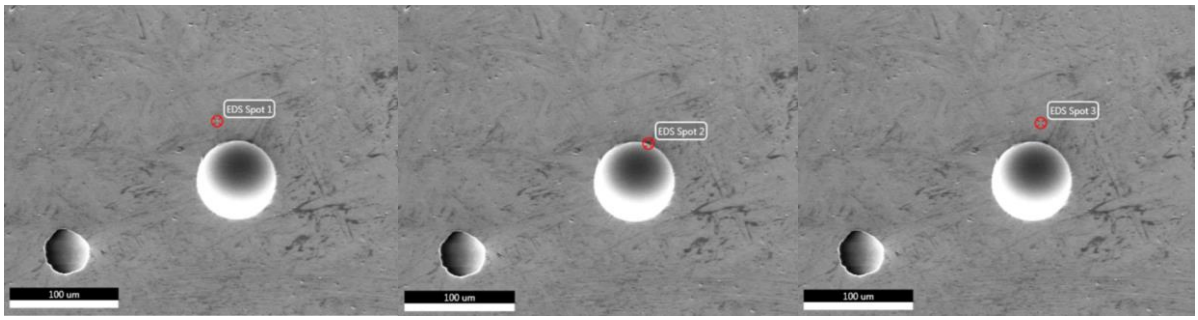

Figure 65. SEM picture showing the position of the three points analysed by EDS, (left) position of point 1 from outside the bubble, (middle) point 2 position at the bubble edge and (right) point 3 position as a reference point.

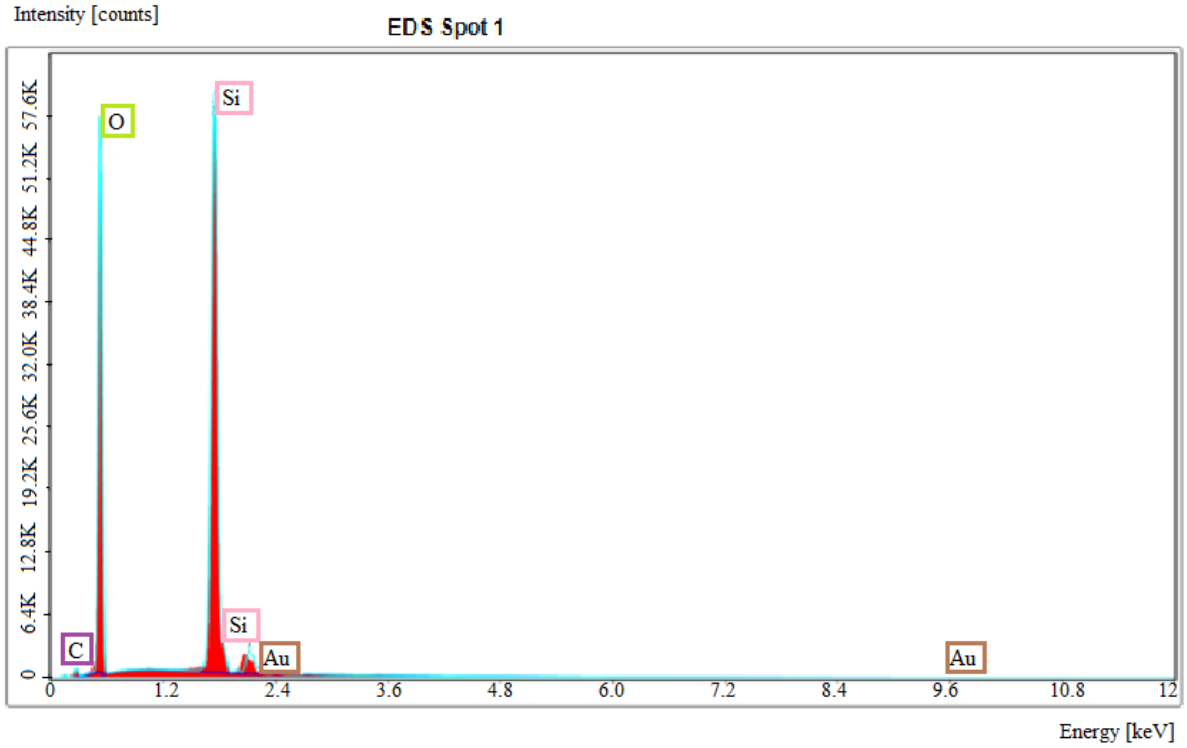

Figure 66. EDS analysis from point 1 on the gold coated sample from position 7 in crucible A.

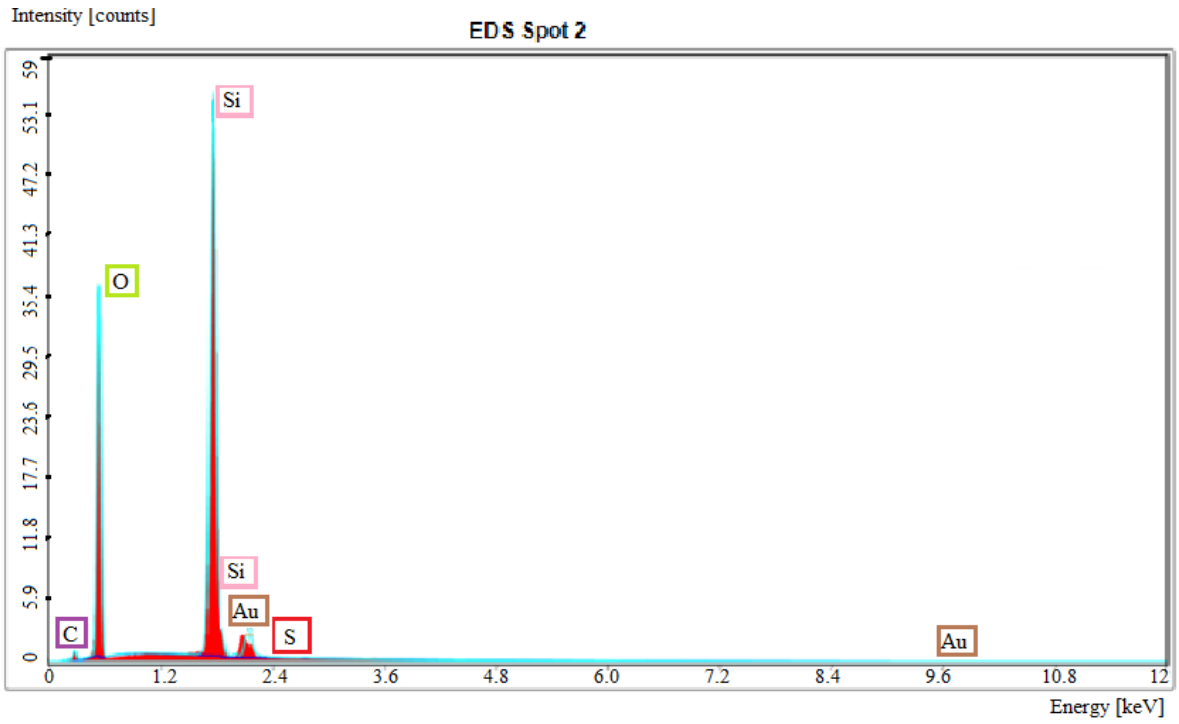

Figure 67. EDS analysis from point 2 on the gold coated sample from position 7 in crucible A.

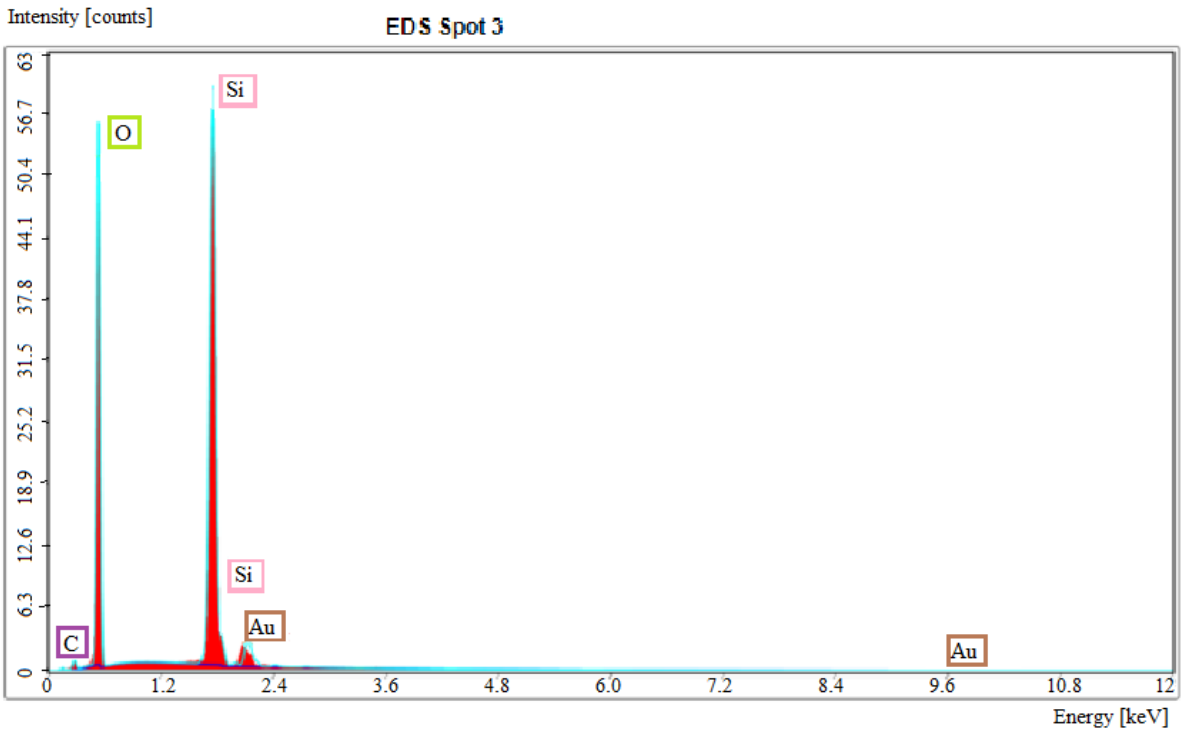

Figure 68. EDS analysis from point 3 on the gold coated sample from position 7 in crucible A.

As seen from Figure 66, 67 and 68, there is a noticeable difference between point 2 and the other points. The oxygen concentration is much lower than in point 1 and 3.

5 DISCUSSION

5.1 Temperature simulation in the crucible

The simulation gives a good indication on what parts of the crucible experience the highest temperatures for the longest time. The corner and bottom parts of the crucible will maintain a much higher temperature than the top, with a longer holding time, as the crucible is raised to let the melt level stay constant relative to the crystal puller. During the body growth of the ingot, the difference in temperature between position 1 and position 7 in the crucible was measured to be around 300 °C. This will have a massive impact on the viscosity properties of the quartz, as discussed in Section 4.1, and hence the growth of the bubbles inside it. It is, however, seen that the temperature difference in position 7 and 10 is only around 20 °C, which will not contribute to a significant change in viscosity. In addition, positions 7 and 10 in the crucible are subjected to the higher temperature for a longer time, as seen in Section 4.1. From these results, it was assumed that the bubbles would grow more in positions 7 and 10 than in position 1. However, as shown in Figure 53 and 54, the data from the X-ray tomography revealed the opposite. The increase in bubble content was significantly higher in position 1 than in positions 7 and 10 when comparing the sample from the unused crucible to the sample from the crucible used in the Cz process.

5.2 Improvement of heat-treatment results

The results from the heat-treatment done in the project thesis (HT1) showed many cracks in the samples due to the formation of a thick cristobalite layer. The bubble analysis data showed a large growth of bubble size in the samples, but this was rejected as it turned out that the image analysis had counted the cracks as bubbles. The bubbles also seemed distorted in shape and looked very different to the bubbles in the unused or the used sample. This gave reason to believe that the heat-treatment model was not representative for the environment experienced during actual crystal pulling.

The heat-treatment methods employed in this thesis gave better and more reliable results than the heat-treatment done in the project [3]. As the temperatures higher than 1400 °C promoted crack formation and growth in HT1, it was decided to use 1400 °C in the following heat-treatments. This should be representative for the temperatures the crucible experiences during a crystal-pulling run, as the crystallization is done below the melting temperature of silicon (1412 °C) [8]. This parameter was therefore fixed, and the pressure and atmosphere was changed to check what effect it would have.

By creating less cracks, the samples from HT2 were easier to analyse, and the results were more trustworthy. On the other hand, the bubble content in the heat-treated sample was not very different from the unused, at least not compared to the used sample. As there were still some cracks in the samples, it could not be determined whether the bubbles had actually grown or if the cracks had been counted as bubbles. It was therefore decided to lower the holding time from 24 h to 4 h, and this was done in HT3 and HT4.

The samples from HT3 and HT4 had no cracks and a barely visible cristobalite layer on the surface. This corresponds well to the work done at SINTEF on cristobalite formation [34]. This means that the results from the bubble analysis could be trusted, and that any change in bubble volume is due to actual bubble growth.

5.3 Bubble content in unused, used and heat-treated samples

As concluded in the project thesis [3], the bubbles grow during the crystal pulling process. The growth of the bubbles was expected to rely on three main parameters: i) temperature, ii) pressure and iii) holding time. The size distribution comparisons show that the samples from the used crucible have a much higher bubble content than the other samples, consisting of bigger bubbles. The bubbles in the used samples are up to 700-800 µm in diameter, while the bubbles in the unused and heat-treated crucibles only just exceed 200 µm. The sample from position 1 in the used crucible had 12.84 % bubble content, which is the highest recorded. This is significantly higher than position 7 and 10, which had 4.97 % and 6.53 % respectively.

The bubble content analysis done after HT1 indicated a significant bubble growth compared to the unused samples. However, this was rejected, as the crack formation in the samples caused the image analysis to produce incorrect results. This was discussed in the project thesis [3].

In HT2, the samples were heated to 1400 °C and kept there for 24 h. This was done in an inert argon atmosphere, at ambient pressure. The image analysis shows some bubble growth in the samples, similar to the bubble growth experienced after HT3. The indicated bubble growth was primarily found in the BC layer. The X-ray tomography data revealed some cracks on the edges of the HT2 samples, as seen in Figure 35, and it was therefore decided that the indicated bubble growth might actually come from the crack formation.

In HT3, the samples were heat-treated for 4 h in vacuum, to investigate if this would enhance the bubble growth. The results show that all the samples from HT3 had higher bubble content than the unused samples. The samples from HT4 were heat-treated for 4 h in 15 mbar argon atmosphere, which is similar to the atmosphere experienced during the Czochralski process, for 4 h. In positions 7 and 10, the bubble content was lower in the HT4 samples than in the unused samples, and in position 1 it grew minutely from 0.22 % to 0.23 % after heat-treatment. The reason for this is not known, but it is possible that the bubbles inside the crucible have a very low pressure, which only grows if the pressure outside is low enough. Still, this is unlikely, since the pressure in the crystal pulling chamber is in the range of 15-50 mbar [8].The fact that the HT3 samples were only heat-treated for 4 h, vs. 24 h for HT2, suggests that, even for the short holding time, the bubbles have actually grown in the HT3 samples.

It is worth noting that the bubbles grew very little during HT3, compared to the used samples. In all the positions, and especially in position 1, the bubble content is a lot higher in the used crucible than in the unused. The bubble content grew 58, 17 and 28 times from the unused to the used sample, in positions 1, 7 and 10, respectively. To compare, the bubble content increased only 1.5, 1.4 and 1.3 times from unused to HT3. The results from the used and unused crucible analysis corresponds to the research done on bubble growth by SINTEF [34].

In order to investigate whether contact with the silicon melt makes any difference to the gas exchange and hence the bubble growth, samples were taken from different positions in the crucible. This might explain why the heat-treatments performed did not give the same results as the used samples. It was expected that the samples that are in contact with the silicon melt therefore would have a higher bubble growth than the samples that are not. In this case, the samples from position 10 should have the biggest change in bubble volume, as they are positioned in the bottom of the crucible where they are in contact with the silicon melt during the entire run.

As seen from Figures 52 and 53, the biggest difference between the unused and used crucible is found in position 1. The B1 sample goes from having an intermediate bubble content to clearly having the largest bubble content. Sample B7 goes from having one of the higher bubble contents in the unused form to having the lowest bubble content after use. B10 has an intermediate bubble content before and after use. It is therefore not conclusive whether contact with the silicon melt actually enhances growth of the bubbles. The unused sample from B7 was the only sample to have bubbles present in the inner part of the BF layer. The image analysis was repeated to see if this was an error, but even though it decreased slightly, the bubble content in the BF layer was still much higher than in the other unused samples. This was surprising, as it seemed to have the largest BF region when inspected visually.

As discussed in the theory, bubble growth has been reported by heat-treating samples from a silica crucible without silicon present. This was done at 1500 °C at 20 Torr (= 26 mbar) in an argon atmosphere. This is 100 °C higher than the heat-treatment done in this thesis. Also, the holding time was longer, 10 h, compared to 4 h in this thesis. This could be the reason for a higher bubble growth reported in the literature than in this thesis.

5.4 Comparison between different crucible types

Crucible A goes from having the highest difference in bubble content between the BC and BF layer in the unused crucible, to having a more evenly distributed bubble content in the used crucible. Sample B7 has a high bubble content in the BF layer before use, but one of the lowest bubble contents after use. The B-crucible has the most equal distribution of bubbles throughout the different positions, that is to say, the distribution profiles are similar. After use, however, the situation is the opposite, and the B-crucible has the least similar bubble distribution profiles. Crucible A has a very even bubble content in the three positions, with 6.60 %, 5.78 % and 6.90 % for A1, A7 and A10 respectively. Both crucibles A and B, except from position B1 which is close to stationary, have lower bubble content after HT4 than before. As discussed in Section 3.9, small variations in bubble content between the samples could be explained by deviation in the cubic shape of the samples. However, this seems unlikely, since all samples except from B1 experienced lower bubble content after HT4. It is worth noting that B1 also had the largest growth in bubble content when comparing used and unused crucibles.

There are big differences between the two crucible types in how the bubbles are distributed through the crucible wall, but the bubbles have similar size. The crucibles have a very low bubble content close to the melt in the bottom position (position 10) before use, while crucible B has a much higher bubble content in this position after use than crucible A. The bubbles in crucible A grow less than the bubbles in crucible B, when compared before and after the crystal pulling process. Crucible A goes from a total bubble content of 0.30% to 6.43%, while crucible B goes from 0.25% to 8.11%. This might indicate that crucible B has a higher carbon content inside the bubbles, which can be due to insufficient quality control in the manufacturing. This, in turn, may affect the quality of the final monocrystalline silicon ingot grown with this type of crucibles.

5.5 Electron microscopy

The uncoated sample showed many bubbles that were too small to be detected by the CT. The charging effect made it difficult to obtain a good contrast and to see the small bubbles in detail.

However, it showed that there are bubbles present down to approximately 1µm in diameter. Unfortunately, it seems that the gold coating covered over the smallest bubbles, and they could not be seen in the SEM when the coated sample was investigated.

The EDS analysis showed that the sample contained oxygen, silicon, gold and carbon. This is not surprising, as the sample consists of silicon and oxygen coated with gold. The carbon is more interesting. It could, as discussed in Section 2.4.2, be traces of carbon that makes the bubbles grow. It could however also be the result of the samples being polished with silicon carbide (SiC) and diamond polishing pads before examination.

6 CONCLUSION

The bubble content and bubble size distribution were investigated in a used and unused crucible from the same producer. The samples from the unused crucible were heat-treated at 1400 °C in three different processes (HT2, HT3 and HT4), and the samples were re-examined and compared. HT2 was done in an argon atmosphere with ambient pressure and 24 h holding time, HT3 was done in vacuum with 4 h holding time, and HT4 was done in a 15 mbar argon atmosphere with 4 h holding time. A method of testing the bubble content was developed, using X-ray tomography and image analysis on samples from positions 1, 7 and 10 in the crucible. Later, the results were compared to similar analysis done on another type of crucible from a different producer.

Both crucibles had, before and after use, two well defined layers inside the wall; one opaque bubble containing layer, and one transparent bubble free layer. The samples from position 7 had a higher thickness than the samples from the other positions. It was found that the bubbles inside the crucible grew significantly in size during the crystal pulling process. The bubbles in the used crucibles were around 200 µm in diameter, but there were bubbles present with up to 1 mm diameter in some samples. Except from position 10 in crucible B, there were bubbles present in the entire BF layer in all the used samples. A thick layer of cristobalite was observed on the surface of the used crucibles.

Except from position 7 from crucible B, all the unused samples had a completely bubble free inner part, consisting of one quarter of the total wall thickness. There was no visible cristobalite layer on the unused samples. The bubbles in the unused crucibles were approximately 50 µm in diameter, and there were very few bubbles measured over 200 µm in diameter. The total bubble content grew from 0.30 % to 6.43 % in crucible A and from 0.25 % to 8.11 % in crucible B after use in the Czochralski process. This means that crucible A had the lowest growth in bubble content, while crucible B had the highest growth in bubble content.

The bubble content increased after HT2 and HT3 compared to the unused samples. These experiments were only done on crucible B. To make a comparison between the crucible types,

crucible A was included in HT4. The bubble content decreased, both in crucible A and B, after HT4. The changes in bubble content between the unused and the heat-treated samples were between one and two orders of magnitude lower than between the unused and the used samples. The amount of cristobalite formed on the samples decreased from HT2 to HT3 and HT4, from being a clearly visible white layer after HT2 to being barely visible after HT3 and HT4. The crack formation was reduced from the heat-treatment results done in the project thesis [3], to HT2, and further in HT3 and HT4. There were some small cracks in the surface after HT2, while there were no cracks in the sample after HT3 and HT4.

The SEM investigation revealed bubbles smaller than the detection limit of the X-ray tomography, down to approximately 1 µm in diameter, in the uncoated samples. The gold coating limited the charging effect but covered over the small bubbles. The smallest bubbles found in the coated sample was around 10 µm in diameter. The EDS analysis showed presence of silicon, oxygen, gold and carbon in the unused samples from crucible A. The carbon can originate from the SiC polishing discs used in the sample preparation, but it may also be incorporated in the crucible material. This could explain the bubble growth [35].

A well defined and easily reproducible testing method was established for the bubble content in the crucibles. The results of the work done in this thesis corresponds well to the work done in the project thesis [3]. The bubble growth during heat-treatment does not correspond to previous work published on this topic. It is, however, believed that the testing method can be used to understand the bubble growth in crucibles during crystal pulling, which will be of great interest to the PV industry.

7 FURTHER WORKS

Continuation of the work in this thesis would include further heat-treatment of samples from the crucibles. This should be done at higher temperature (1500 °C) and for a longer time (24 h). To see which of these parameters make the most impact on the bubble growth, they should be done separately. By following the testing procedure described in Chapter 3 in this thesis, the data can be compared to the results from this thesis.

In order to obtain correct data to perform the further heat-treatments, the simulation model should be improved to contain simulation of the meltdown process. This is the part of the pulling process that requires the highest temperature, and is therefore the part that is most interesting with respect on the bubble growth.

A further investigation on the softness of the crucible material should also be done. Calculations on the material softness at different temperatures and pressures will build a fundament on which more knowledge about the bubble growth can be improved.

To improve the chemical analysis of the crucibles, Wavelength-Dispersive Spectrometry (WDS) could be used. This has a lower detection limit than the EDS, (0,1 % vs 2 %), and could help understand what impurities are present in the crucible. As well, the content in the bubbles should be investigated by chemical probe analysis. This would help understanding what happens inside the bubbles during crystal pulling.

The work with the SEM should be continued, to obtain high resolution images from both crucible A and B, and to compare them. In addition, the carbon coating should be tried. In-situ analysis by SEM and/or X-ray could also be performed and help understanding the mechanisms of bubble formation and distribution.

8 REFERENCES

(1): Fraunhofer Institute for Solar Energy ISE: Photovoltaics Report, Freiburg, 2016, Downloaded 13.06.16 from https://www.ise.fraunhofer.de/de/downloads/pdf-files/aktuelles/photovoltaics-report-in-englischer-sprache.pdf

(2): A. Willoughby: Solar Cell Materials: Developing techniques, Wiley Series in Materials for Electronic & Optoelectronic Applications, Somerset, GB, 2014

(3): F. Thorsen: Bubble formation in quartz crucibles for industrial applications (project thesis), NTNU, 2015

(4): M. Di Sabatino: Silicon Production, Lecture slides from TMT4322 Solar Cells and Photovoltaic nanostructures, NTNU, 23.09.2015

(5): P. Kofstad & B. Pedersen: Silisium, Store Norske Leksikon, 2012. Downloaded 13.03.16 from: https://snl.no/silisium

(6): S. Pizzini: Towards solar grade silicon: Challenges and benefits for low cost photovoltaics, Solar Energy Materials and Solar Cells, vol 94(9), 2010

(7): J. Czochralski: Ein neues Verfahren zur Messung der Kristallisations-geschwindigkeit der Metalle, Z. Phys. Chem., 92, 1918

(8): V. Lindroos, M. Tilli, A. Lehto, T. Motooka: Handbook of Silicon Based MEMS Materials and Technologies, William Andrew Publishing, 2010

(9): J. Friedrich, W. von Ammon and G. Müller: Handbook of Crystal Growth: Bulk Crystal Growth (Second edition), Elsevier, 2015

(10): Picture of silicon wafer cutting apparatus. Downloaded 13.06.16 from: http://www.pveducation.org/node/496

(11): Picture of solar cell module. Downloaded 13.06.16 from: http://assets.inhabitat.com/wp-content/blogs.dir/1/files/2015/07/solar-panels1.jpg

(12): B. Larsen: P-type halvleder, Store Norske Leksikon, 2010. Downloaded 13.06.16 from: https://snl.no/p-type_halvleder

(13): W. Zulehner, D. Huber: Czochralskigrown silicon, Crystals, vol. 8, SpringerVerlag, 1982

(14): P. Capper: Bulk Crystal Growth of Electronic, Optical and Optoelectronic Materials, John Wiley & Sons, 2005

(15): J. Roberts: High purity quartz: Under the spotlight. Industrial Minerals, 2012. Downloaded 13.06.16 from: http://search.proquest.com/docview/993118306?accountid=12870

(16): R. Haus, S. Prinz, C. Priess: Quartz: Deposits, Mineralogy and Analytics, Springer Geology, 2012

(17): US Patent US 4632686 A (1986). Downloaded 28.05.16 from: https://www.google.com/patents/US4632686?dq=quartz+crucible&hl=en&sa=X&ved=0CB0Q6AFqFQoTCO6elZiNhccCFQVZkgod1-kCow

(18): US Patent US 4416680 A (1983). Downloaded 13.06.15 from: https://www.google.com/patents/US4416680

(19): Picture of Quartz crucible. Downloaded 09.12.15 from: http://www.ferrotec.co.jp/images/english/products/pv/crucible.jpg

(20): A. Abyzov, R. Androsch, V. Baidakov: Glass: Selected Properties and Crystallization, De Gruyter, Boston/Berlin, 2014

(21): Liu et al.: Reaction Between Liquid Silicon and Vitreous Silica, J. Mater. Res., 7(2), 1992

(22): US Patent US 5976247 A (1999). Downloaded 13.06.16 from: http://www.google.com/patents/US5976247

(23): X. Huang, T. Hoshikawa, S. Uda: Analysis of the reaction at the interface between Si melt and Ba-doped silica glass, Journal of Crystal Growth 306, 2007

(24): T. Minami, S. Maeda, M. Higasa, K. Kashima: In-situ observation of bubble formation at silicon melt–silica glass interface, Journal of Crystal Growth, Volume 318(1), 2011. Downloaded 13.06.16 from: http://dx.doi.org/10.1016/j.jcrysgro.2010.10.075

(25): W. Zulehner: Czochralski growth of silicon, J. Cryst. Growth, vol. 65, 1983

(26): N. Kobayashi: Effect of fluid flow on the formation of gas bubbles in oxide crystals grown by the Czochralski method, Journal of Crystal Growth, 54(3), 1981. Downloaded 13.06.16 from: http://www.sciencedirect.com/science/article/pii/0022024881904929

(27): US Patent US 6605149 B2 (2003). Downloaded 13.06.16 from: http://www.google.com/patents/US6605149

(28): T. Fukuda et al.: Lifetime improvement of photovoltaic silicon crystals grown by Czochralski technique using “liquinert” quartz crucibles, Journal of Crystal Growth 438, 2016

(29): X. Yu, J. Chen, X. Ma, D. Yang: Impurity engineering of Czochralski silicon, Materials Science and Engineering, Volume 74(1-2), 2013. Downloaded 13.06.16 from: http://dx.doi.org/10.1016/j.mser.2013.01.002

(30): M. Higasa, Y. Nagai, S. Nakagawa and K. Kashima: Abstract No 20a, 75th Jpn. Soc. Appl. Phys. Autumn Meeting, 2014.

(31): H. Wababayashi, M. Tomozawa: Diffusion of Water into Silica Glass at low Temperature, Materials Engineering Department, Rensselaer Polytechnic Institute, New York, J. Am. Cerum. Soc., 72, 1989

(32): E. W. Lemmon, M. L. Huber, M. O. McLinden: NIST Standard Reference Database 23: Reference Fluid Thermodynamic and Transport Properties-REFPROP, Version 9.1, National Institute of Standards and Technology, Standard Reference Data Program, Gaithersburg, 2013

(33): B. Gallien, T. Duffar, J.P. Garandet: On the detachment of Si ingots from SiO2 crucibles, Journal of Crystal Growth, Volume 390, 2014

(34): M. Juel, O. Paulsen, B. Ryningen, M. Syvertsen: Characterization of Crucibles, SINTEF, 2015

(35): Huang et al.: Expansion Behavior of Bubbles in Silica Glass Concerning Czochralski (Cz) Si Growth, Saitama 369-1108, Shinshu University Japan, 1999

(36): Picture of thermal properties of fused quartz. Downloaded 13.06.16 from: http://www.momentive.com/page.aspx?id=4294968966

(37): L.W. Hobbs: Introduction to Analytical Electron Microscopy, Scanning Microscopy International, Chicago, 1979

(38): Y.D. Yu, M.P. Raanes, J. Hjelen: Characterization of Nonconductive Polymer Materials Using FESEM, 17th International Microscopy Congress, 2010

(39): D. Bell, N. Erdman: Low Voltage Electron Microscopy: Principles and Applications, John Wiley & Sons, 2013

(40): G. Höflinger: Brief Introduction to coating technology for electron microscopy, Leica Microsystems, 2013. Downloaded 13.06.16 from: http://www.leica-microsystems.com/science-lab/brief-introduction-to-coating-technology-for-electron-microscopy/

(41): S. M. Schnurre, R. Schmid-Fetzer: Reactions at the liquid silicon/silica glass interface, Institute of Metallurgy, Technical University of Clausthal, Clausthal-Zellerfeld, Germany, 2002

(42): R. F. Egerton: Physical Principles of Electron Microscopy, An Introduction to TEM, SEM, and AEM, Springer, Dordrecht, 2005

9 APPENDIX

To make further works possible on bubble formation and growth in quartz crucibles, the image analysis macro used to calculate the bubble volume from the X-ray tomography data is included here (with permission from Stein Rørvik, SINTEF):

```
//SR20150416_SiO2_NHC-A2-1-bef_10mm_W-130kV-100uA-nf  181
     1300


root = "E:\\Exported Stacks SiO2 2015-04\\Results\\";

run("Set Measurements...", "area mean standard modal min
centroid center perimeter bounding fit stack redirect=None
decimal=8");

run("Set Measurements...", "area mean bounding fit stack
redirect=None decimal=8");


root = "Desktop";

ProcessStack(""  , 100, 1200);

/*

ProcessStack("SR20150416_SiO2_NHC-A2-1-bef_10mm_W-130kV-100uA-
nf-8bit(350.00).tif"  , 181, 1300);

ProcessStack("SR20150416_SiO2_NHC-A2-2-bef_10mm_W-130kV-100uA-
nf-8bit(350.00).tif"  , 221, 1340);

ProcessStack("SR20150416_SiO2_NTQCI-B2-1-bef_10mm_W-130kV-
100uA-nf-8bit(350.00).tif", 301, 1420);

ProcessStack("SR20150416_SiO2_NTQCI-B2-2-bef_10mm_W-130kV-
100uA-nf-8bit(350.00).tif", 231, 1350);

ProcessStack("SR20150422_SiO2_NHC-A2-1-aft_10mm_W-130kV-100uA-
nf-8bit(350.00).tif"  , 231, 1350);

ProcessStack("SR20150422_SiO2_NHC-A2-2-aft_10mm_W-130kV-100uA-
nf-8bit(300.00).tif"  , 241, 1360);

ProcessStack("SR20150422_SiO2_NTQC1-B2-1-aft_10mm_W-130kV-
100uA-nf-8bit(350.00).tif", 221, 1340);

ProcessStack("SR20150422_SiO2_NTQC1-B2-2-aft_10mm_W-130kV-
100uA-nf-8bit(300.00).tif", 241, 1360);

*/
```

```
function ProcessStack(file, start, stop) {


     call("java.lang.System.gc");

     //open(root + "..\\" + file);

     //open("");

     selectImage(1);

     title1 = getTitle();

     title1 = replace(title1,".tif","");

     run("Select None");


     selectImage(1);

     setThreshold(0,34);

     //run("Analyze Particles...", "size=0-1 show=Masks display
clear stack");

     run("Analyze  Particles...",  "size=0-50000  show=Nothing
display clear stack");

     saveAs("Results", root + title1 + " Result Pores.txt");


     selectImage(1);

     setThreshold(34,350);

     //run("Analyze Particles...", "size=10-Infinity show=Masks
display clear stack");

     run("Analyze     Particles...",     "size=500000-Infinity
show=Nothing display clear stack");

     saveAs("Results", root + title1 + " Result Glass.txt");


     selectImage(1);

     close();

}
```